7-12-2018

A Study on the Influence of Degree of Saturation and Dry Unit Weight on the Shear Strength of Unsaturated Peoria Loess at Fulton, Tennessee

Sudip Bahadur Khadka

A STUDY ON THE INFLUENCE OF DEGREE OF SATURATION AND DRY UNIT WEIGHT ON THE SHEAR STRENGTH OF UNSATURATED PEORIA LOESS AT FULTON, TENNESSEE

by

Sudip Bahadur Khadka

A Thesis

Submitted in Partial Fulfillment of the

Requirements for the Degree of

Master of Science

Major: Civil Engineering

The University of Memphis

August 2018

ACKNOWLEDGMENTS

First and foremost, I offer my sincere gratitude and respect to my advisor Dr. David Arellano, Associate Professor, Department of Civil Engineering, for his invaluable guidance and insight throughout the course of this research. I consider myself extremely fortunate to have had the opportunity of associating myself with him. I would also like to thank my committee members Dr. Roger W. Meier, Associate Professor and Graduate Coordinator, Department of Civil Engineering, and Dr. Daniel Larsen, Professor and Chair, Department of Earth Sciences for helping me to complete my thesis with their valuable guidance and thorough review of my thesis.

I wish to express my deep gratitude to all those who extended their helping hands towards me in various ways during my tenure at the University of Memphis. I greatly appreciate and convey my heartfelt thanks to my colleagues, dear ones and all those who helped me in the completion of this work.

I am especially indebted to my parents, beloved wife and brother for their love, sacrifice and support. They have set the great examples for me about how to live, study and work hard.

I also express my sincere gratitude to Dr. Shahram Pezeshk, Professor and Chair, Department of Civil Engineering for valuable departmental facilities.

ABSTRACT

Khadka, Sudip Bahadur. MS. The University of Memphis. May 2018. A Study on the Influence of Degree of Saturation and Dry Unit Weight on the Shear Strength of Unsaturated Peoria Loess at Fulton, Tennessee. Major Professor: David Arellano, Ph.D.

Loess is a windblown deposit comprised primarily of silt particles that has a metastable structure characterized by randomly open and loose particle packing with high porosity. It has an ability to stand in a near-vertical slope in its unsaturated state but collapses with an increase in the degree of saturation apparently due to the loss of the effective cohesion and matric suction. The higher degree of saturation decreases the shear strength of the soil, which makes structures on loess vulnerable to collapse or excessive settlement and instability. The overall objective of this research was to find the effect of degree of saturation and dry unit weight on the shear strength of loess. To accomplish the overall objective of this research, disturbed soil samples were collected from the field and direct shear tests were performed in the laboratory for specimens with various saturation levels. The drained shear strength parameters, cohesion (c′) and internal friction angle (φ′), were determined. Soil water characteristic curves (SWCCs) were prepared to determine the matric suction at different degrees of saturation. For determining the unsaturated shear strength, the friction angle indicating the increase in shear strength due to change in matric suction (φ^b) was estimated using three models, which were evaluated for loess. Using both test results, the shear strength of unsaturated soil was determined. It was found that the shear strength of loess decreases with an increase in saturation levels mainly due to a decrease in apparent cohesion resulting from the reduction in matric suction.

TABLE OF CONTENTS

List of Tables

List of Figures

1 Introduction

1.1 Background

Loess is a loosely compacted soil formed due to the accumulation of wind-blown dust, and has a metastable structure characterized by a randomly open and loose particle packing with high porosity. Unsaturated loess is a problematic soil due to its high collapse potential and displays high loss in shear strength upon increase in water content. It is widespread around the world and in the United States. In Tennessee, it is generally found along the Mississippi River deposited as a steep bluff. Structures built upon unsaturated loess are vulnerable to collapse or excessive settlement with an increase in water content. Therefore, an understanding of unsaturated shear strength behavior is needed.

1.2 Goals and objectives

The primary goal of this research is to find the influence of degree of saturation and dry unit weight on the shear strength of unsaturated loess. In addition, soil water characteristic curves (SWCCs) will be obtained to define the relationship between water content and matric suction since there is an influence of matric suction on the shear strength of unsaturated loess.

1.3 Research approach

In order to achieve the primary goal of this research, disturbed soil samples were collected from the field. Laboratory index tests such as gradation, Atterberg limits, and specific gravity were performed in the laboratory. Compaction curves that provide the dry unit weight and water content relationship were determined on specimens prepared using the static compaction method. To estimate the unsaturated shear strength, drained shear strength parameters, cohesion (c') and internal friction angle (φ'), along with the matric suction values are important in this research. Thus, direct shear tests were performed on the loess specimens for estimating the drained shear

strength parameters and soil water characteristic curves were prepared to determine the matric suction values at various degrees of saturation. These test results were combined to estimate the unsaturated shear strength of loess. An important parameter, the angle indicating the rate of change of shear strength with respect to matric suction (φ^b), was estimated using models suggested by Fredlund et. Al. (1996), Vanapalli et. Al. (1996), and Khalili & Khabbaz (1998). Since the applicability of these models was unknown for loess, an attempt was made to compare these models. The influence of degree of saturation and dry unit weight on the unsaturated shear strength of loess was determined.

1.4 Outline of thesis

This thesis is divided into six different chapters. Chapter 1 provides an introduction on loess along with the goals and objectives of this study. Chapter 2 provides the literature review on loess and provides a summary of the literature on shear strength of saturated and unsaturated soil. Chapter 3 presents the test methodologies utilized to accomplish the research goals and objectives. Also, this chapter provides the procedure used for sampling the soil, the physical properties of the soil, and the procedures used for conducting direct shear tests and preparing soil water characteristic curves. Chapter 4 provides a summary of the test results obtained in this study. Chapter 5 presents the analysis and discussion of the test results. Finally, Chapter 6 presents the overall summary and conclusions of the research and recommendations for future research.

2 Literature review

2.1 Introduction

In this chapter, a summary of the physical properties of loess is presented. Since the shear strength is an important property of any soil in geotechnical engineering, a brief discussion is provided on the shear strength of saturated as well as unsaturated soil. Moreover, a brief discussion on the soil water characteristic curve (SWCC) is presented as these curves are important to define the shear strength of unsaturated soil.

2.2 Introduction to loess

Loess, an aeolian sediment formed by the accumulation of wind-blown dust, is mainly comprised of silt-sized particles, and a small percentage of clay and may contain sand. Loess has a metastable structure characterized by a randomly open and loose particle packing with high porosity. This metastable structure displays a high loss in shear strength or great increase in compressibility upon an increase in the water content Wen and Yan (2014).

2.3 General physical properties

Loess is present worldwide including in the United States as shown in Figure 2-1. As indicated in Figure 2-1, loess is present in West Tennessee especially along the bluffs adjacent to the Mississippi River as shown in Figure 2-2.

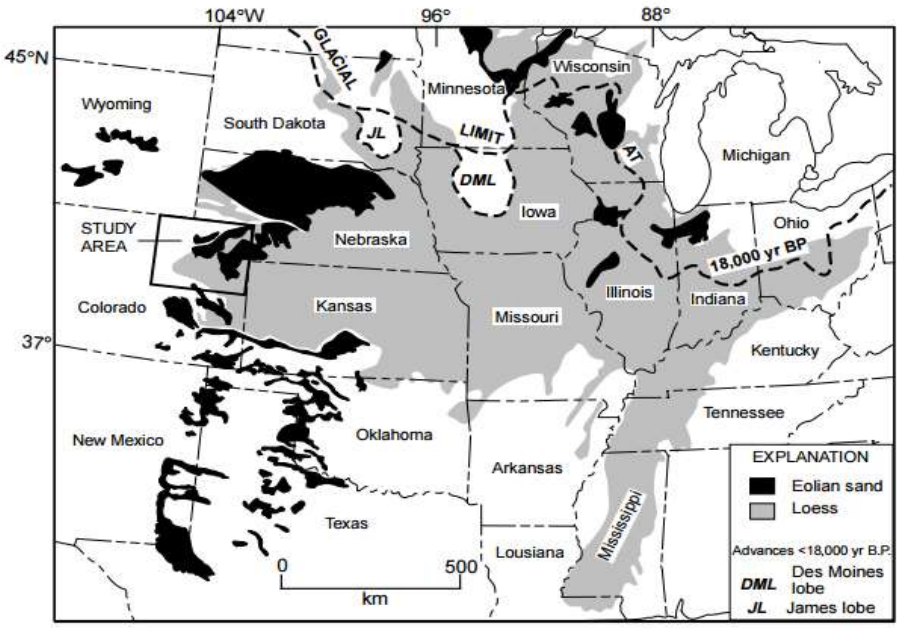

Figure 2-1: Loess distribution in North America (Muhs et al. 1999)

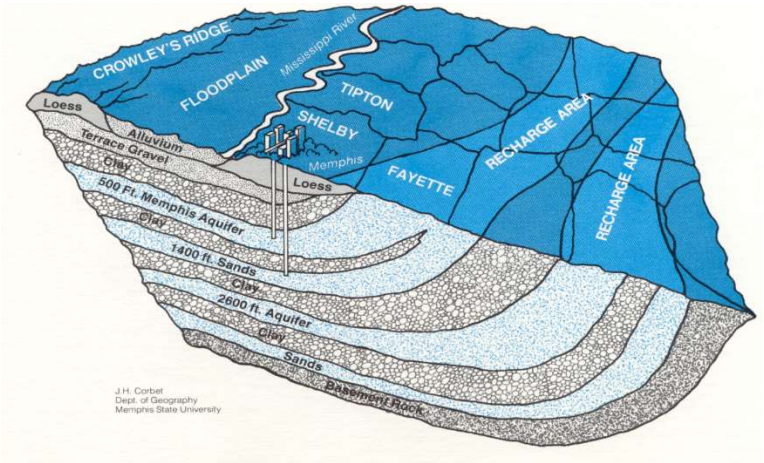

Figure 2-2: Loess distribution in Memphis (Corbet)

A literature search revealed the availability of characterization study results on the physical properties of loess obtained in France, China, and the United States. A summary of these physical properties is presented in Table 2-1.

Table 2-1: General physical properties of loess

Researcher	Country	Atterberg	Dry unit weight	Grain size
Krinitzsky and Turnbull (1967)	Mississippi Valley, TN, USA	----------	----------	Silt = 75 – 90% Clay = 10 – 25%
Delage et al. (2005)	Northern France	LL = 30 PL = 21	14.9	Silt = 80 - 84% Sand = 1 - 2% Clay = 15 - 18%
Wen and Yan (2014)	Lanzhou, China	LL = 26 - 32 PL = 17 - 19	12.1-16.3	Silt = 75 - 92% Clay = 3 - 22% Sand = 3-5%
Zhong et al. (2015)	Shanxi, China	LL = 34.2 PL = 16.7	19.8	----------
Bowders et al. (2000)	Missouri, USA	LL = 35 PL = 20	----------	----------
Parsons et al. (2009)	Kansas, USA	LL = 31 - 38 PL = 16 - 18	----------	----------
Adrian (2012)	Fulton Lake, West TN, USA	LL = 38 PL = 25	19.2	Silt = 82% Clay = 18%
Stinson (2014)	Eagle Lake, West TN, USA	LL = 30 PL = 23	17.1	Silt = 48.6% Clay = 23% Sand = 28.5%
Kane (1968)	Iowa, USA	LL = 25-45 PL = 5-25	----------	Clay = 10 - 30%

Holtz and Gibbs (1951) and Gibbs and Holland (1960) separated loess into three types based on grain size distribution. Figure 2-3 shows that the three loess types based on the predominant composition of sand, silt or clay are (1) sandy loess (2) silty loess, and (3) clayey loess. A study on loess from different locations in the United States showed that the gradations fell within the bounds established by Holtz and Gibbs (1951) and Gibbs and Holland (1960) with the exception of Alaskan loess, which tends to be slightly coarser (Higgins and Modeer Jr, 1996).

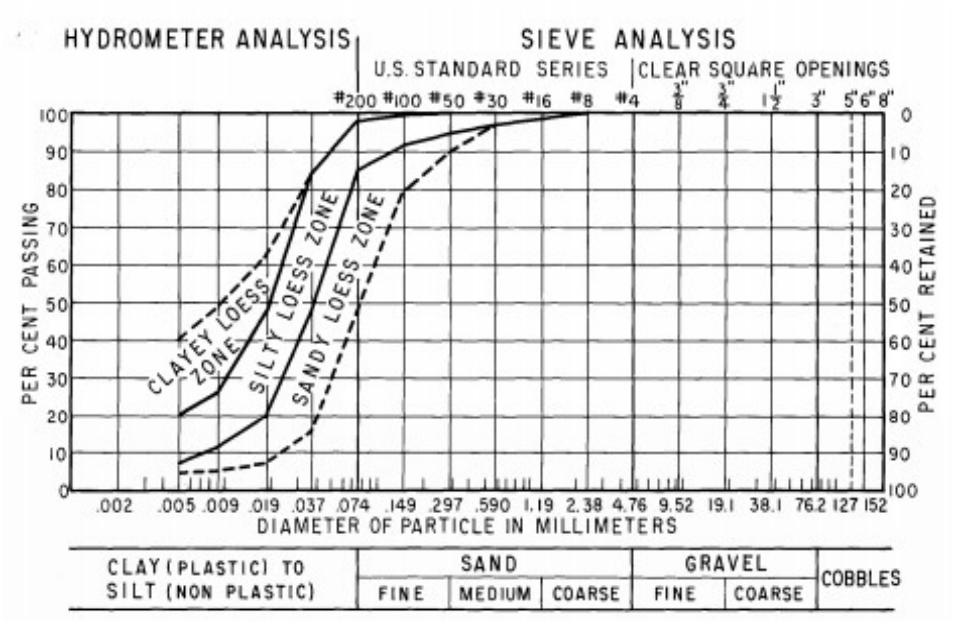

Figure 2-3: Trends of gradation curves for loess
(Gibbs and Holland 1960; Holtz and Gibbs 1951)

2.4 Shear strength

Shear strength is the internal resistance per unit area that the soil can offer to resist failure and sliding along any plane inside it. Generally, soil consists of solid particles that are randomly distributed with voids between the particles. The voids can be occupied by air, water or both. According to the percentage of voids occupied by water, also referred to as degree of saturation (S), soil can be classified into three groups:

1) For voids occupied by air only or S=0%, dry soil.
2) For voids occupied by water only or S=100%, saturated soil.
3) For voids occupied partly by air and water or 0% < S < 100%, unsaturated soil.

A summary of shear strength concepts for both saturated and unsaturated soil is presented next.

2.4.1 Shear strength of saturated soil

The shear strength of soil is a function of effective stress, which is the difference between applied external stress and porewater pressure. Since transient excess pore-water pressures

generated by applied loads will affect effective stress and thereby the shear strength as well, geotechnical engineers typically evaluate the shear strength of soil under two limiting conditions: undrained and drained. The undrained condition occurs when the pore water in the soil voids cannot drain out during load application and excess pore water pressures are generated. As a result, the pore water takes most of the external loading. Figure 2-4 shows the Mohr-Coulomb failure criterion for a saturated soil under undrained conditions and Equation 2-1 provides the shear strength in terms of total stresses for undrained condition,

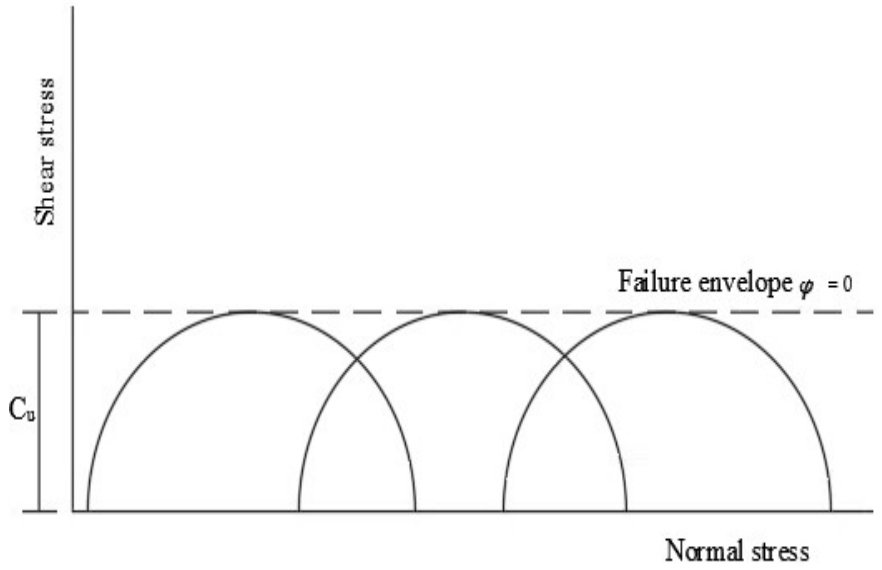

Figure 2-4: Mohr-Coulomb failure criterion for a saturated soil for undrained condition (Ekawita and Nawir 2015)

$$\tau_f = c_u \tag{2-1}$$

where, τ_f is the shear stress on the failure plane, and c_u is undrained shear strength.

As shown by Figure 2-4 and Equation 2-1, the shear strength of saturated soil for undrained conditions is the undrained shear strength because the failure envelope for the total stress Mohr's circles becomes a horizontal line and thus $\phi = 0$.

The drained condition occurs when there is no change in pore water pressure due to external loading because water can flow into or out of a mass of a soil in the length of time that the soil is subjected to the external loading. Analyses based on effective stresses are common in evaluating the shear strength of soil under drained conditions. Figure 2-5 shows the Mohr-Coulomb failure criterion for a saturated soil under drained conditions and Equation 2-2 provides the shear strength of soil in terms of effective stresses,

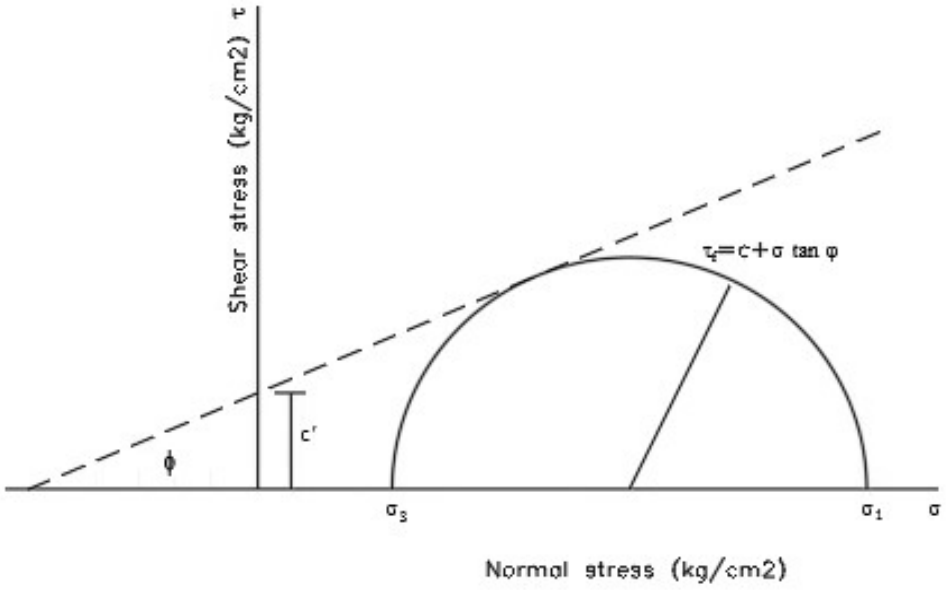

Figure 2-5: Mohr-Coulomb failure criterion for saturated soil for drained condition (Ekawita and Nawir 2015)

$$\tau_f = c' + \sigma' \tan \phi' \tag{2-2}$$

where, c′ is drained or effective cohesion, σ′ is the effective normal stress = $\sigma - u$, u is pore-water pressure, σ is the total stress, and φ′ is the effective or drained internal angle of friction.

2.4.2 Shear strength of unsaturated soil

Unsaturated soil is soil that exists at a degree of saturation less than 100%. For an unsaturated soil, the Mohr-Coulomb failure criterion corresponding to failure conditions can be

plotted in a three-dimensional plot as shown in Figure 2-6. Shear stress (τ) is the ordinate and the two stress state variables, net normal stress (σ-u_a) and matric suction (u_a-u_w), are the abscissas.

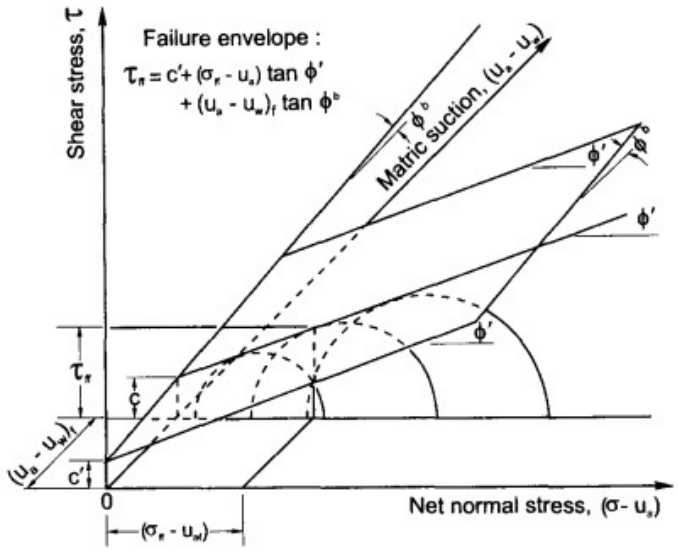

Figure 2-6: Mohr-Coulomb failure criterion for unsaturated soil (Fredlund et al. 2012)

The Mohr circles are plotted with respect to the net normal stress axis (σ-u_a) for an unsaturated soil as shown in Figure 2-6. The line tangent to the Mohr circles intersects the shear stress axis at a point that represents the drained cohesion (c′). The third axis is in terms of matric suction, which is the difference between pore air pressure and pore water pressure (u_a-u_w), and the Mohr circles are represented as a function of matric suction. The surface tangent to the Mohr circles at failure is referred to as the extended Mohr-Coulomb failure envelope and defines the shear strength of an unsaturated soil, with strength parameters φ' and φ^b that are slope angles associated with the net normal stress and matric suction, respectively, and drained cohesion (c′).

The failure envelope intersects the shear stress versus matric suction plane along a line of intercepts as shown in Figure 2-7. The line of intercepts shows the increase in shear strength with

an increase in matric suction as defined by slope angle φ^b. A linear equation of the line of intercepts is given by Equation 2-3,

$$c = c' + (u_a - u_w)_f \tan \varphi^b \tag{2-3}$$

where, c is the intercept of the extended Mohr-Coulomb failure envelope with the shear stress axis at a specific matric suction, c′ is the intercept of the "extended" Mohr-Coulomb failure envelope on the shear stress axis where the net normal stress and the matric suction at failure are equal to zero, also referred to as ″drained cohesion‟, $(u_a-u_w)_f$ is the matric suction on the failure plane at failure, and φ^b is the angle indicating the rate of increase in shear strength with respect to a change in matric suction, $(u_a-u_w)_f$.

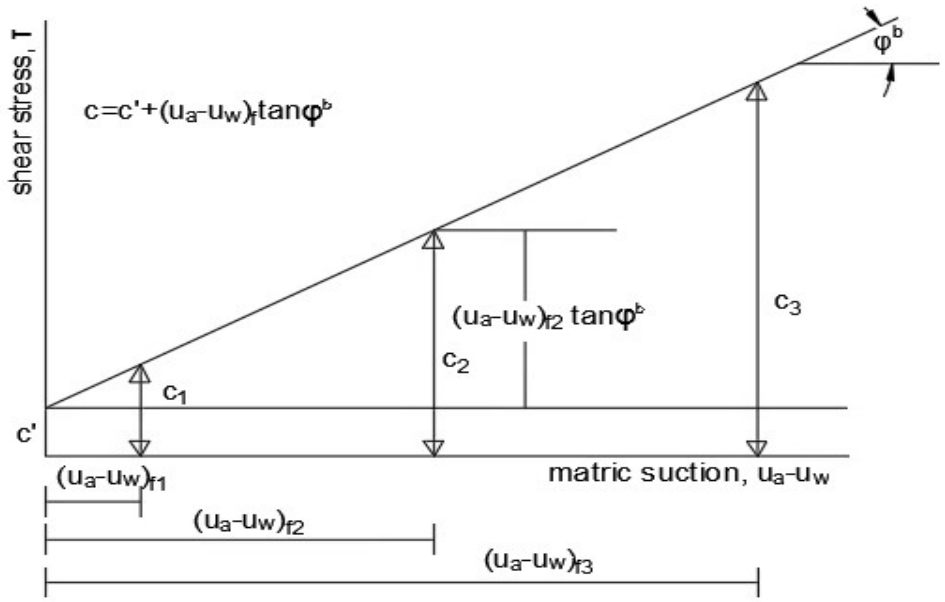

Figure 2-7: Line of intercepts along failure plane on τ versus u_a-u_w plane (Fredlund et al. 2012)

The linear form of the shear strength equation of an unsaturated soil in terms of the net normal stress state $(\sigma_f-u_a)_f$ on the failure plane at failure, shown in Figure 2-6, can be written in mathematical terms as seen in Equation 2-4,

$$\tau_{ff} = c + \left(\sigma_f - u_a\right)_f \tan\varphi' \tag{2-4}$$

where τ_{ff} is the shear strength of an unsaturated soil in terms of the net normal stress state on the failure plane at failure, $(\sigma_f\text{-}u_a)_f$ is the net normal stress state on the failure plane at failure, and φ' is the angle of internal friction associated with the net normal stress state variable, $(\sigma_f\text{-}u_a)_f$.

Equation 2-3 can be substituted into Equation 2-4 to get the shear strength of an unsaturated soil as shown in Equation 2-5,

$$\tau_{ff} = c' + \left(\sigma_f - u_a\right)_f \tan\phi' + \left(u_a - u_w\right)_f \tan\phi^b \tag{2-5}$$

The shear strength provided by Equation 2-5 can also be expressed in terms of other combinations of stress state variables such as effective stress $(\sigma_f\text{-}u_w)$ and matric suction $(u_a\text{-}u_w)$ as shown in Equation 2-6,

$$\tau_{ff} = c' + \left(\sigma_f - u_w\right)_f \tan\phi' + \left(u_a - u_w\right)_f \tan\phi'' \tag{2-6}$$

where $(\sigma_f\text{-}u_w)_f$ is the net normal stress state with respect to pore-water pressure on the failure plane at failure, and φ'' is the friction angle associated with the matric suction stress state variable and is given by Equation 2-7.

$$\tan\phi'' = \tan\phi^b - \tan\phi' \tag{2-7}$$

Although a linear shear strength theory such as Equations 2-5 and 2-6 has been presented for an unsaturated soil using an extended Mohr-Coulomb failure envelope, research on a wider variety of soil types under a wider range of soil suctions has revealed that the shear strength versus matric suction relationship, i.e., φ^b, is not a linear relationship Fredlund et al. (2012). Many researchers have provided estimation equations based on saturated shear strength

parameters for explaining the non-linearity of the shear strength versus matric suction curve. Some of the most popular relationships are presented next with their estimation equations.

One φ^b estimation equation to explain the non-linearity of shear strength is given by Equation 2-8 (Fredlund et al. 1996),

$$\tan\phi^b = \left(\frac{\theta}{\theta_s}\right)^{\kappa} \tan\phi' \tag{2-8}$$

where θ is the volumetric water content of the soil, θ_s is the volumetric water content at saturation, and κ is a fitting parameter related to the plasticity index (PI) of soil as given by Equation 2-9 provided by Garven and Vanapalli (2006),

$$\kappa = -0.0016\,(PI)^2 + 0.0975\,(PI) + 1 \tag{2-9}$$

Another estimation equation to explain the non-linear behavior of shear strength is given by Equation 2-10 (Vanapalli et al. 1996),

$$\tan\phi^b = \left(\frac{\theta - \theta_r}{\theta_s - \theta_r}\right)\tan\phi' \tag{2-10}$$

where θ_r is the volumetric water content at residual suction.

Similarly, Equation 2-11 (Khalili and Khabbaz 1998) gives another estimation equation based on air entry value,

$$\tan\phi^b = \left[\frac{u_a - u_w}{(u_a - u_w)_b}\right]^{-0.55} \tan\phi' \tag{2-11}$$

where $(u_a\text{-}u_w)_b$ is the air entry value of the soil.

In an unsaturated loess, the shear strength is provided by the combined effect of cohesion, internal friction angle, and matric suction as seen in Equation 2-5. Cohesion is mainly provided by clay binding of soil particles such as between clay and silt particles and with the cementation

provided by various agents that are present in the soil such as calcium carbonates ($CaCO_3$), ferric oxides (Fe_2O_3), sodium chloride (NaCl), etc. Internal friction angle is provided by the interlocking between the soil particles that mainly depends on the orientation of the soil particles. Matric suction is provided by the combined effect of capillarity and short-range adsorption. Capillarity is defined as the tendency of a liquid to rise or fall in a capillary tube due to the action of surface tension. In an unsaturated soil, the concept of capillarity can be used to describe the matric suction development. The pores between the soil particles act as a capillary tube and the capillary action allows water menisci to form between soil particles creating compressive normal forces between them. This force holds the particles together and the difference between the air and water pressure is the matric suction. Short-range adsorption is defined as the effects that are present within the soil due to electrical and Van der Waals forces occurring at the soil-water interface. Short-range adsorption can be found both in saturated and unsaturated soil; however, capillarity effects are unique to unsaturated soil.

Generally, loess soils are found in unsaturated conditions and their shear strength is affected by changes in water content. Direct shear tests conducted on unsaturated loess samples of China with varying water contents have shown that the drained cohesion, c', of loess is more sensitive than the drained internal friction angle, φ'. The primary mechanism for the reduction in shear strength of the unsaturated loess was the breakage in the cementation bonding provided predominantly by the clay and calcium carbonates and secondly by magnesium carbonates and soluble salts (Wen and Yan 2014). Similarly, Zhong et al. (2015) performed consolidated undrained triaxial tests on unsaturated loess specimens and consolidated drained triaxial tests on saturated loess samples from the same province of Wen and Yan (2014) samples previously described. They concluded that the shear strength of unsaturated loess is greater than the shear

strength of saturated loess due to the fact that the cohesion and internal friction angle values are higher when loess soils are in an unsaturated state. Once they saturate, the values decrease, resulting in the lower shear strength.

Because matric suction plays an important role in determining the shear strength of unsaturated soil, the relationship between water content and matric suction is important in this study. The soil water characteristics curve (SWCC) provides this relationship and a summary of SWCC is presented next.

2.5 Soil-water characteristic curve (SWCC)

SWCC relates the water content in a soil to the pore water suction, which is referred to as matric suction. The amount of water in a soil is typically defined in one of three ways: gravimetric water content (w), volumetric water content (θ_w), and degree of saturation (S). Gravimetric water content is the ratio of the mass of water in a given soil sample (M_w) to the mass of soil solids in the sample (M_s) as given by Equation 2-12.

$$w = \frac{M_w}{M_s} \tag{2-12}$$

Volumetric water content relates the volume of water in a given soil sample (V_w) to the total volume of the soil sample (V_T) as shown in Equation 2-13.

$$\theta_w = \frac{V_w}{V_T} \tag{2-13}$$

Degree of saturation is the ratio of the volume of water in a given soil sample (V_w) to the volume of voids in the soil sample (V_v) as seen in Equation 2-14.

$$S = \frac{V_w}{V_v} \tag{2-14}$$

SWCC is primarily a relationship between the amount of water in terms of volumetric water content and the suction in a soil. Figure 2-8 illustrates a typical SWCC for a silty soil along with some of its key features such as air entry value, residual water content, residual air content, desorption (drying) curve and adsorption (wetting) curve. A desorption curve is determined initially with a saturated specimen and then the degree of saturation is gradually decreased and the increase in the matric suction is measured until the soil specimen is dried. From the dried soil specimen, the adsorption curve is determined by gradually increasing the degree of saturation and the decrease in the matric suction is measured until the specimen is saturated. In the desorption curve, the air-entry value is the value of matric suction that must be exceeded for air to enter the pores of the soil. The residual water content is the water content at which an increase in the matric suction does not significantly affect the water content. The residual air content is the difference between the volumetric water content of the desorption and adsorption curve at suction values near zero. Although it is not shown in the Figure 2-8, a value analogous to the air entry value on desorption curve is called the air-occlusion value on the adsorption curve. This value is the suction value at which air bubbles becomes trapped in a soil that is being wetted, preventing the soil from reaching 100% saturation. As seen in Figure 2-8, there is hysteresis between the desorption and adsorption curves that needs to be considered when using SWCC for analyzing unsaturated soil properties. The reasons for the hysteresis include the inkbottle effect (this refers to the effects of pore size distribution), the contact angle between the air-water interface and the soil grains, entrapped air, and swelling and shrinking of the soil.

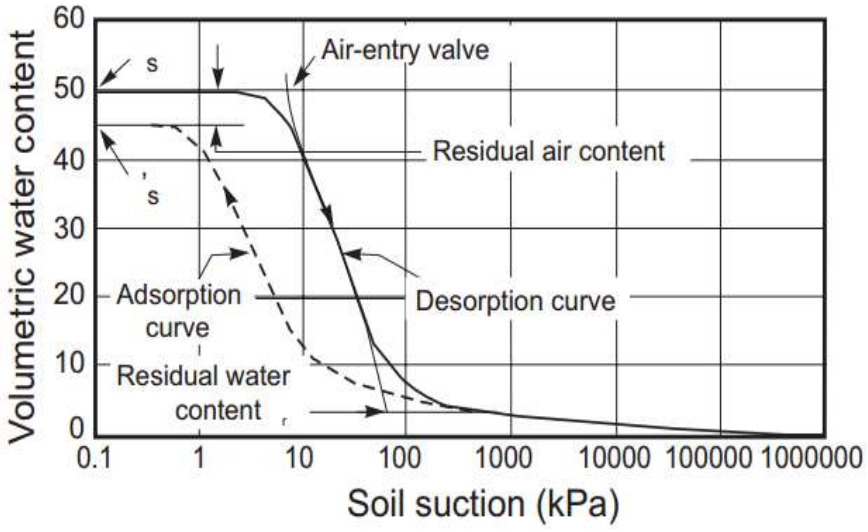

Figure 2-8: Soil-water characteristics curve for a silty soil (Fredlund and Xing 1994)

Figure 2-9 illustrates the typical SWCC (i.e. desorption curve) for a sandy, a silty and a clayey soil. It can be inferred that the saturated water content and the air entry value generally increase with soil plasticity. The SWCCs of Figures 2-8 and 2-9 can also be expressed in terms of degree of saturation instead of volumetric content as shown by Equation 2-14.

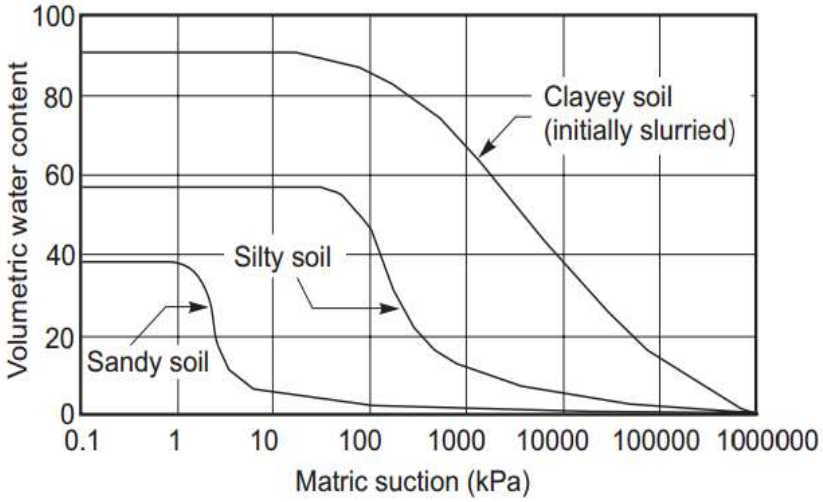

Figure 2-9: Soil-water characteristics curves for sandy, silty, and clayey soil (Fredlund and Xing 1994)

The primary purpose of obtaining SWCCs is to determine the matric suction and the angle associated with the matric suction stress variable {i.e., $(u_a-u_w)_f \tan \varphi^b$} portion of the shear strength of loess as indicated by Equation 2-5.

2.6 Summary

In this chapter, general physical properties of loess found around the world were presented. Additionally, a summary of both saturated and unsaturated shear strength concepts is presented and a summary of shear strength results from the literature of loess is provided. In this study, Equation 2-5 will be used to obtain the shear strength of loess from Fulton, TN. SWCCs will be obtained of the loess as described in this chapter to determine the matric suction and the angle associated with the matric suction stress variable.

3 Testing methodology

3.1 Introduction

The primary research tasks include obtaining soil samples, performing laboratory physical property tests, preparing test specimens from the field soil samples, performing direct shear strength tests, and determining soil-water characteristic curves. A summary of the methodologies employed to accomplish these tasks is provided next.

3.2 Soil Sample collection

On May 26 and June 16, 2016, soil samples were collected from the bluffs around Fulton, TN at coordinates (35.6344400N, -89.8219360E). This site is close to the site from which Stinson (2014) and Adrian (2012) collected samples for their research. The soil, referred to herein as ″Fulton loess‟ due to its geographic location, is part of the Peoria Loess formation that was deposited throughout North America during the Last Glacial Maximum.

Prior to sample collection, 1.5 feet of surficial soil was removed to clear debris such as plant roots. Disturbed soil samples were obtained at depths from about 2 to 4 feet by shoveling soil from the ground and placing the soil sample into a 5-gallon bucket that was subsequently closed with a lid. A small portion of soil was also placed in a plastic bag and sealed to prevent moisture loss so that the in-situ moisture content could be measured.

3.3 Loess physical property tests

3.3.1 Grain size distribution

Grain size distribution provides the relative quantities of different grain sizes of particles in the soil. It is used in soil classification, soil filter design and prediction of the behavior of a soil concerning shear strength, settlement, and permeability. Figure 3-1 provides the grain size distribution of Fulton loess based on hydrometer tests per the ASTM D422 procedure. Table 3-1

summarizes the percentages of gravel-sized, sand-sized, silt-sized, and clay-sized particles. Fulton loess consists of 87% silt-sized particles and 13% clay-sized particles. These particle size distribution results agree with the values obtained by Adrian (2012), which were previously summarized in

Table 2-1.

Also shown in Figure 3-1 are the three loess zones based on particle size proposed by Gibbs and Holland (1960) as described in Section 2.3. Figure 3-1 shows that Fulton loess falls near the silty and clayey loess zone transition areas.

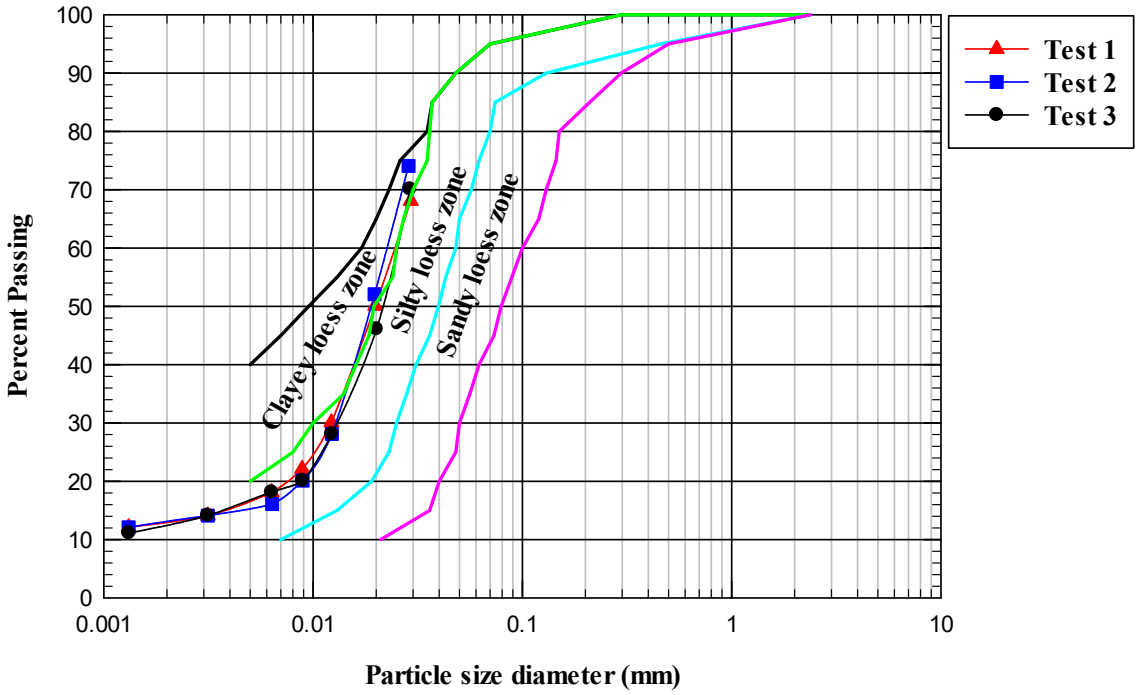

Figure 3-1: Grain size distribution of Fulton loess

Table 3-1: Grain size distribution of Fulton loess

Test	Gravel % >4.75 mm	Sand % 0.074<dia<4.75 mm	Silt % 0.002<dia<0.074 mm	Clay % <0.002 mm
Test 1	0.0	0.0	86.9	13.1
Test 2	0.0	0.0	87.0	13.0
Test 3	0.0	0.0	87.1	12.9

3.3.2 Specific gravity test

The specific gravity of soil is the ratio of the unit weight of soil solids to the unit weight of water. This property is useful in the calculation of soil weight and volume quantities like void ratio and degree of saturation. Specific gravity tests were performed on Fulton loess following ASTM D854, test method A. According to the test, Fulton loess has a specific gravity of 2.81.

3.3.3 Atterberg limits

The liquid limit (LL) and plastic limit (PL) of Fulton loess were obtained in the laboratory in accordance with ASTM D 4318. The LL of Fulton loess is 30 and the PL is 29. The plasticity index (PI), which is the difference between LL and PL, is 1. These Atterberg limit values are also in agreement with the values obtained by Stinson (2014) and Adrian (2012), which were previously summarized in Section 2.2 of this thesis. The in-situ moisture content of Fulton loess as sampled in the field is 26.6 % and is less than the PL.

3.4 Specimen preparation procedure

3.4.1 Introduction

Remolded specimens are typically prepared using a compaction procedure. Compaction is a mechanical process in which stress is applied to a soil layer through the application of mechanical energy. This process is used to densify the soil by expelling out air trapped in the voids. A compaction curve, which is the dry density versus moisture content relationship, can be developed in the laboratory utilizing this process. A compaction curve represents the resulting dry unit weight from several soil specimens from the same soil sample that are compacted at different moisture contents while applying the same compaction effort. Each soil type has a unique dry unit weight versus moisture content relationship, i.e., compaction curve, for a given compaction effort. The shape of the compaction curve depends on soil type, method of

compaction, and compaction effort applied. Typical compaction curves are illustrated in Figure 3-2.

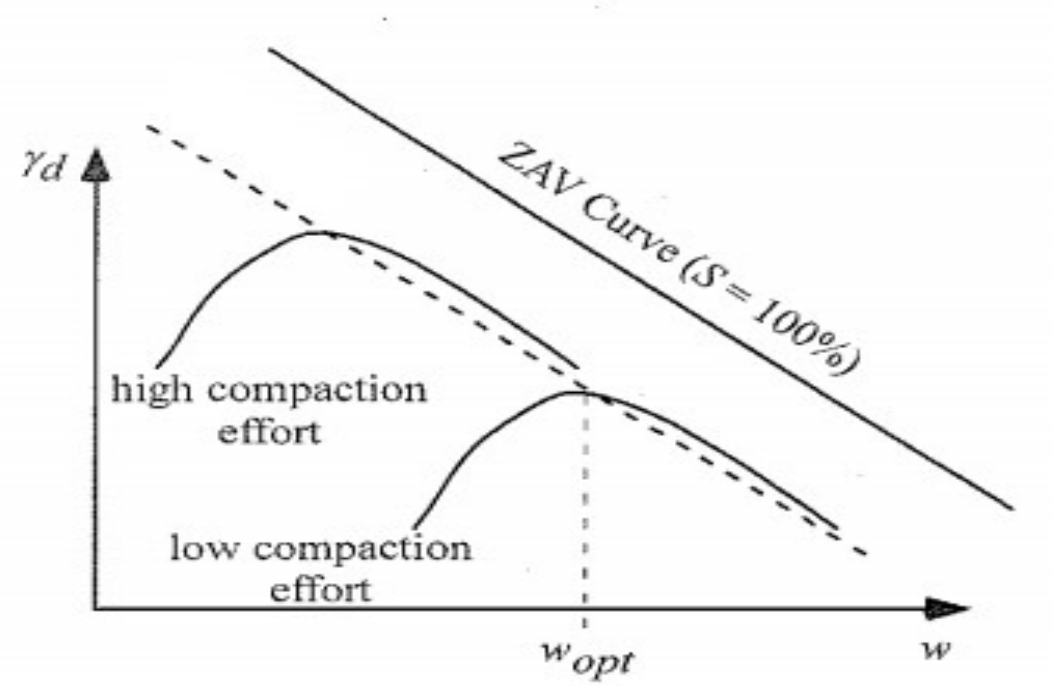

Figure 3-2: Typical compaction curve

As shown in Figure 3-2, moisture content (w) is plotted as the abscissa and dry unit weight (γ_d) as the ordinate. Two compaction curves are plotted for different compaction efforts. The moisture content where the dry unit weight is the maximum for a compaction curve is known as the optimum moisture content (w_{opt} or OMC). The portion of the curve to the left of OMC is called dry-of-optimum, and the portion of the curve to the right is called wet-of-optimum. In the field, the soil can be compacted dry-of-optimum or wet-of-optimum. A zero-air void (ZAV) curve, which represents the coordinates of dry unit weight and moisture content for the 100% saturated condition, is usually drawn with the compaction curve. The slope of the ZAV curve and the slope of the wet-of-optimum portion of the compaction curve are nearly parallel.

Two types of compaction methods typically used in the laboratory to obtain the compaction curve are (1) dynamic or impact compaction and (2) static compaction.

Dynamic or impact compaction is a method of compaction in which a standard hammer with a specific weight is dropped from a specific height for a specific number of times. Dynamic compaction is typically achieved by one of two methods: (1) standard Proctor method, in which soil is compacted in three separate layers, termed lifts, of equal thickness using 25 blows per lift with a 5.5-lb hammer falling through 12 inches of height, and (2) modified Proctor method, in which soil is compacted in five lifts of equal thickness using 25 blows per lift with a 10-lb hammer falling through 18 inches of height.

Static compaction is a method in which the soil is compacted by applying a static uniform force per unit cross-section of soil specimen. Static compaction is achieved by one of two methods: (1) constant peak stress-variable stroke compaction, in which the stress is applied at a constant rate until a specific peak stress is reached, and (2) variable peak stress-constant stroke compaction, in which a static force is applied at a constant rate of strain in the soil mass until a desired thickness of specimen is achieved.

Doris Asmani et al. (2013) performed a study using both static (constant peak stress) and dynamic (standard Proctor) laboratory compaction tests on different categories of soils and compared the condition of the compacted specimens. They tested the homogeneity of both compacted specimens using X-ray imagery. They found that the specimens prepared by static compaction were more homogenous. Stinson (2014) also used the static compaction method (constant peak stress) to develop a static compaction curve and to prepare soil specimens for maximum collapse potential testing using oedometer tests. He found that the static compaction

method provided more consistent soil specimens. Therefore, test specimens for this research were prepared using the static compaction method (constant peak stress).

3.4.2 Procedure

Soil that passed through the #4 sieve was oven dried for 24 hours and a predetermined amount of distilled water was added to achieve a targeted moisture content. The soil and water mixture was kept in airtight plastic bags for 24 hours. The purpose of this curing period is to allow the moisture content to equilibrate. After curing, a small amount of the prepared soil was weighed and the moisture content was determined according to ASTM D2216-10 by using a drying oven to evaporate the water within the soil. The remaining soil was used to prepare soil specimens for testing.

Soil specimens were prepared using a prefabricated aluminum mold that allowed for static compaction of the soil directly into a 2.5-inch-diameter by 1-inch-high confining ring as shown in Figure 3-3.

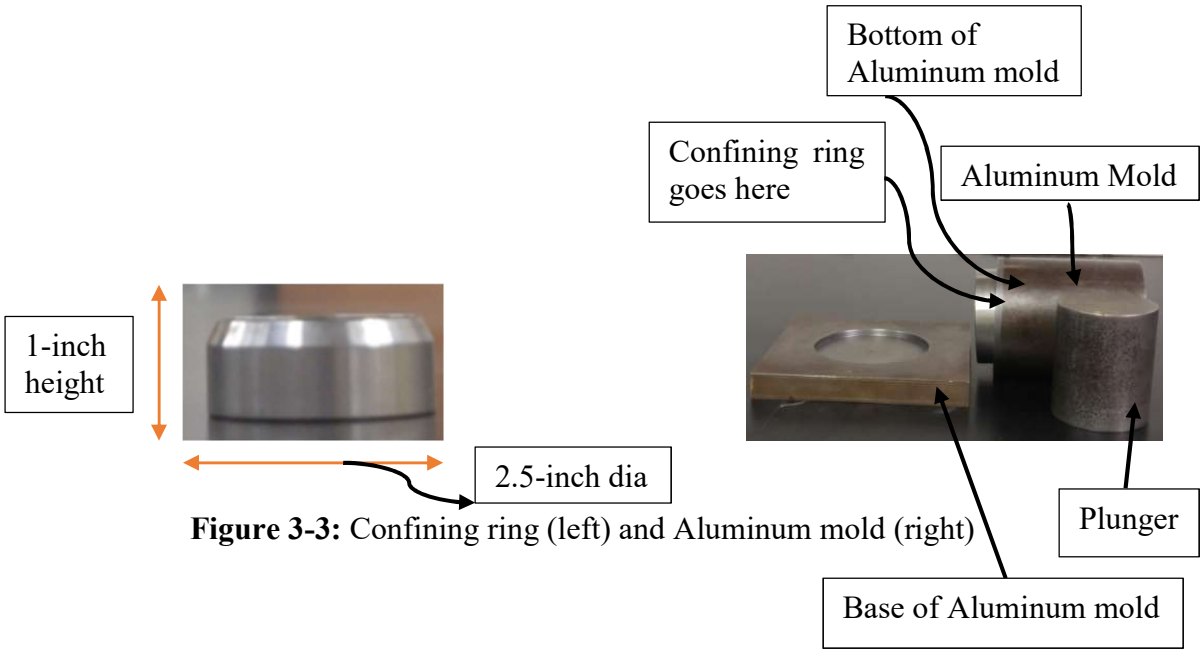

Figure 3-3: Confining ring (left) and Aluminum mold (right)

The interior of the confining ring was sprayed and rubbed with canola oil to reduce friction between the soil particles and confining ring wall during compaction, and then the confining ring was inserted in the bottom of the mold.

Several soil-water mixtures were prepared with different targeted moisture content values. To create a specimen for testing, a predetermined amount of soil was chosen so that the final height of the soil after compaction would be at least one inch. The amount for the first specimen was selected after various trials. The amount of soil for the other specimens was calculated based on the increase in moisture content of the other mixtures. This means a soil specimen with higher moisture content will have higher mass at the start of the compaction. The amount of soil ranged between 110 grams and 160 grams for all of the specimens. The soil was then placed in the aluminum mold using a cone so that soil would not get lost. After leveling the soil inside the mold, a plunger was placed into the top of the mold. Then, the aluminum mold was taken to the loading frame of the GCTS Fredlund device as shown in Figure 3-4.

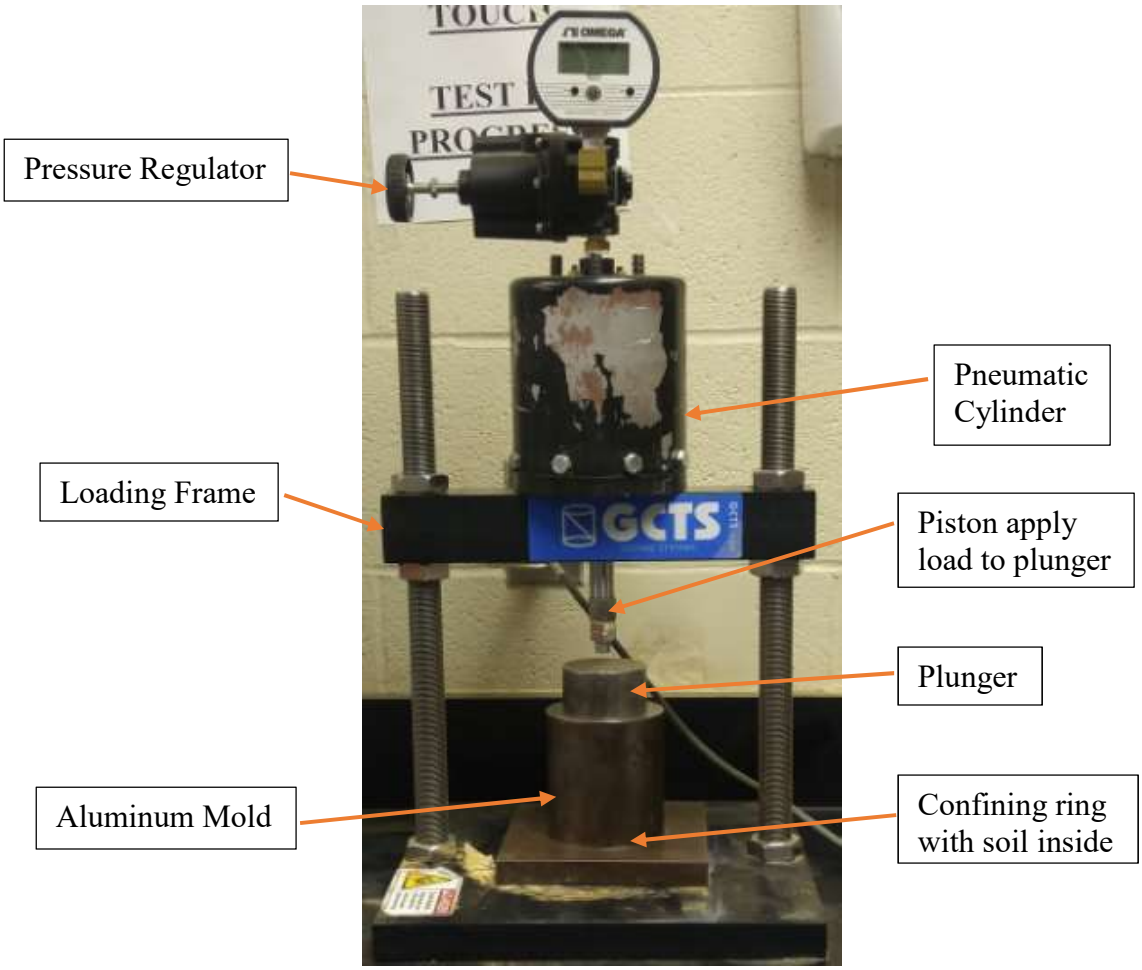

Figure 3-4: Pneumatic cylinder attached to the loading frame on GCTS Fredlund device

The targeted stress was applied from the pneumatic cylinder attached to the loading frame. Soil compaction curves were prepared using peak stresses of 143.8 kPa, 229.2 kPa, and 561.7 kPa. Initially, stresses of 50 kPa, 70 kPa, and 175 kPa were intended to develop the compaction curves because these stresses would resemble the in-situ overburden stress in the field, at depths 2.9 m, 4 m, and 10 m, respectively, based on an assumed in-situ moist unit weight of 17.5 kN/m^3. However, the stresses were adjusted to 143.8 kPa, 229.2 kPa, and 561.7 kPa because the specimens prepared below 140 kPa disintegrated upon extraction from the confining ring.

At the start of the compaction process, the compaction stress was uniformly increased during a 2-minute period and then held constant for another 3-minute period. These time intervals were also utilized by Stinson (2014) for preparing his compaction curve specimens. After compaction, all of the specimens had their final height at or slightly greater than one inch.

After the compaction procedure was completed, the confining ring was carefully taken out of the mold, and excess soil above the top of the confining ring was trimmed off using a wire saw to obtain a soil specimen that was totally within the confining ring and 1 inch in height. The specimen within the confining ring was then weighed, and the moist mass of the specimen was recorded by deducting the weight of the confining ring. The moist unit weight was determined based on the volume of the confining ring, which was 8.04e-5 m^3. The specimen was then extracted from the ring and placed in the oven at 115 °C for at least 24 hours to determine the post-compaction moisture content. There was no significant difference in the pre-compaction and post-compaction moisture contents. The dry unit weight of each specimen was determined from the moist unit weight and the moisture content.

Three compaction curves were prepared for this research as shown in Figure 3-5.

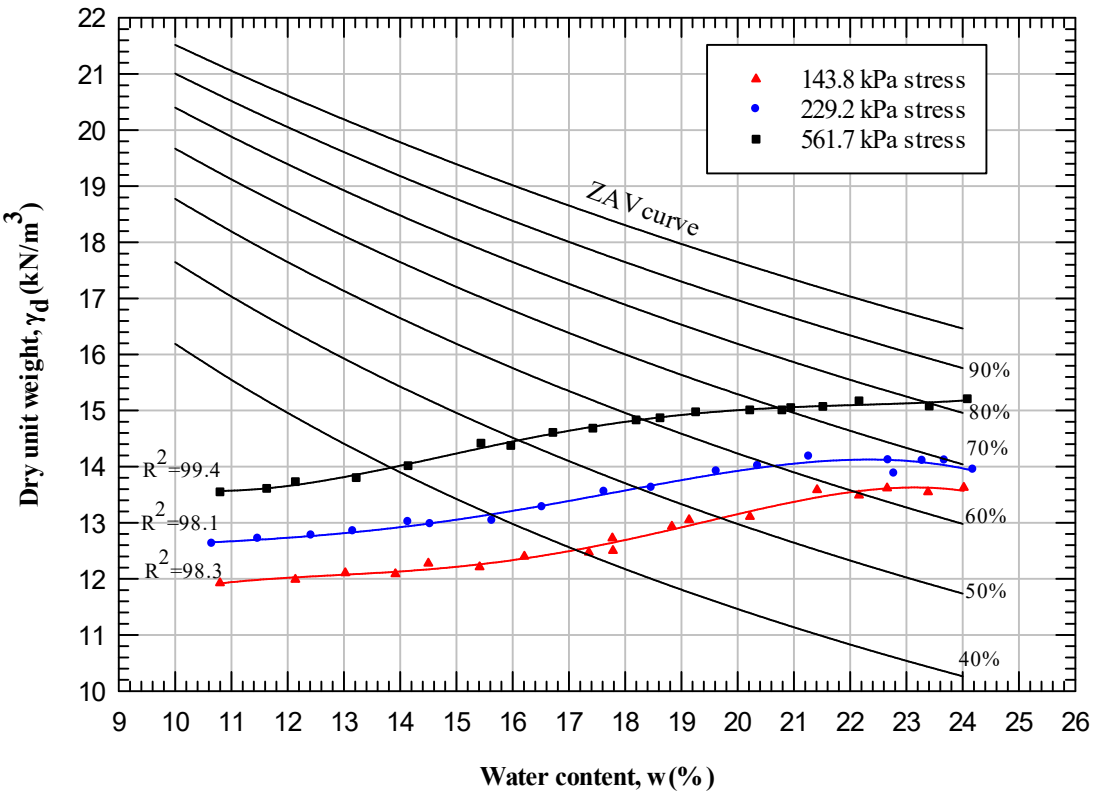

Figure 3-5: Static compaction curves for Fulton loess

For developing the compaction curve at a given stress level, seventeen specimens were prepared at moisture contents ranging from 11% to 27%. However, the results of specimens that exhibited water expulsion during compaction were not utilized in the development of the compaction curve. Thus, the moisture contents of the compaction curves were all less than 25%.

The compaction curve for a given compaction stress level was obtained by fitting a curve to the series of measured dry unit weight and moisture content values obtained for that given stress level using the polynomial regression option included in the SigmaPlot12 software. Figure 3-5 shows the three fitted compaction curves and the R-squared values for each curve. It also shows the theoretical zero air-void curve and curves for 90%, 80%, 70%, 65%, 60%, 50%, and 40% saturation levels based on a specific gravity of 2.81. R-squared values for the compaction curves exceed 0.98, indicating that the constant stress procedure of specimen preparation yielded

reasonably consistent specimens, which is in agreement with the studies of Doris Asmani et. al. (2013) and Stinson (2014). The compaction curves shown in Figure 3-5 were used to prepare additional specimens for the determination of shear strength and soil-water characteristics curves as will be described in Sections 3.3.3.2 and 3.7.3.1.

As previously noted, the results of specimens that exhibited water expulsion during compaction were not utilized in the development of the compaction curve. Thus, the moisture contents of the compaction curves were less than 25% and only the dry-of-optimum portion of the compaction curves was obtained.

3.5 Test matrix

The test matrix shown in Table 3-2 provides the targeted test variables utilized in performing the direct shear tests for Fulton loess. The test matrix shows the compaction stresses used to prepare the specimens and the various targeted degrees of saturation and dry unit weights for the specimens that were tested. The targeted dry unit weights were obtained from the compaction curves of Figure 3-5 at the corresponding degrees of saturation. Each test series consists of three identical specimens prepared at the same targeted degree of saturation and dry unit weight. Each specimen was used to perform a direct shear strength test at one of three different normal stresses as listed in the Table 3-2 (i.e., one specimen for each normal stress).

Table 3-2: Text matrix for direct shear tests

Direct Shear Test				
Remolded Specimens	Test Series	Degree of Saturation, S (%)	Dry Unit Weight, γ_d (kN/m^3)	Normal Stresses for Direct Shear Tests (kPa)
Specimens to be prepared at compaction stress of 143.8 kPa	1	40%	12.6	110, 143.8, and 600
	2	50%	13.1	110, 143.8, and 600
	3	60%	13.5	110, 143.8, and 600
	4	65%	13.4	110, 143.8, and 600
	5	100%	γ_{100}	110, 350, and 600
Specimens to be prepared at compaction stress of 229.2 kPa	6	40%	13.2	110, 229.2, and 600
	7	50%	13.6	110, 229.2, and 600
	8	60%	13.9	110, 229.2, and 600
	9	65%	14.1	110, 229.2, and 600
	10	100%	γ_{100}	110, 350, and 600
Specimens to be prepared at compaction stress of 561.7 kPa	11	40%	14.1	110, 561.7, and 600
	12	50%	14.5	110, 561.7, and 600
	13	60%	14.8	110, 561.7, and 600
	14	65%	14.9	110, 561.7, and 600
	15	100%	γ_{100}	110, 350, and 600

For each direct shear test series shown in Table 3-2, two normal stress values are kept the same for all test series, i.e., 110 kPa and 600 kPa, which are stress values that are lower and higher, respectively, than the compaction stresses of 143.8 kPa, 229.2 kPa, and 561.7 kPa that will be used to prepare the specimens to determine the effect of over-consolidation ratio, i.e., the ratio of compaction stress to normal stress, on shear strength. The intermediate third stress value will be the same stress value that will be used to prepare the respective specimen as shown in Table 3-2 to simulate a normally consolidated soil, i.e., the ratio of compaction stress to normal stress equal to 1.

3.6 Direct shear test

3.6.1 Introduction

The primary goal of this research is to evaluate the effects of degree of saturation and dry unit weight on the shear strength of unsaturated loess. Shear strength is an important engineering property of soil because soil strength controls the stability of geotechnical structures. Determination of applicable shear strength parameters is a key objective in the design of geotechnical structures. A direct shear strength test is a common test for determining shear strength parameters because it is an easier and quicker method to measure the drained shear strength parameters, i.e., c′ and φ′ in Equation 2-2, of soil or rock or discontinuities in soil or rock masses compared to triaxial tests. The direct shear test methodology is described next.

3.6.2 Direct shear device

A schematic diagram of a typical direct shear device is shown in Figure 3-6.

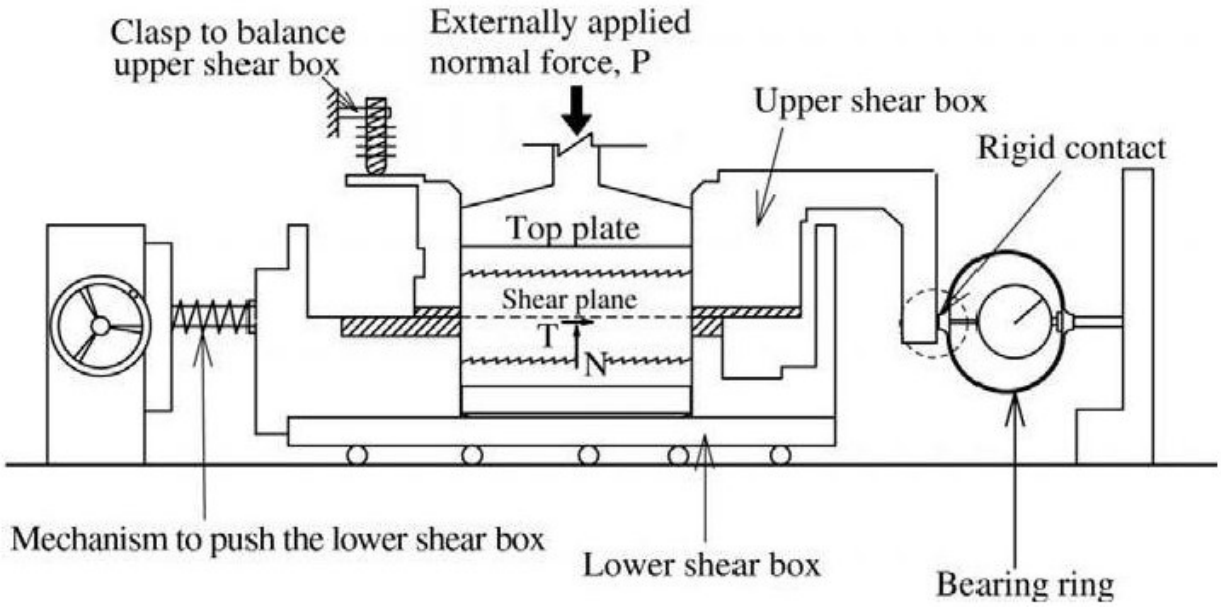

Figure 3-6: Schematic diagram of a direct shear device (Liu 2006)

The direct shear test device consists of a metal shear box that splits horizontally into an upper and lower shear box. The upper shear box is fixed, and the lower shear box is pushed or pulled horizontally relative to the other box section with the help of a motor. The direct shear box used in this study was manufactured by Durham Geo-Slope Indicator (DGSI) and is shown in Figure 3-7.

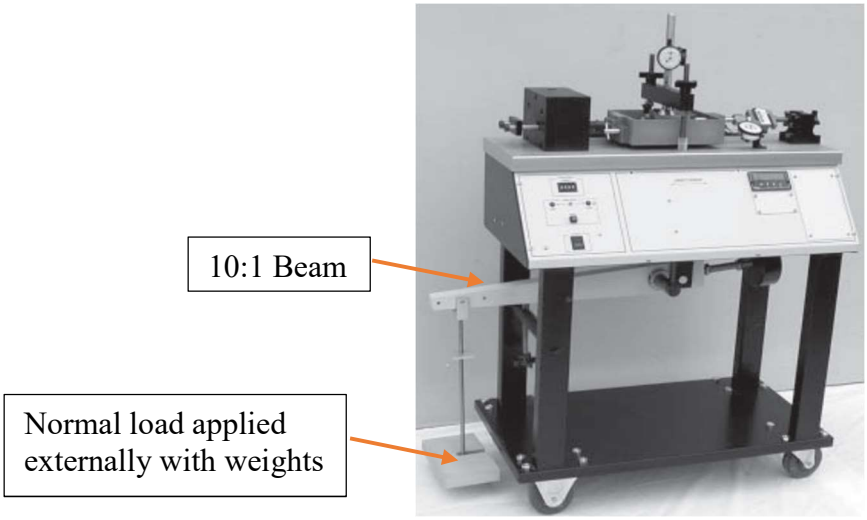

Figure 3-7: Direct shear device manufactured by DGSI

The motor can apply a shear (horizontal) load at a rate ranging from 0.0001 in/mm to 0.2999 in/mm. This applied horizontal load causes the soil specimen to shear along the horizontal plane created by the horizontal split of the shear box. The device includes sensors and digital indicators for measuring the shear load and horizontal deformation during the test. The normal load is applied externally to the specimen with weights as shown in Figure 3-7. The lever arm (beam) of the device used in this study has a ratio of 10:1, which means if a 1 lb. load is applied to the beam, 10 lbs. of load is applied to the specimen. External linear variable differential transducers (LVDTs) are used to measure the horizontal and vertical deformation of the soil

specimen. The DGSI direct shear device transfers the data directly to a computer during the test through software called Windows Based Serial Acquisition Software (WINSAS).

ASTM D 3080, which is the standard test method for direct shear strength test of soils, provides shear loading rates for minimizing the potential for the development of pore water pressures during shear loading. The shear loading rate varies with the type of soil to be tested. ASTM D 3080 suggests using consolidation test results on the type of soil to be tested to determine the shear loading rate.

3.6.2.1 Determination of Shear Loading Rate

ASTM D 3080 provides recommended shear loading rates based on the time required for soil to reach 90% consolidation, t_{90}, under the highest normal stress that will be applied during the direct shear test because the highest normal stress will induce the greatest excess pore water pressure in the soil. Therefore, a consolidation test was performed on a specimen of Fulton loess to obtain t_{90}. Consolidation is a process of reduction in the bulk volume of soil under loading due to the expulsion of excess pore water from the soil. The ASTM D2435 procedure was followed in performing the consolidation test.

The specimen was prepared using a compaction stress of 561.7 kPa because it is the highest compaction stress that will be used for preparing the direct shear test specimens. A targeted moisture content of 21% was chosen to prepare the specimen. As explained in Section 3.4.2, the specimens with a moisture content greater than 24% were not utilized to prepare the compaction curve because of the expulsion of water. Thus, a target moisture content of 21% was chosen slightly below 24% to reduce the risk of preparing inferior specimens. An upper value of moisture content was selected because it would provide a greater potential for excess pore water pressure development. From Figure 3-5, for a moisture content of 21% and compaction stress of

561.7 kPa, the targeted dry unit weight was determined to be 15.03 kN/m^3. This dry unit weight was utilized to calculate the dry soil mass (123.3 gm) and then the moist soil mass (149.2 gm) using the targeted moisture content. From the estimated moist soil mass, a soil specimen was prepared using the procedure described in Section 3.4.2.

After the soil specimen was prepared, the specimen and the confining ring were weighed to verify that the target unit weight of 15.03 kN/m^3 was achieved. The specimen degree of saturation was calculated to be 70.7%. Consolidation tests are typically performed on nearly fully saturated specimens. Therefore, an attempt was made to fully saturate the soil specimen by placing the confining ring with the soil specimen in a tray full of distilled water. Porous stones of the same diameter as the inside diameter of the confining ring were placed at the top and bottom of the confining ring to confine the soil specimen within the confining ring. Filter paper was placed between the soil specimen and the porous stones to prevent loss of soil into the porous stones. The height of the water in the tray was maintained just below the top of the confining ring. This allows the soil to be saturated from the bottom up, reducing the risk of entrapping air in the specimen. A small load of 0.5 N was placed on the top of the top porous stone to ensure contact was maintained between the porous stone and tray during saturation.

The specimen was saturated for 30 hours. The specimen and confining ring were periodically weighed during the saturation period to calculate the degree of saturation. The initial degree of saturation was calculated to be 70.7%, and after the saturation period, a final degree of saturation of 92.6% was obtained. After the saturation process, the specimen was taken out of the water tray and any free water present on the exterior of the specimen and the confining ring was removed with a paper towel. The specimen and the confining ring were then placed in the consolidation cell of the consolidation test device.

A small seating load of 3 kPa was applied first and immediately after load application the deformation indicator was zeroed. Then, the first load of 13.41 kPa was applied to the specimen. Vertical deformation readings at time intervals of 0.1, 0.25, 0.5, 1, 2, 4, 8, 15, and 30 minutes, and 1, 2, 4, 8, and 24 hours were recorded as per the ASTM D2435 standard. Then, after 24 hours, the load was increased to 26.4 kPa, and the vertical deformation reading was retaken. The process of load increase and deformation readings continued by increasing the load in increment ratios of 2 (new load = 2 x previous load) until the highest normal stress that was to be used to perform the direct shear test of 600 kPa as noted in Table 3-2 was exceeded. The final consolidation test load was 801.4 kPa based on the load increment ratio used.

Each load increment was sustained for a period of 24 hours as recommended by ASTM D 2435 to ensure that the end of primary consolidation was reached, which is defined as the time it takes for all excess pore water pressure due to the load to dissipate. The end of primary consolidation for each load increment was confirmed by obtaining additional vertical deformation readings near the 24-hour period and checking that additional vertical deformations did not occur. The consolidation test data is provided in Table A-1 in Appendix A.

For each load increment, vertical deformations at specified time intervals were recorded. Although vertical deformation data were recorded for each load increment, to obtain a shear rate, ASTM D 2435 recommends using the vertical deformation versus time interval data for the highest load applied to the specimen. This means the data for the final load increment of 801.4 kPa was utilized to calculate shear rate. Initially, the axial strain was calculated, which is defined as the ratio of change in specimen height to the original height. Figure 3-8 shows the plot of axial strain versus the square root of time consolidation curve using the vertical deformation versus time interval data for the final load of 801.4 kPa that was utilized to obtain the time for

90% consolidation (t_{90}). This process of obtaining the t_{90} is called Taylor's square root of time method as outlined in ASTM 2435. In this test, the square root of t_{90} is obtained to be 2.04 $min^{1/2}$. Then, t_{90} was obtained by squaring the value, i.e., $2.04^2 = 4.16$ min.

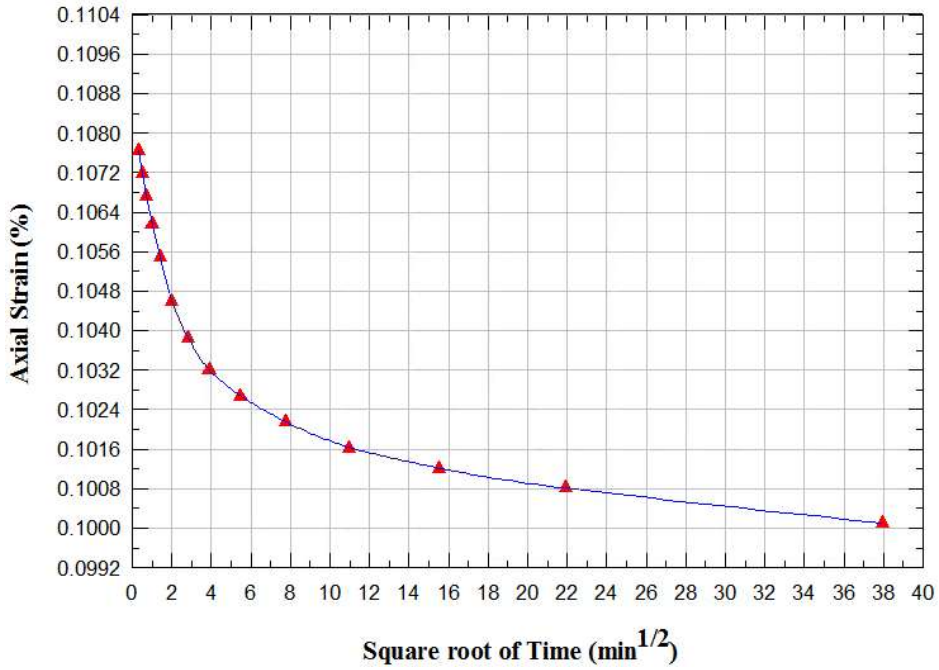

Figure 3-8: Square root of time consolidation curve

As explained in section 9.10.2 in ASTM D3080, the shearing rate was found using Equation 3-1:

$$R_d = \frac{d_f}{t_f} \tag{3-1}$$

where R_d is the shear loading rate (in/min or mm/min), d_f is the estimated relative shear displacement at failure (in or mm), and t_f is the total estimated elapsed time to failure (min) as given by Equation 3-2:

$$t_f = 11.6 t_{90} \tag{3-2}$$

where t_{90} is the time required for the specimen to achieve 90% consolidation under the maximum normal stress.

Based on the t_{90} of 4.16 min, a shear rate based on an estimated relative shear displacement at failure (d_f) of 5 mm (for over-consolidated fine-grained soil: to be more conservative on the shearing rate) was obtained to be 0.104 mm/min or 0.00408 in/min. The shear rate was taken to be 0.004 in/min for performing the direct shear tests.

3.6.2.2 Direct shear specimen preparation

The test matrix in Table 3-2 provides the target saturation levels at which the specimens for a given direct shear test series are prepared. Based on the specimen compaction stress and the target degree of saturation, the dry unit weight and the moisture content is obtained from Figure 3-5. The intersection points of the compaction curve for a targeted compaction stress and the curve for the targeted degree of saturation shown in Figure 3-5 gives the required dry unit weight and the moisture content. The moisture content that corresponds to the targeted saturation level and dry unit weight was also verified using Equation 3-3,

$$w = S\left(\frac{\gamma_w}{\gamma_d} - \frac{1}{G_s}\right) \tag{3-3}$$

where G_s is the specific gravity of loess, w is the moisture content, S is the degree of saturation, γ_w is the unit weight of water, and γ_d is the dry unit weight of the loess.

The weight of dry soil is calculated from the dry unit weight. The volume of water required to obtain the targeted saturation level is then calculated from the moisture content obtained using Equation 3-3. The moist soil is prepared using the dry weight of soil and the required volume of water and the prepared moist soil is placed in air-tight double plastic bags to prevent loss of moisture. The plastic bags were kept in a humidity-controlled room in the

laboratory for 24 hours to ensure moisture equilibrium. The soil-water mixture was then taken out after 24 hours and the direct shear specimens were prepared following the procedure explained in Section 3.4.2.

As shown in Table 3-2, for a given direct shear test series, e.g., Test Series 1, three specimens, with each specimen subjected to a different normal stress, e.g., 110, 143.8, and 600 kPa, were used to determine the shear strength at a given degree of saturation and dry unit weight.

Figure 3-9 shows how c′ and φ′ are obtained from the series of three direct shear strength test results performed at varying normal stresses.

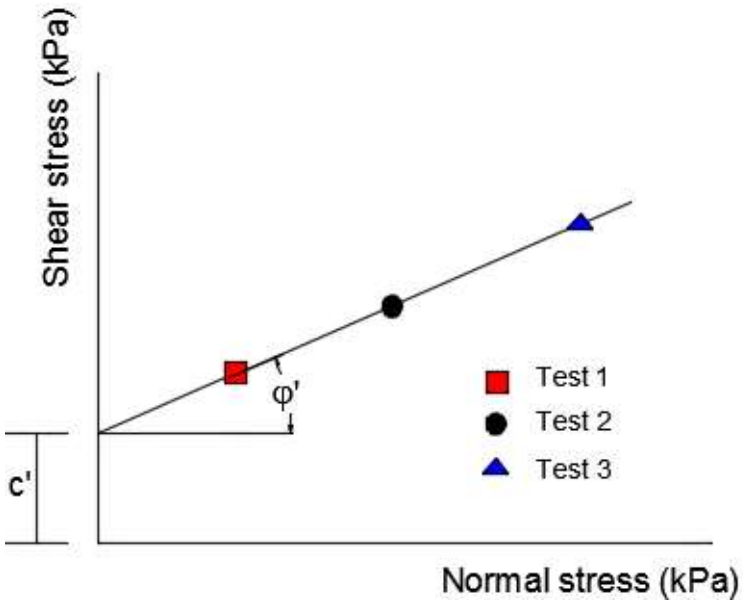

Figure 3-9: Typical plot of shear stress versus normal stress

The shear stress versus horizontal displacement plots are obtained for each normal stresses shown in Table 3-2. From these plots, peak shear stress for each normal stress is determined. Each peak shear stress is plotted against its respective normal stress to estimate c′ and φ′ as shown in Figure 3-9. Each specimen was weighed after compaction to verify the unit

weight and a representative portion of the soil specimen were taken out of the prepared mixture for verification of moisture content. As will be presented in Chapter 4, the actual specimen dry unit weight values and water contents varied slightly from the target values of Table 3-2.

3.6.2.3 Direct shear test procedure

The shear box was initially assembled with no gap between the upper and lower boxes with the use of two screws. A saturated porous stone was placed on the bottom box and a filter paper was placed at the porous stone soil interface. After the soil specimen was prepared per the procedure described in Section 3.4.2, the specimen was extracted out of the confining ring utilizing an extractor available in the laboratory. The specimen was then placed carefully in the shear box on top of the filter paper and porous stone previously placed at the bottom of the shear box. Another filter paper and porous stone were placed on the top of the specimen.

The top cap of the shear box was then placed over the top porous stone followed by placement of the load frame device. The shear force loading system and the shear displacement measurement system was appropriately adjusted so that there was no force and displacement imposed on the specimen. Then, the lever for providing the normal force was leveled, and the sensor for measuring the vertical displacement was adjusted. Initially, a small seating load of 5 kPa was applied on the specimen ensuring no significant vertical displacement or compression. The purpose of this load was to ensure all the components are in contact and alignment. The initial vertical displacement reading was recorded. Then, the required normal load was applied on the specimen externally through the cantilever dead weight system.

After the application of the required normal load, the vertical deflection was monitored until the compression rate was below 0.0001 in/min per the ASTM D 3080 procedure to allow dissipation of excess pore water pressure. This typically occurred 10 to 15 minutes after load

application. After the compression rate was below 0.0001 in/min, the screws that kept the two boxes connected were removed, and a gap was created between the upper and lower box using gap screws.

The shearing rate was adjusted to 0.004 in/min as previously described in Section 3.6.2.1. The shear force, shear displacement, and vertical displacement were checked to ensure that all were set to zero and then the test was started. The test was continued until the maximum shear displacement of the shear box reached 0.7 inches. A single test took about 3 hours to finish.

To check the water contents of the prepared specimens against the targeted water contents, a representative portion of soil was taken from the prepared soil mixture placed in the plastic bags during specimen preparation and placed in the oven for at least 24 hours at 115 °C. Also, after the direct shear test was completed, the shear box was disassembled, and a representative portion of soil was taken from the failure surface of the specimen to ensure the uniformity of the moisture content. A slight difference was measured between the water content measured during specimen preparation and the water content measured after the direct shear testing. The difference in moisture content is due to the moisture loss during the testing period. The water content measured during the specimen preparation was utilized to calculate the achieved degree of saturation. Since this research is based on the degree of saturation instead of water content, the achieved water content values were utilized to calculate achieved degree of saturation and will be shown in Chapter 4. The complete direct shear test results (shear stress versus normal stress, vertical displacement versus shear displacement, and shear stress versus shear displacement) for each test series of the test matrix are provided in Appendix B.

As shown in Table 3-2, direct shear tests on fully saturated specimens were also performed following the same procedure described above. The specimens for fully saturated tests were

initially prepared with a moisture content of 20.5% and the appropriate compaction stress. The specimen was extracted from the confining ring and then placed in the shear box with the filter paper and porous stones on the top and bottom of the specimen. Then, the device with the specimen was placed in a tray full of distilled water. The specimen was saturated within the shear box because the extraction of the specimen in its original circular shape and soil structure is not possible after saturation. The degree of saturation of the specimens was periodically measured. A specimen was initially saturated for four days but the degree of saturation during the 3rd day and the 4th day showed no difference. Thus, the saturation of other specimens was performed for three days, ensuring the maximum saturation that the loess can attain. The average saturation of all the saturated specimens was found to be 94.5%. The reason that the maximum saturation was less than 100% may be the inherent differences in soil fabric that results from the soil specimen preparation procedure. The shear box was then taken out of the tray, and direct shear testing was performed as per the test procedure explained above.

3.7 Soil water characteristics curves (SWCCs) determination

3.7.1 Introduction

SWCCs were obtained per the procedure explained in the GCTS Testing Systems SWC-150 manual (GCTS 2007). SWCCs provide the matric suction with varying degrees of saturation as described in Section 2.4 of this thesis. Various factors might have an influence on the SWCC such as sample dry unit weight, molding compaction stress and applied vertical stress during testing. Olson and Langfelder (1965) conducted extensive research into the influence of specimen molding moisture content, molding dry density and method of compaction on the SWCC. They incorporated five different soil types with different static compaction pressures ranging from 290 to 876 kPa. They found that variations in the static compaction stress does not

influence the SWCC. Thus, they concluded that for a given soil, matric suction is almost independent of dry unit weight and primarily a function of moisture content. Vanapalli et al. (1996) also confirmed that there is no influence of initial dry unit weight on the SWCC. Stinson (2014) prepared SWCCs for Memphis loess with specimens compacted statically with the application of different pressures. He also found that dry unit weight did not impact the SWCC. The SWCCs prepared by Stinson can be seen in Figure 3-10. Therefore, since specimen preparation stress and dry unit weight does not influence the SWCC, SWCCs were only determined at a single compaction stress and dry unit weight.

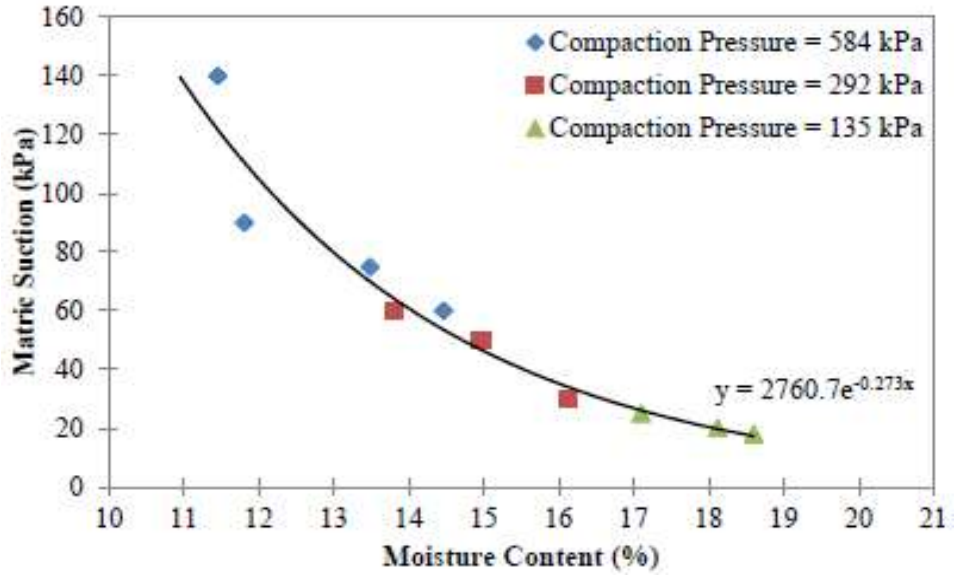

Figure 3-10: SWCC of Eagle Lake loess, Memphis, TN (Stinson 2014)

The literature search also revealed that the application of vertical stress during testing does influence the SWCC. The higher the vertical stress, the lower is the moisture content and the greater the matric suction (Elkady and Al-Mahbashi 2012; Li et al. 2007; Oh and Lu 2014; Ng and Pang 2000). Thus, five SWCCs were prepared at vertical stresses of 110 kPa, 143.8 kPa, 229.2 kPa, 561.7 kPa, and 600 kPa. These stresses were utilized because the direct shear tests were also performed using the same normal stress values as shown in Table 3-2.

3.7.2 Fredlund device

The SWC-150 Fredlund device manufactured by GCTS was used in the determination of the SWCCs. The GCTS Fredlund device can apply vertical stress, measure volume change during the test, and generate an SWCC using a single specimen. A schematic diagram of the device can be seen in Figure 3-11, and a picture of the actual device is shown in Figure 3-12.

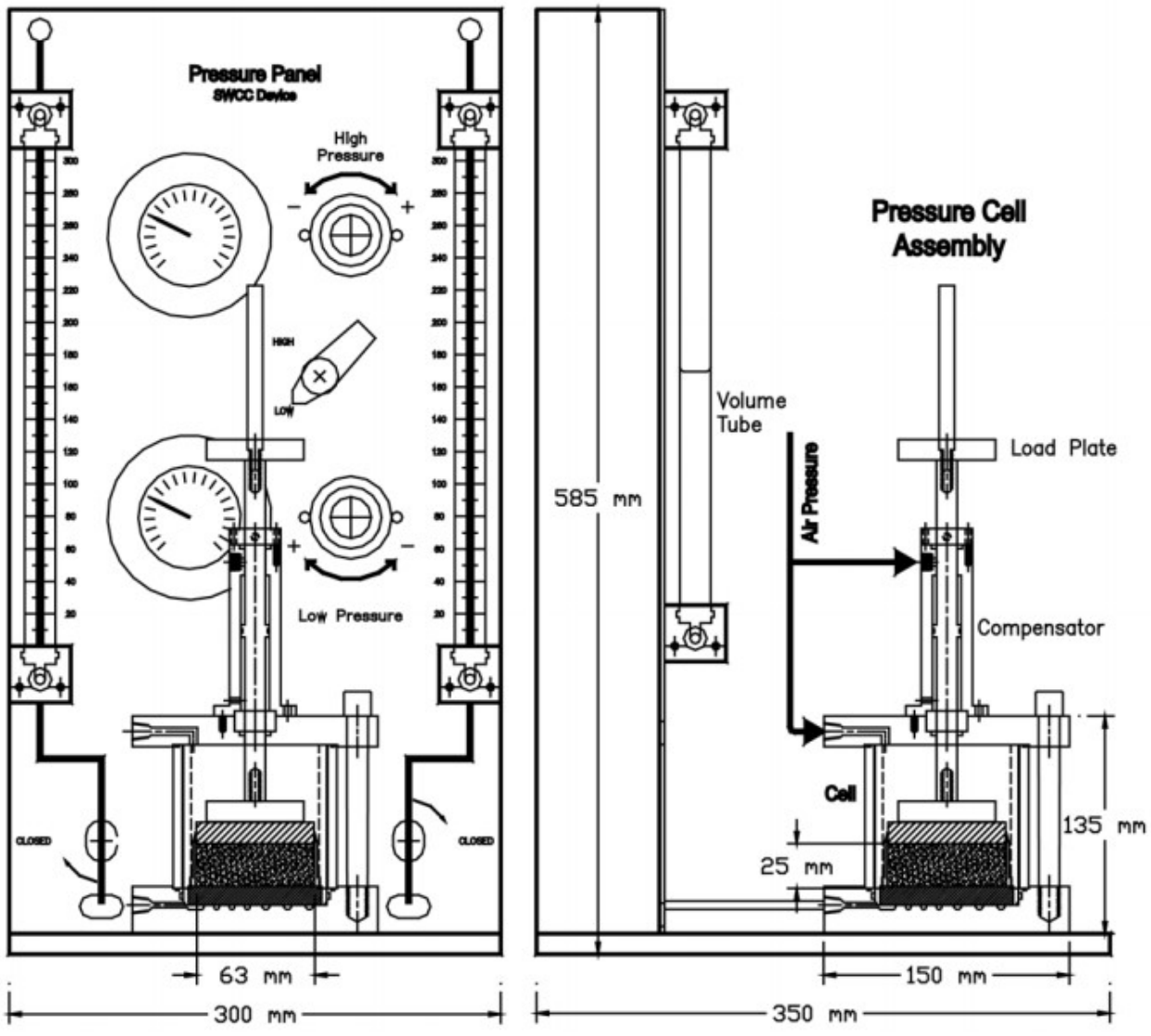

Figure 3-11: Schematic diagram of Fredlund device (Perez-Garcia et al. 2007)

The Fredlund device utilizes an axis translation technique like other pressure plate-type devices that generates negative pore-water pressures by elevating pore-air pressure. The device has a high air entry ceramic disk that is epoxied in a ring. The disk is fitted in a recess on the base plate of the apparatus. The base plate has a grooved water compartment that allows saturation of the ceramic disk during the test. Also, the diffused air is flushed out through the compartment. The compartment is connected to two external ports that facilitate the drainage to the two graduated volume tubes with 1 mm marks, which translates to 0.07 cc in volume measurements thus providing accuracy in volume measurements. The device has two pressure regulators: one low-pressure regulator with a range from 0 to 200 kPa and another high-pressure regulator with a range from 0 to 2000 kPa. A loading rod serves to apply overburden or normal stress on the soil specimen. A loading frame with a pneumatic cylinder is available to apply external loads to the loading rod. The cell of the device contains a pressure compensator that nulls the uplift loads generated during the application of air pressure inside the cell. The soil specimen is kept inside the cell that is laterally constrained into a stainless-steel ring. The device is capable of testing soil samples with diameters from 50 mm to 75 mm and height of 25 mm. The loading rod and top platen of the device move up and down as the soil specimen expands and contracts.

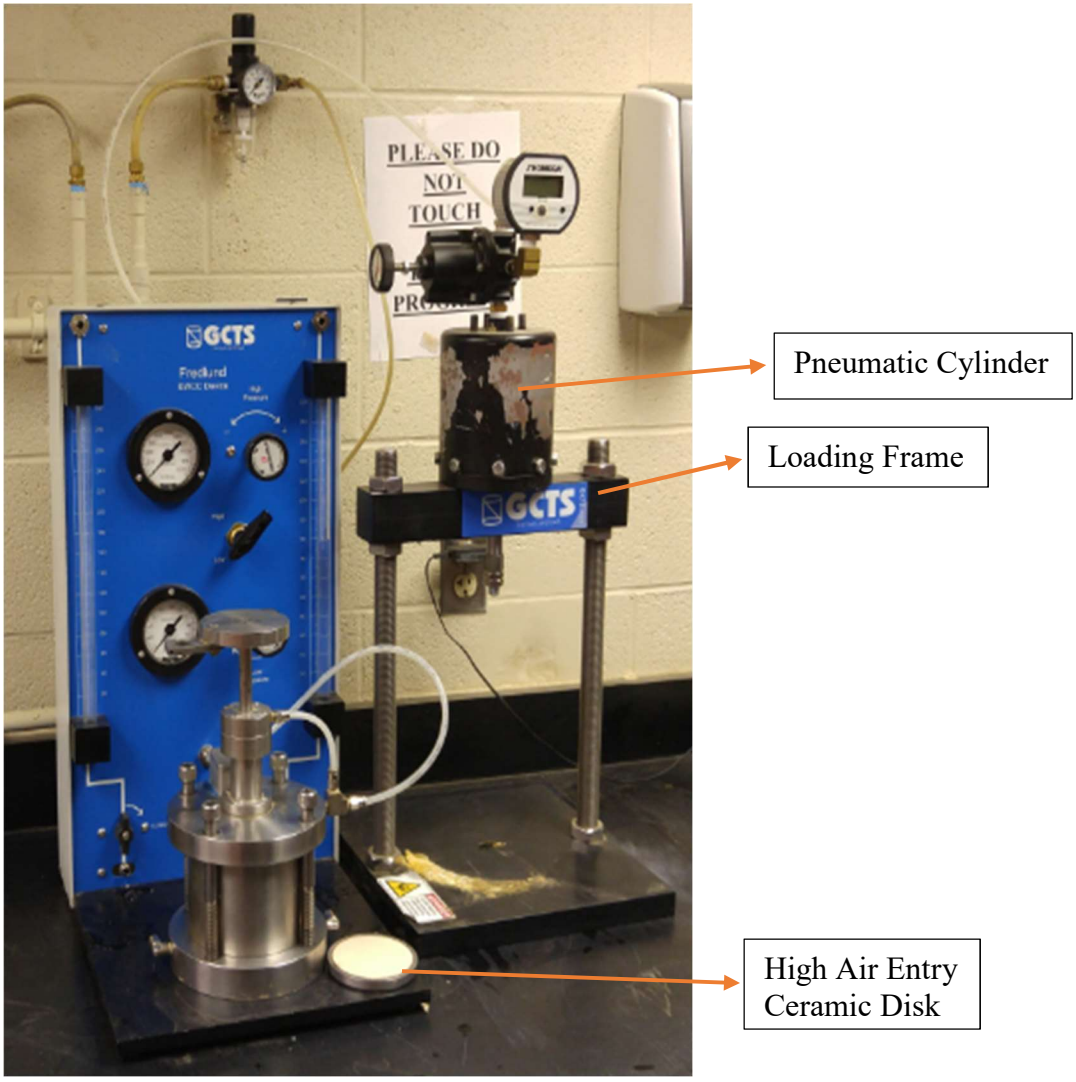

Figure 3-12: Fredlund device manufactured by GCTS

3.7.3 Specimen preparation

The specimen preparation procedure explained in Section 3.4.2 of this thesis was used to prepare soil specimens for determining the SWCCs. The specimen was prepared using a single compaction stress of 561.7 kPa since there was no significant influence of dry unit weight or compaction energy as explained in Section 3.7.1. A targeted moisture content of 21% was chosen for the preparation of each specimen. This moisture content was adopted to be consistent with the specimens prepared for the consolidation test and the direct shear strength tests. From

Figure 3-5, for a moisture content of 21% and compaction stress of 561.7 kPa, a dry unit weight of 15.03 kN/m^3 was determined. The target dry unit weight and moisture content were utilized to calculate the dry and moist soil masses for use in preparing the soil specimen. After the soil specimen was prepared, it was weighed to verify the unit weight. The specimen was then further saturated following the same procedure as for consolidation test specimens as explained in Section 3.6.2.1. The average final degree of saturation for all the specimens was around 93.5% with dry unit weight of 15.03 kN/m^3. After saturation, the specimen, along with the confining ring, was taken out of the saturation tray and then placed in the Fredlund device.

3.7.3.1 SWCC test procedure

The procedure explained in the GCTS Testing Systems SWC-150 manual (GCTS 2007) was followed to determine the SWCCs. Initially, a high air entry ceramic disk was chosen and saturated overnight, and the saturated mass was recorded. Then, a dry glass plate was selected, and its weight was recorded. The saturated specimen (average final degree of saturation of 93.5% and average dry unit weight of 15.03 kN/m^3) within the confining ring was placed on the glass plate so that excess water could drain from the specimen. Then, any water that accumulated on the glass plate and outside of the ring was dried. The soil specimen along with the glass plate were weighed.

The soil specimen was then transferred to the saturated ceramic disk, and the weight of the saturated specimen with the saturated ceramic disk was recorded. The base plate of the Fredlund device was cleaned to ensure no foreign particles were present. The two external ports were connected to the corresponding graduated volume tubes. Then, distilled water was added to the grooved water compartments in the base plate. Also, the outside of the ceramic stone was moistened. Then the ceramic stone with the specimen was pressed carefully into the recess in the

base plate. The load plate was centered on the specimen. After that, the top plate, compression ring, compensator body, compensator cap and the load shaft were assembled quickly. The top plate and bottom plate were secured by tightening the four socket-head cap screws.

The left volume tube was filled with distilled water through the opening located on the top left-hand corner of the panel until a level of water was seen in the volume tubes. Water also flowed to the right volume tube through the grooved water component on the base plate. Air was flushed through the volume tube to expel any entrapped air in the base. An LVDT was placed on the top plate to measure the volume change of the specimen. The initial reading of the LVDT was set to zero. After the water in the volume tubes was leveled, the initial volume tube readings were recorded with date and time. The target pressures to be applied to the soil specimen were determined, and the first selected pressure was added by using the low-pressure regulator. The required normal stress was supplied by the pneumatic cylinder attached to the loading frame of the GCTS Fredlund device as shown in Figure 3-12. The first pressure was maintained for at least 30 hours until the water levels in the volume tubes did not change significantly. Before applying the next pressure increment, the volume tube readings were taken, and the change in the height of the specimen was recorded until the water levels did not change significantly, approx. 30 hours. The final pressure adopted in this test was 800 kPa due to the constraint in the air pressure supply line in the laboratory. After the final increment of the pressure was applied, the volume tube readings were recorded along with the change in height from the LVDT. Then, the pressure was reduced to zero slowly, and the apparatus was disassembled. The soil specimen was extracted from the confining ring and placed in the oven for at least 24 hours to determine the final moisture content of the specimen. For each normal stress utilized to prepare SWCCs, identical soil specimens were prepared, and similar procedure as described were followed.

3.8 Summary

This chapter provided a summary of the methodologies that were employed to obtain soil samples, perform laboratory physical property tests, prepare test specimens from the field soil samples, perform direct shear tests, and determine soil-water characteristic curves. The test matrix shown in Table 3-2 includes the targeted degrees of saturation and dry unit weight values of the test specimens as well as the normal stresses for performing direct shear tests. The next chapter provides a summary of the test results.

4 Summary of test results

4.1 Introduction

The primary goal of this research is to study the influence of the degree of saturation and dry unit weight on the shear strength of unsaturated Fulton loess. This chapter provides a summary of direct shear strength test results and soil-water characteristics curves obtained on Fulton loess specimens. Observations of the influence of degree of saturation, OCR, and dry unit weight on shear behavior, the influence of degree of saturation and dry unit weight on shear strength parameters, and the influence of normal stress on the SWCCs are also presented.

4.2 Direct shear strength test results

The direct shear strength tests were performed on the Fulton loess in accordance with the ASTM D 3080 procedure explained in Section 3.6.3.3. This test was selected because it is commonly used in practice to determine the drained shear strength parameters of soil because it is an easier and quicker method compared to triaxial tests.

As shown in the test matrix of Table 3-2, specimens with targeted degrees of saturation of 40%, 50%, 60%, and 65% were initially planned for each compaction stress. However, the specimen preparation procedure that was described in Section 3.6.1.2 produced specimens with actual degrees of saturation that were slightly different than the targeted values as shown in Table 4-1. Table 4-1 shows the targeted and achieved degrees of saturation as well as the achieved dry unit weight values obtained for each specimen. The differences between the targeted and achieved degrees of saturation were within +5.5% to -6.3% for targeted degrees of saturation less than and equal to 65%; the difference was -5.7% for the 100% target. The reason for not achieving 100% saturation might be the inherent differences in soil fabrics that result

from the soil specimen preparation procedure. The difference between the targeted and achieved dry unit weight values was ±0.04 kN/m^3.

Table 4-1: Targeted and measured degree of saturation and dry unit weight for all specimens

143.8 kPa compaction stress			229.3 kPa compaction stress			561.7 kPa compaction stress		
Targeted saturation level (%)	Achieved saturation level (%)	Dry unit weight (kN/m^3)	Targeted saturation level (%)	Achieved saturation level (%)	Dry unit weight (kN/m^3)	Targeted saturation level (%)	Achieved saturation level (%)	Dry unit weight (kN/m^3)
40	39.9	12.6	40	39.6	12.9	40	40.1	14
50	51.2	12.9	50	50.4	13.5	50	51.7	14.3
60	56.7	13.3	60	56.2	13.7	60	57.1	14.6
65	66.2	13.5	65	66.5	14	65	66.8	15.1
100	94.3	13.3	100	94.4	13.9	100	94.5	15

The direct shear strength test results and observations made on the drained shear strength parameters are presented next.

4.2.1 Drained shear strength parameters

This section summarizes the influence of the degree of saturation and dry unit weight on the drained shear strength parameters of Fulton loess. Plots of drained cohesion versus degree of saturation, drained cohesion versus dry unit weight, drained friction angle versus degree of saturation, and drained friction angle versus dry unit weight are presented.

In a direct shear test, the cross-sectional contact area of the specimen on the shearing plane decreases as the horizontal displacement between the upper and lower portions of the specimen occurs during the application of horizontal force. The decrease in contact area influences both the horizontal shear stress and the normal stress that is applied to the specimen. In this research, the cross-sectional area was corrected using the area correction factor proposed by Olson (2004).

The original area (A_o) for the circular specimen with diameter D is given by Equation 4-1.

$$A_o = \frac{\pi}{4} D^2 \tag{4-1}$$

For a circular specimen, horizontal displacement leads to a contact area between the upper and lower portions of the specimen indicated by the hatched area as shown in Figure 4-1. For a horizontal displacement of Δh indicated in Figure 4-1, the area correction factor F and the corrected area A is given by Equations 4-2 and 4-3, respectively.

$$F = \frac{2}{\pi}\left\{\cos^{-1}\left(\frac{\Delta h}{D}\right) - \left(\frac{\Delta h}{D}\right)\sqrt{1-\left(\frac{\Delta h}{D}\right)^3}\right\} \tag{4-2}$$

$$A = A_o F \tag{4-3}$$

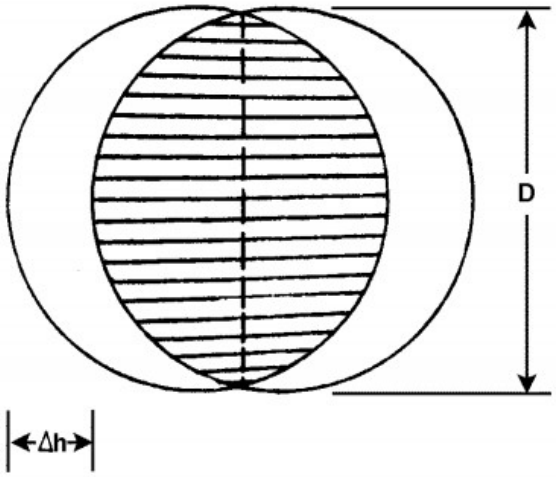

Figure 4-1: Contact area of the circular soil specimen (Olson 2004)

Both horizontal shear stress and normal stress were corrected for the decrease in area with an increase in shearing using the correction factor shown in Equation 4-2. The plots of corrected shear stress versus horizontal displacement and vertical displacement versus horizontal displacement for each compaction stress and each test series shown in Table 3-2 are presented in Appendix B. The figure captions provide the degree of saturation and compaction stress used to prepare the specimens.

To estimate the drained shear strength parameters, as explained in Section 3.6.2.2, the plots included in Appendix B were utilized. As an example, a plot showing the procedure to determine the corrected peak shear stress is shown in Figure 4-2.

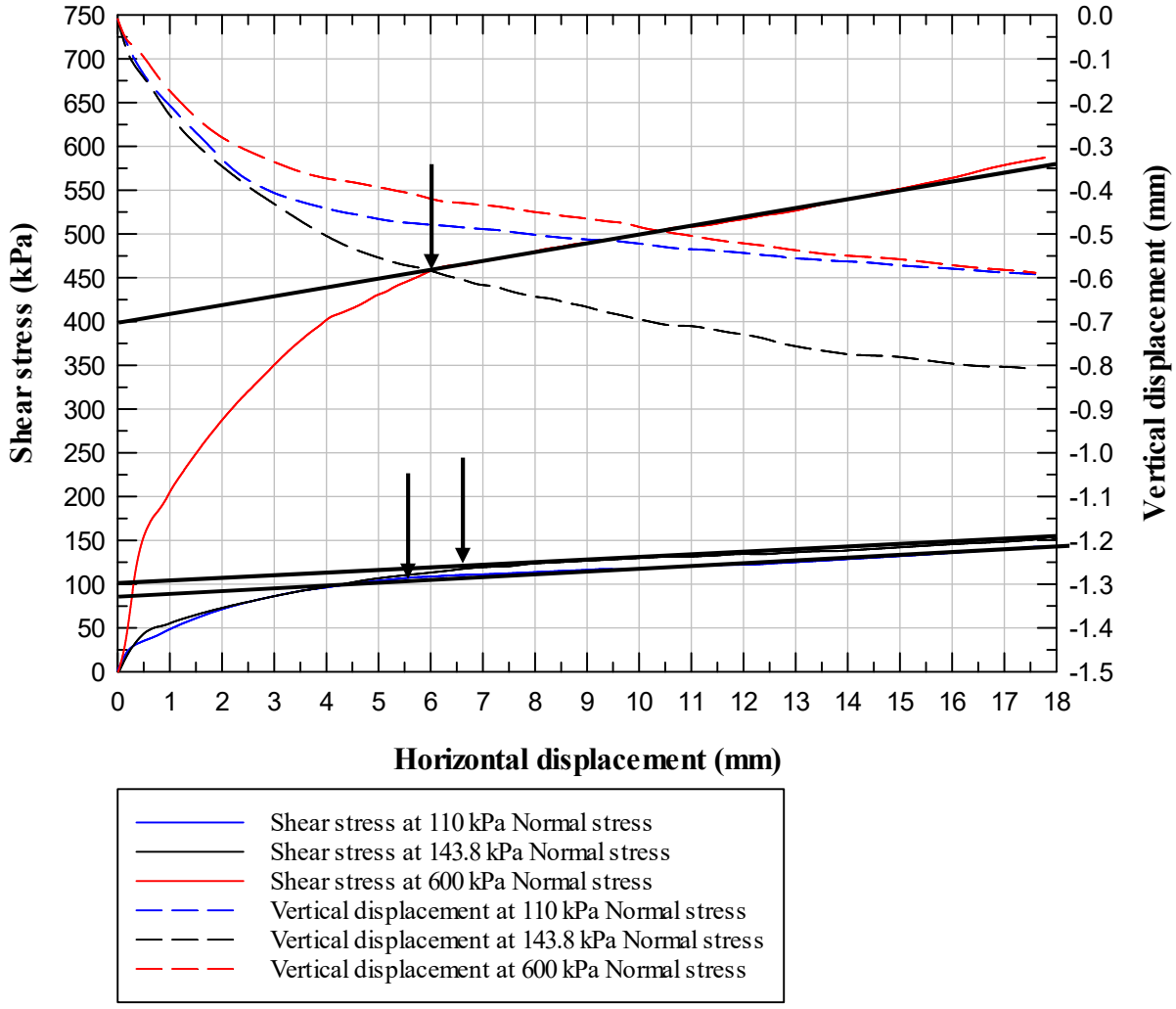

Figure 4-2: Example plot for determination of peak shear stress

A straight line was drawn through the final portion of each curve for every plot, which tends to be linear as shown in Figure 4-2. The horizontal displacement for the point with the lowest deformation that is tangent to the shear stress versus horizontal displacement curve was determined, as shown by the vertical arrow for each curve, and this point was used to determine

the peak shear stress. The corrected peak shear stress values were plotted against the corrected normal stress values to estimate the drained shear strength parameters.

Figures 4-3 through 4-5 include the points of corrected peak shear stress for each corresponding corrected normal stress value obtained from the corrected shear stress versus horizontal displacement curves shown in Figures B-1 through B-15 in Appendix B using the procedure described above. The figure captions provide the compaction stress utilized to prepare the specimens. The legends in each figure provide the saturation level of the specimens during preparation.

After the series of corrected peak shear stress and corrected normal stress points were plotted, a best-fit line was drawn through each series of points to obtain the drained shear strength parameters, i.e., c' and ϕ'. The use of a best-fit line assumes that the peak shear stress varies linearly with normal stress, which is a common assumption that is made to determine drained shear strength parameters from direct shear test results. The best-fit line was plotted using the R-squared (linear) approach option included in the SigmaPlot12 software. The R-squared values exceeded 95%, indicating that the shear and normal stress data points are very close to the fitted regression line. In each figure, five best-fit lines are plotted, with each line representing the different saturation levels of the series of test specimens as shown in the legends. For example, the black line represents the best-fit line for the specimens with the lowest degree of saturation of 39.9%, and the pink line represents the best-fit line for the specimens with the highest degree of saturation of 94.3%.

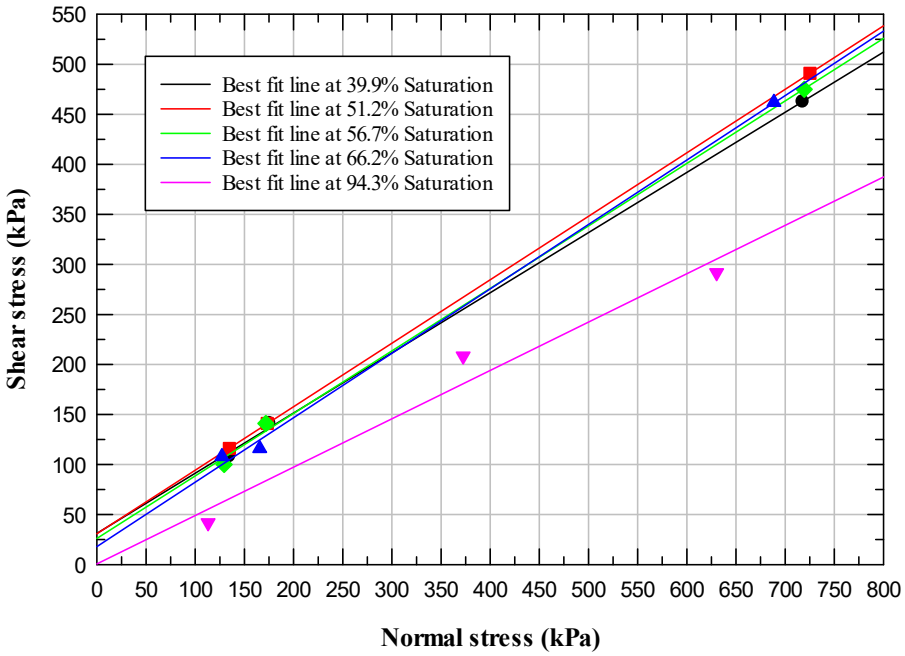

Figure 4-3: Shear stress versus normal stress plot for specimens prepared with compaction stress of 143.8 kPa

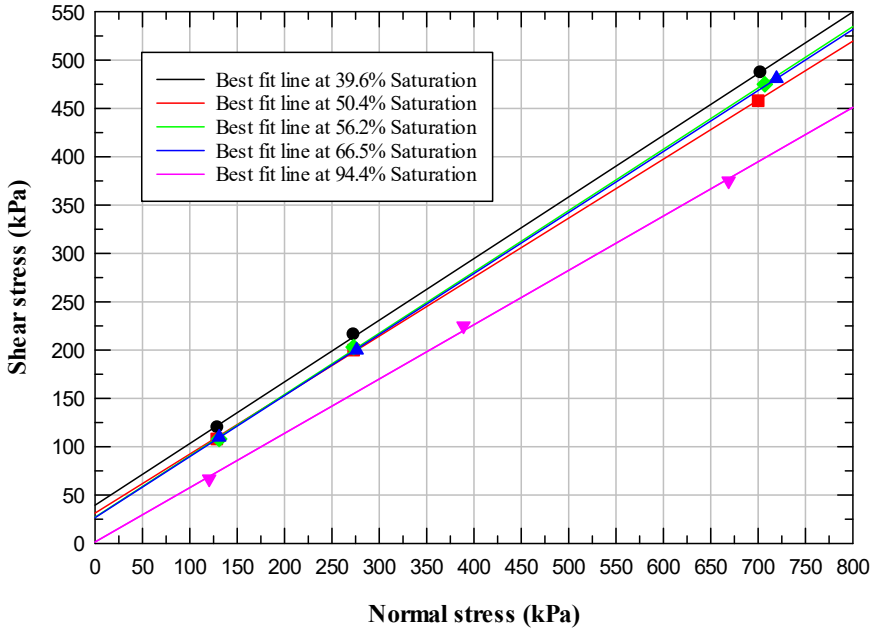

Figure 4-4: Shear stress versus normal stress plot for specimens prepared with compaction stress of 229.2 kPa

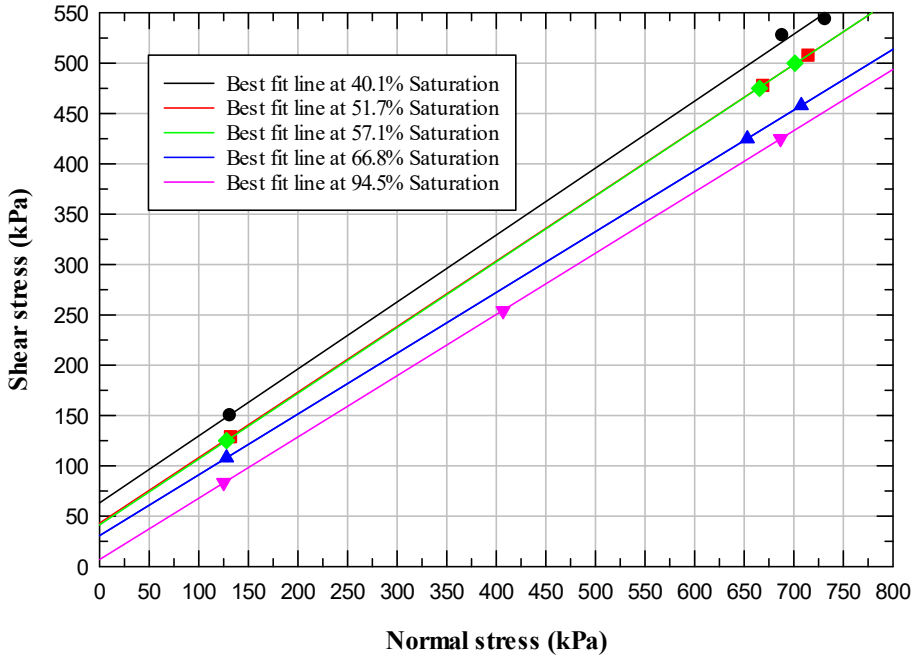

Figure 4-5: Shear stress versus normal stress plot for specimens prepared with compaction stress of 561.7 kPa

After the best-fit lines were drawn, the drained shear strength parameters were estimated using the procedure described in Section 3.6.2.2. The y-intercept (shear stress) of the best-fit lines at zero normal stress represents the drained cohesion (c′) and the slope of the best-fit line to the x-axis provides the drained internal friction angle (φ′). Table 4-2 presents a summary of the drained shear strength parameters obtained for each compaction stress and degree of saturation. Table 4-2 also provides the specimen dry unit weights (γ_d) for each compaction stress.

Table 4-2: Summary of the drained shear strength parameters

143.8 kPa compaction stress				229.2 kPa compaction stress				561.7 kPa compaction stress			
%S	γ_d (kN/m^3)	c′ (kPa)	φ′ (°)	%S	γ_d (kN/m^3)	c′ (kPa)	φ′ (°)	%S	γ_d (kN/m^3)	c′ (kPa)	φ′ (°)
39.9	12.6	31.2	31	39.6	12.9	39.5	32.5	40.1	14	63.2	33.6
51.2	12.9	30.8	32.4	50.4	13.5	31.3	31.4	51.7	14.3	43.2	33.1
56.7	13.3	26.2	32	56.2	13.7	27	32.4	57.1	14.6	41.4	33.2
66.2	13.5	18.1	32.8	66.5	14	26.6	32.3	66.8	15.1	30.8	31.1
94.3	13.3	0.7	25.8	94.4	13.9	1.5	29.3	94.5	15	7	31.3

The following subsections present the influence of the degree of saturation and dry unit weight on drained shear strength parameters.

4.2.1.1 Influence of degree of saturation on drained cohesion

This section summarizes the influence of the degree of saturation on the drained cohesion of the Fulton loess specimens. The values of drained cohesion provided in Table 4-2 are plotted with their respective degrees of saturation for each compaction stress in Figure 4-6.

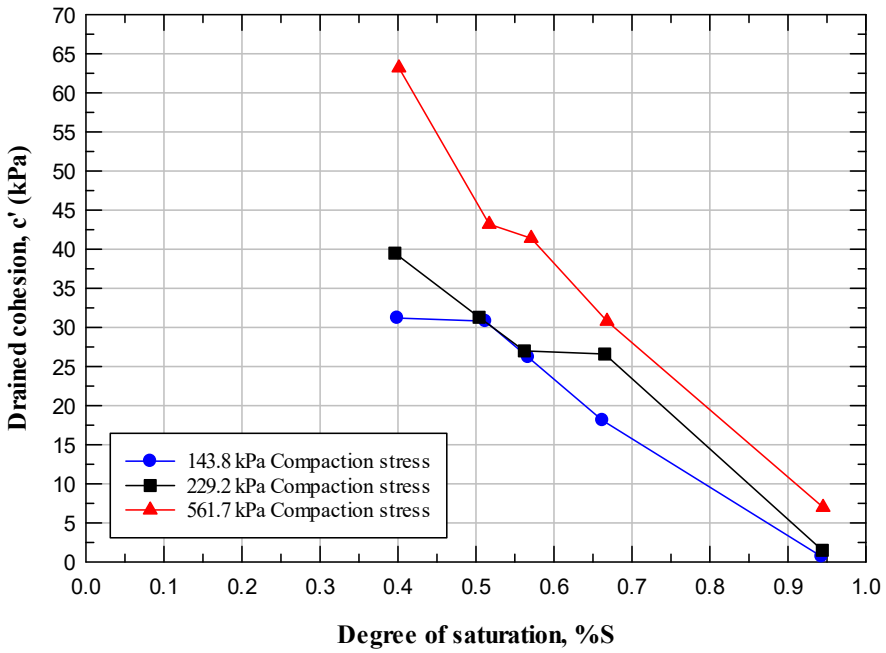

Figure 4-6: Influence of degree of saturation on drained cohesion

Figure 4-6 shows that the drained cohesion decreases with an increase in the degree of saturation for all compaction stress levels used to prepare the specimens. This trend in cohesion is in agreement with the results of Wen and Yan (2014) and Zhong et al. (2015). Additionally, the results of Figure 4-6 indicate that cohesion may trend to zero at 100% saturation for specimens prepared at compaction stresses of 143.8 and 229.2 kPa but a slight cohesion may remain for the specimens prepared at 561.7 kPa. The slight cohesion for the specimens prepared

at 561.7 kPa is similar to the behavior of saturated over-consolidated clay, which tends to exhibit a drained cohesion. The specimens prepared at the highest compaction stress of 561.7 kPa could be behaving similarly to an over-consolidated clay especially when tested at the low normal stress of 110 kPa. On the other hand, Akiyama (1964) indicates that the drained cohesion that is obtained in loess at high moisture contents is unreliable and can be considered to be zero.

4.2.1.2 Influence of dry unit weight on drained cohesion

This section summarizes the influence of dry unit weight on the cohesion intercept of the Fulton loess specimens. The values of drained cohesion and their respective dry unit weight values indicated in Table 4-2 are plotted in Figure 4-7 by the degree of saturation. As shown in Table 4-2, the dry unit weight values of the specimens will vary with the compaction stress used to prepare the specimens. Therefore, the three points on each line represent the different compaction stresses used to prepare the specimens. The leftmost point represents the specimens prepared using a compaction stress of 143.8 kPa, the middle point represents the specimens prepared using a compaction stress of 229.2 kPa, and the rightmost point represents the specimens prepared using a compaction stress of 561.7 kPa.

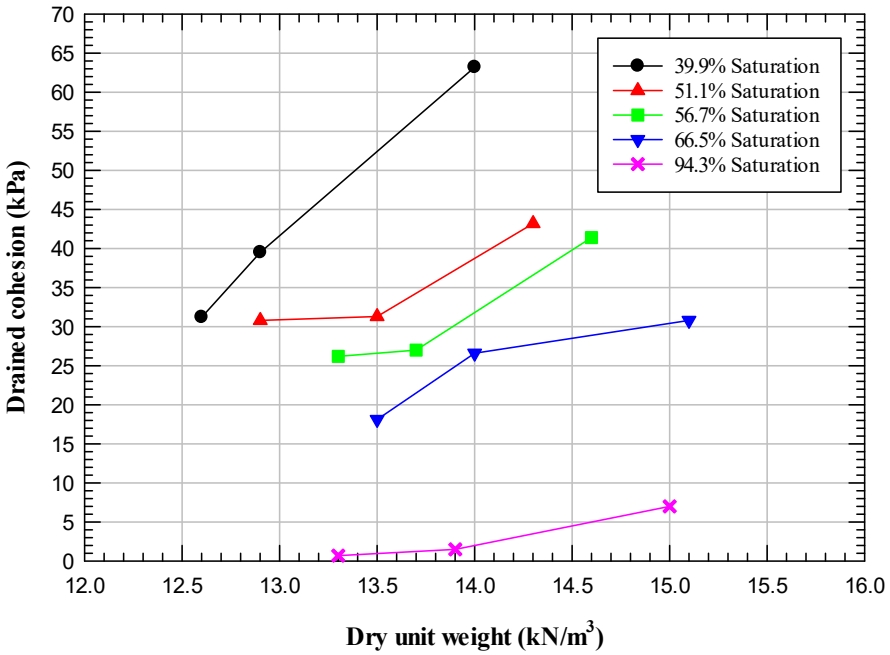

Figure 4-7: Influence of dry unit weight on drained cohesion

Figure 4-7 shows that the drained cohesion increases with an increase in dry unit weight or an increase in compaction stress. This observation is in agreement with the results of Wen and Yan (2014). It can also be seen in Figure 4-7 that the drained cohesion values are higher for the specimens with lower degrees of saturation. For a given dry unit weight, the drained cohesion value is highest for the specimens with a lower degree of saturation, which is the same observation made in Figure 4-6.

4.2.1.3 Influence of degree of saturation on drained friction angle

This section summarizes the influence of the degree of saturation on the drained internal friction angle of the Fulton loess specimens. The values of drained internal friction angle with their respective degrees of saturation are plotted for each compaction stress in Figure 4-8.

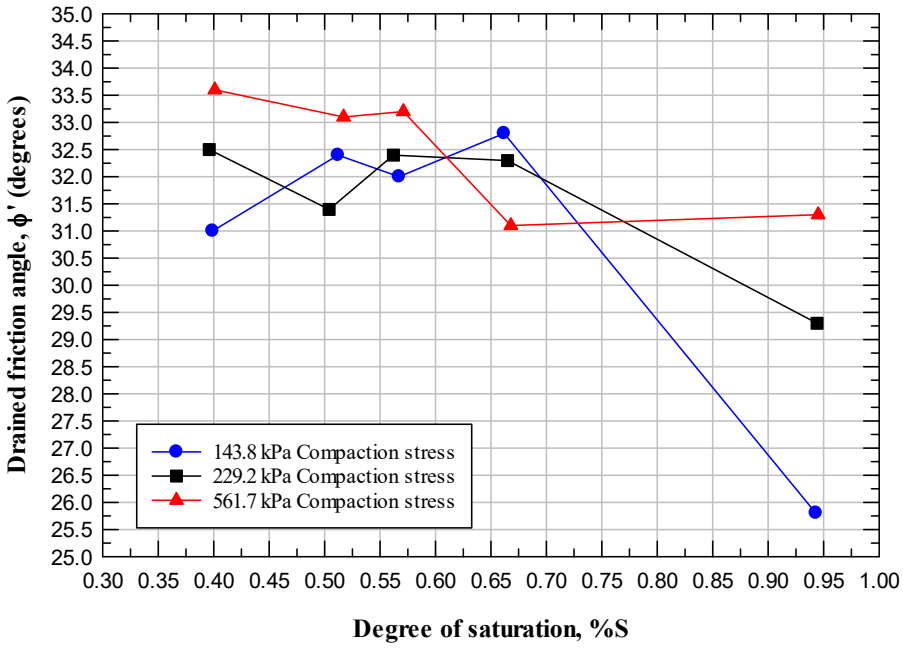

Figure 4-8: Influence of degree of saturation on the drained internal friction angle

Figure 4-8 shows that the there is a small variance in drained friction angle with respect to the increase in degree of saturation except the specimens compacted using compaction stresses of 143.8 kPa and 229.2 kPa and having highest degree of saturation around 94.3%. As observed in Figures 4-3 through 4-5, all the plots have a similar slope except for the two best-fit lines in Figures 4-3 and 4-4 represented by pink lines, which are those for specimens with the highest degrees of saturation and compacted using stresses of 143.8 kPa and 229.2 kPa, respectively. These two lines tend to have a different slope resulting in the comparatively lower friction angle. The reason behind this decrease in drained friction angle is unknown.

4.2.1.4 Influence of dry unit weight on internal friction angle

This section summarizes the influence of dry unit weight on the drained internal friction angle of the Fulton loess specimens. The values of drained internal friction angle with their respective dry unit weight provided in Table 4-2 are plotted in Figure 4-9. Similar to Figure 4-8,

the three points on each line represent the different compaction stresses used to prepare the specimens.

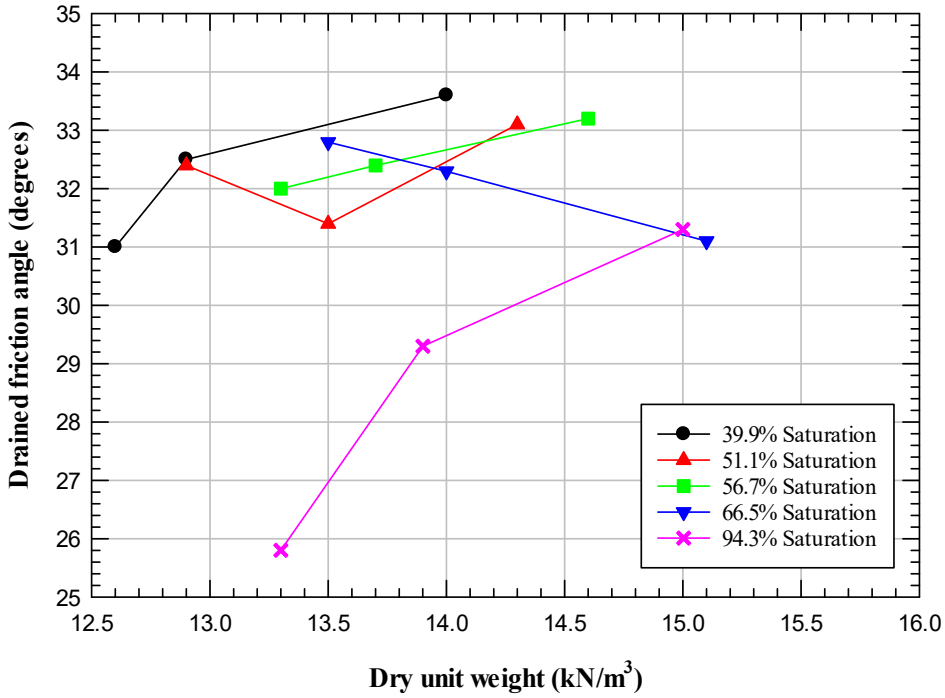

Figure 4-9: Influence of dry unit weight on internal friction angle

Figure 4-9 shows that in general, for a given degree of saturation, the drained friction angle increases with an increase in dry unit weight and this behavior is typical for most soil types. However, the drained friction angle for the 66.5% saturation level shows the opposite result, which may be due to some inherent property differences arising from the specimen preparation.

4.3 Soil-water characteristic curve (SWCC) results

Soil-water characteristic curves (SWCCs) were determined for the Fulton loess in accordance with the procedure in the GCTS Testing Systems SWC-150 manual (GCTS 2007) as explained in Section 3.7.3.1. SWCCs were determined to obtain the matric suction values at various targeted degrees of saturation. The SWCC specimens were prepared using a single

compaction stress of 561.7 kPa and a molding moisture content of 21% and then saturated before the test. The final average degree of saturation of all five specimens tested was about 93.5% with a dry unit weight of 15.03 kN/m^3.

Figures 4-10 through 4-14 illustrates five SWCCs prepared by applying normal stress values of 110 kPa, 143.8 kPa, 229.2 kPa, 561.7 kPa, and 600 kPa, respectively, during the test. The figure caption provides the normal stress value used during each test. As described in Section 3.7.3.1, the SWCCs were obtained using suction values up to 800 kPa due to laboratory constraints on air pressure. However, Figures 4-10 through 4-14 provide a full set of SWCCs having suction values up to 1,000,000 kPa using the Fredlund and Xing (1994) model available in the "SWRC fit" web interface by Seki (2007). Moreover, the soaked test specimens could not attain 100% saturation to start the test. Thus, the SWCCs are corrected for the degree of saturation near 100% following the procedure provided by Perez-Garcia et al. (2007).

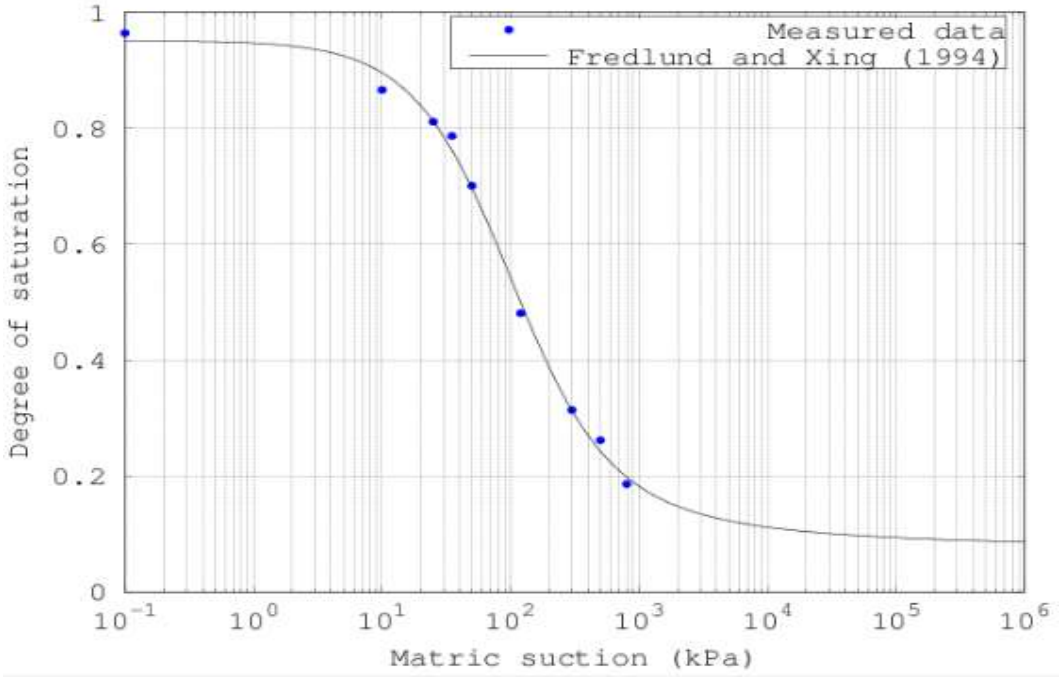

Figure 4-10: SWCC obtained at a normal stress of 110 kPa

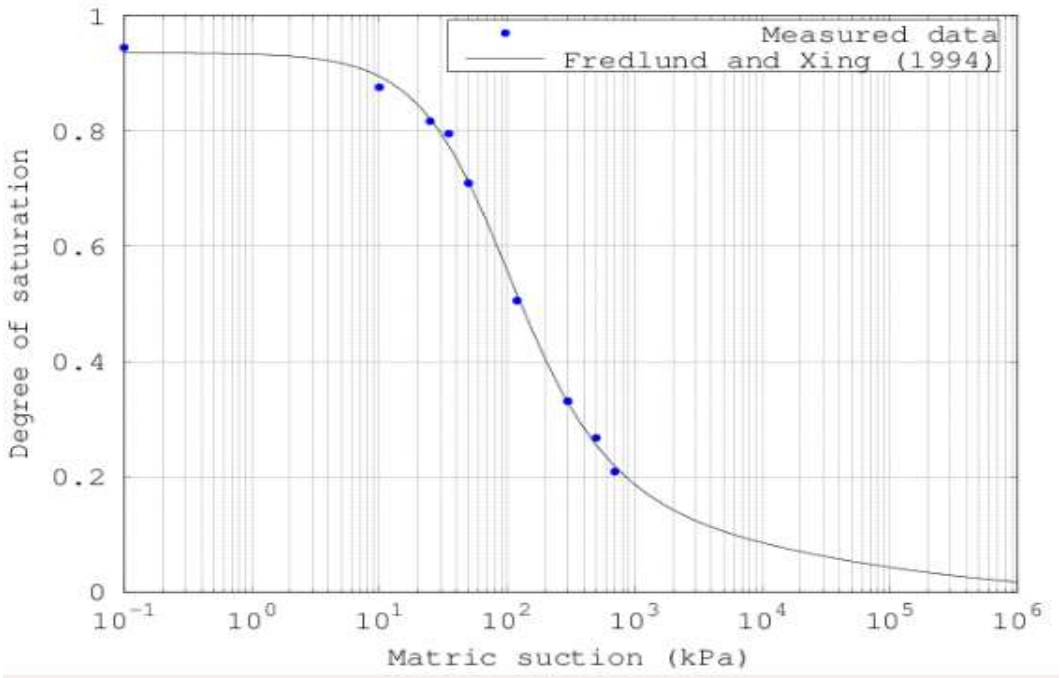

Figure 4-11: SWCC obtained at a normal stress of 143.8 kPa

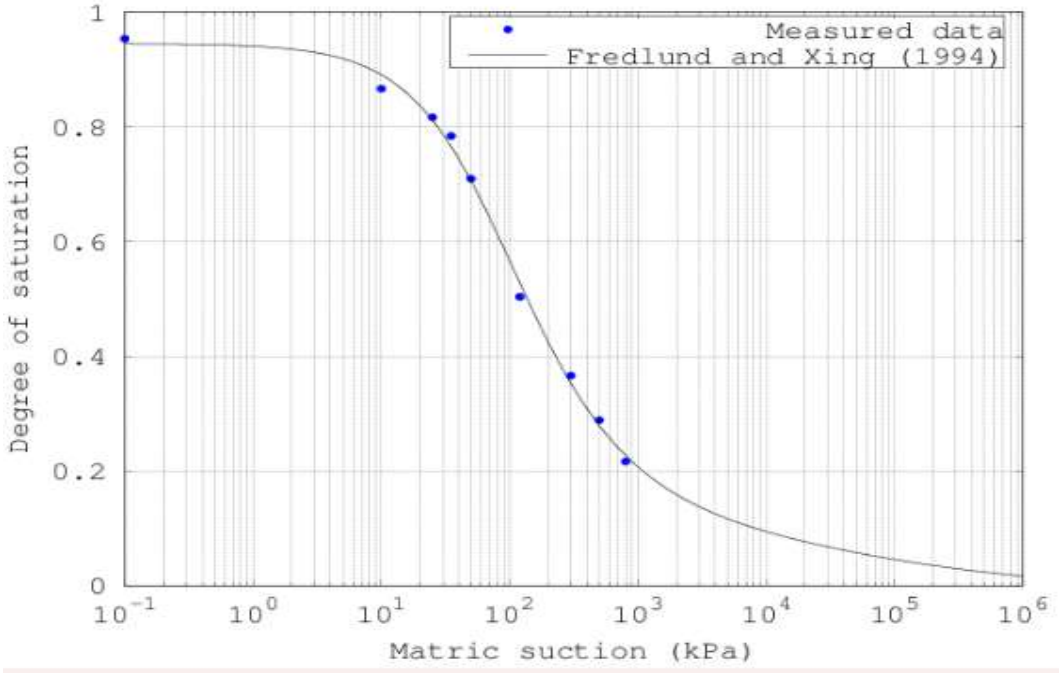

Figure 4-12: SWCC obtained at a normal stress of 229.2 kPa

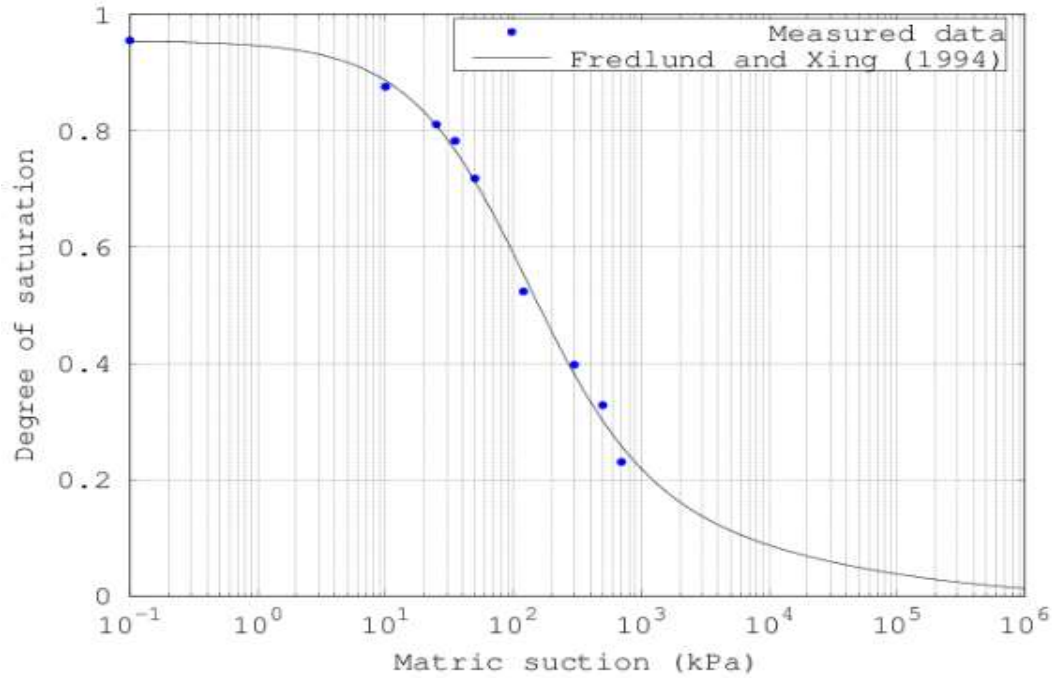

Figure 4-13: SWCC obtained at a normal stress of 561.7 kPa

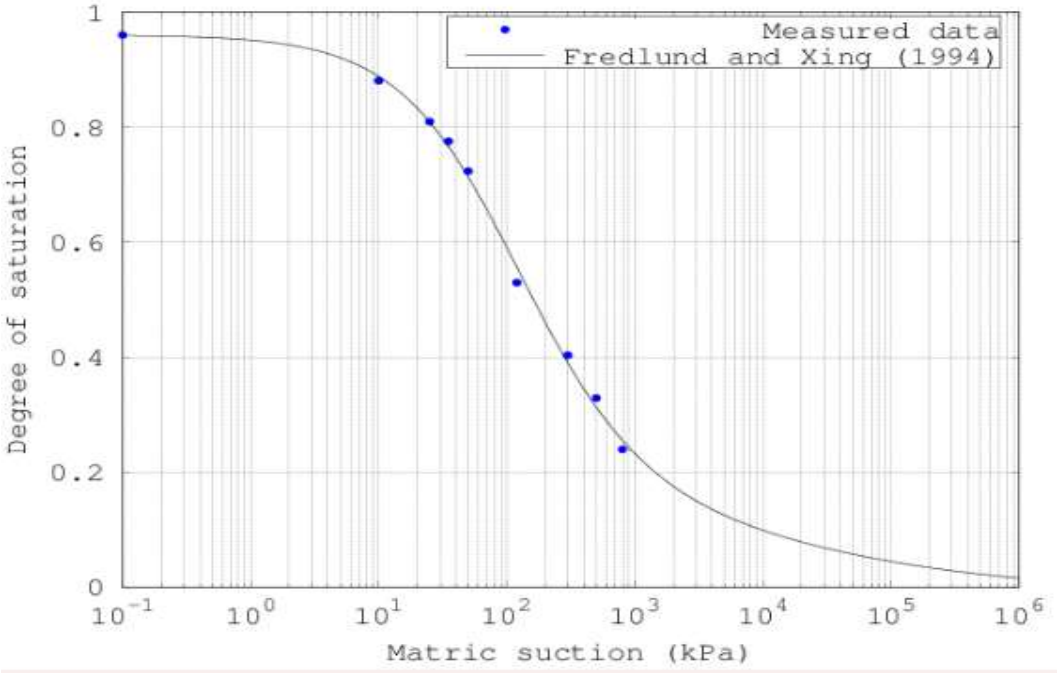

Figure 4-14: SWCC obtained at a normal stress of 600 kPa

Figures 4-10 through 4-14 show that at lower matric suction values of 0.1 kPa to 10 kPa, the change in the degree of saturation is slight. However, at higher matric suction values of 10 kPa through 2000 kPa, the degree of saturation drops quickly. Then, at matric suctions above 2000 kPa, the change in the degree of saturation is lower again. Zhong et. al. (2015) shows a similar trend of matric suction reduction with an increase in the degree of saturation for undisturbed loess. As explained in Section 2.5, the change in the degree of saturation is clearly observed as the matric suction value exceeds the air-entry value, which is defined as the matric suction value that must be exceeded before air recedes into the soil pores. Similarly, as the degree of saturation approaches the residual degree of the saturation value, the change in the degree of saturation is lower although the matric suction is much higher. SWCCs are influenced by the normal stress applied to the specimen during testing as explained in Section 3.7.1. The influence of this normal stress on matric suction values in this research is presented next.

4.3.1 Influence of normal stress on the SWCCs

As explained in Section 3.7.1, for a given degree of saturation, higher vertical stresses applied to the specimen during testing give higher values of matric suction (Elkady and Al-Mahbashi 2012; Li et al. 2007; Oh and Lu 2014; Ng and Pang 2000). Zhong (2015) also presented the effect of confining pressure on matric suction of undisturbed loess. For a given degree of saturation, higher confining stresses provide a higher value of matric suction for undisturbed loess. This effect of normal stress on loess is also clearly seen in the SWCCs prepared using the various normal stress values listed in the previous section. Figure 4-15 shows all of the SWCCs to illustrate the influence of applied normal stress on SWCCs. For example, for a normal stress of 110 kPa and a degree of saturation of 40%, the matric suction value is about

200 kPa, but for the normal stress of 229.2 kPa, the matric suction value is about 250 kPa and increases further as the normal stress increases.

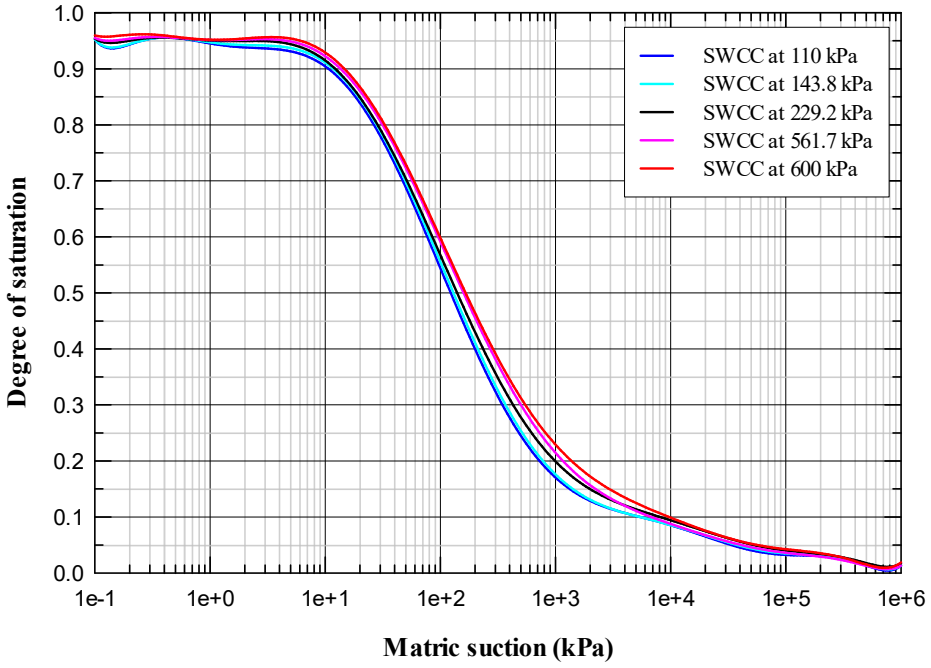

Figure 4-15: SWCCs prepared at various normal stresses

4.4 Summary

This chapter provides a summary of the results of the direct shear strength tests and soil water characteristic curves (SWCCs) obtained on the Fulton loess specimens. Also, a summary on the influence of the degree of saturation and dry unit weight on the drained shear strength parameters is presented along with a summary of the influence of normal stress on the SWCCs.

The drained shear strength parameters are significantly influenced by the change in the degree of saturation. Drained cohesion decreases considerably with an increase in saturation level and may trend to zero at 100% saturation, but a slight cohesion may remain for specimens compacted at the highest compaction stress of 561.7 kPa. The drained friction angle varies slightly with an increase in degree of saturation except for the decrease in drained friction angle for the specimens compacted at the lower stress levels of 143.8 kPa and 229.2 kPa at the higher

degree of saturation of 94.3%. Also, the dry unit weight plays a significant role in cohesion, as the cohesion of denser specimens is higher compared to loose specimens. The drained friction angle also increased with an increase in dry unit weight. The SWCCs show that the matric suction decreases with an increase in the degree of saturation. Normal stresses applied during the preparation of SWCCs also influence the matric suction. At a given degree of saturation, the matric suction is higher for the SWCCs prepared using higher normal stress values.

5 Analysis and discussion of unsaturated shear strength of Fulton loess

5.1 Introduction

This chapter provides the analysis and discussion of the shear strength of unsaturated Fulton loess. The fully saturated shear strength parameters and the matric suction values are estimated first. The angle indicating the rate of change in shear strength due to matric suction is estimated using various models discussed in Chapter 2 and then compared for Fulton loess. The shear strength of the unsaturated Fulton loess is estimated using the results from the direct shear tests and SWCCs and the influence of degree of saturation and the dry unit weight are discussed .

5.2 Estimate of fully saturated shear strength parameters

Fredlund et al. (1987) provided Equation 2-5 for calculating the shear strength of unsaturated soil based on the drained shear strength parameters (c' and φ'), matric suction (u_a-u_w), and the angle indicating the rate of change of shear strength with respect to matric suction (φ^b). For an unsaturated soil, the first part of the shear strength relationship of Equation 2-5 (i.e., $c' + \sigma' \tan \varphi'$) is provided by the drained shear strength parameters of a saturated soil (i.e., c' and φ') and the second part of the equation (i.e., $(u_a-u_w) \tan \varphi^b$) is provided by the matric suction and the angle φ^b.

An attempt was made to fully saturate the soil specimens for direct shear testing per the procedure explained in Section 3.6.2.3 to obtain the drained shear strength parameters of the Fulton loess at 100% saturation. However, it was only possible to achieve a degree of saturation of about 94%. Therefore, the drained shear strength parameters at 100% were indirectly estimated.

To estimate the drained shear strength parameters of the Fulton loess, direct shear tests on the unsaturated specimens were performed per the procedure explained in Section 3.6.2.3. The

direct shear test provides drained shear strength parameters through the relationship between normal stress and shear stress as discussed in Section 3.6.2.2. The plots of drained cohesion and drained friction angle with respect to degree of saturation were plotted as seen in Figures 4-6 and 4-8, respectively. Figure 4-6 shows that the drained cohesion decreases rapidly with an increase in the degree of saturation and tends to zero at 100% saturation for the lower two compaction stresses. The behavior at a compaction stress of 561.7 kPa is similar to the behavior of saturated over-consolidated clay, which tends to possess a low but non-zero drained cohesion at 100% saturation. However, Akiyama (1964) suggests that the low cohesion at 100% saturation for loess is unreliable and can be considered to be zero. Thus, the drained cohesion value for the saturated loess specimens in this research is assumed to be zero. The drained friction angle values at around 94.3% saturation are utilized to represent the drained friction angles for saturated specimens despite the fact that the drained friction angle values for the nearly saturated specimens compacted using compaction stress of 143.8 kPa and 229.2 kPa don't follow the same trend exhibited by the less-saturated specimens as discussed in Section 4.2.1.

Table 5-1 provides the estimated fully saturated shear strength parameters incorporated in this study.

Table 5-1: Fully saturated shear strength parameters

Compaction stress (kPa)	Drained cohesion (kPa)	Drained friction angle (°)
143.8	0	25.8
229.2	0	29.3
561.7	0	31.3

5.3 Estimate of matric suction values based on SWCCs

The SWCCs were prepared as explained in Section 3.7.3.1 and presented in Section 4.3. The matric suction values were estimated using the SWCCs in Figures 4-10 through 4-14 for the measured degree of saturation for each compaction stress shown in Table 4-1. Tables 5-2

through 5-6 show the values of matric suction estimated from each SWCC prepared at various normal stresses. The table caption provides the value of normal stress that was used to obtain the SWCCs.

Table 5-2: Matric suction values from SWCC obtained at 110 kPa Normal stress

143.8 kPa compaction stress		229.2 kPa compaction stress		561.7 kPa compaction stress	
Degrees of saturation (%)	Matric suction (kPa)	Degrees of saturation (%)	Matric suction (kPa)	Degrees of saturation (%)	Matric suction (kPa)
39.9	198	39.6	200	40.1	198
51.2	106	50.4	103	51.7	101
56.7	90	56.2	92	57.1	90
66.2	60	66.5	58	66.8	58
94.3	0.8	94.4	0.8	94.5	0.8

Table 5-3: Matric suction values from SWCC obtained at 143.8 kPa Normal stress

143.8 kPa compaction stress		229.2 kPa compaction stress		561.7 kPa compaction stress	
Degrees of saturation (%)	Matric suction (kPa)	Degrees of saturation (%)	Matric suction (kPa)	Degrees of saturation (%)	Matric suction (kPa)
39.9	202	39.6	204	40.1	200
51.2	110	50.4	112	51.7	107
56.7	98	56.2	99	57.1	95
66.2	65	66.5	63	66.8	60
94.3	0.8	94.4	0.8	94.5	0.8

Table 5-4: Matric suction values from SWCC obtained at 229.2 kPa Normal stress

143.8 kPa compaction stress		229.2 kPa compaction stress		561.7 kPa compaction stress	
Degrees of saturation (%)	Matric suction (kPa)	Degrees of saturation (%)	Matric suction (kPa)	Degrees of saturation (%)	Matric suction (kPa)
39.9	210	39.6	212	40.1	208
51.2	112	50.4	118	51.7	110
56.7	100	56.2	102	57.1	98
66.2	67	66.5	65	66.8	63
94.3	0.9	94.4	0.9	94.5	0.9

Table 5-5: Matric suction values from SWCC obtained at 561.7 kPa Normal stress

143.8 kPa compaction stress		229.2 kPa compaction stress		561.7 kPa compaction stress	
Degrees of saturation (%)	Matric suction (kPa)	Degrees of saturation (%)	Matric suction (kPa)	Degrees of saturation (%)	Matric suction (kPa)
39.9	280	39.6	285	40.1	278
51.2	138	50.4	150	51.7	145
56.7	104	56.2	105	57.1	101
66.2	69	66.5	68	66.8	66
94.3	1.3	94.4	1.3	94.5	1.3

Table 5-6: Matric suction values from SWCC obtained at 600 kPa Normal stress

143.8 kPa compaction stress		229.2 kPa compaction stress		561.7 kPa compaction stress	
Degrees of saturation (%)	Matric suction (kPa)	Degrees of saturation (%)	Matric suction (kPa)	Degrees of saturation (%)	Matric suction (kPa)
39.9	292	39.6	298	40.1	285
51.2	151	50.4	160	51.7	148
56.7	106	56.2	107	57.1	102
66.2	70	66.5	68	66.8	67
94.3	1.7	94.4	1.7	94.5	1.7

5.4 Shear strength of unsaturated Fulton loess

To estimate the shear strength of an unsaturated soil, Equation 2-5 was utilized, which is also shown in Equation 5-1.

$$\tau_{ff} = c' + (\sigma_f - u_a)_f \tan\phi' + (u_a - u_w)_f \tan\phi^b \quad (5\text{-}1)$$

Saturated shear strength — Shear strength due to matric suction

where τ_{ff} is the shear strength of the unsaturated soil at failure, c′ is the drained cohesion intercept, $(\sigma_f\text{-}u_a)_f$ is the net normal stress, φ′ is the drained friction angle, $(u_a\text{-}u_w)_f$ is the matric suction, and φ^b is the angle indicating the rate of change of shear strength with respect to matric suction.

The initial portion of Equation 5-1 is the shear strength provided by the drained shear strength parameters and these parameters are listed in Table 5-1 for the loess tested in this research. The second portion of the shear strength is provided by the matric suction and the angle φ^b. Matric suction values for the loess are provided in Tables 5-2 through 5-6. In this research, the empirical estimation equations shown in Equations 2-8, 2-10, and 2-11 are utilized to estimate the angle φ^b. These estimation equations were provided for general unsaturated soils by the respective researchers. However, the validity of these equations is still unknown for the Fulton loess, and an attempt will be made to compare the results of these models with test results. After estimating the angle φ^b from each estimation equation, a predicted apparent cohesion will be calculated using Equation 5-2.

$$c = (u_a - u_w)_f tan\phi^b \tag{5-2}$$

where c is the predicted apparent cohesion, $(u_a\text{-}u_w)_f$ is the matric suction and φ^b is the angle indicating rate of change of shear strength with respect to matric suction. Note that Equation 5-2 was obtained from Equation 2-3 with $c'=0$.

In this study, apparent cohesion for an unsaturated soil will be defined as the cohesion provided by matric suction, which is shown in Equation 5-2, because it is assumed that cohesion provided by cementation from precipitates and clay binding is minimal compared to the contribution of matric suction. The predicted apparent cohesion will be compared with the measured apparent cohesion values shown in Table 4-2. Although this research is not performed for validating a specific model for estimation of angle φ^b for loess, a comparison of the models is made herein.

One estimation equation that can be used to explain the nonlinear relationship between the degree of saturation and apparent cohesion shown in Equation 2-8 is again shown in Equation 5-3 (Fredlund et al. 1996).

$$\tan \phi^b = \left(\frac{\theta}{\theta_s} \right)^{\kappa} \tan \phi' \tag{5-3}$$

where θ is the volumetric water content of the soil, θ_s is the volumetric water content at saturation, and κ is a fitting parameter related to the plasticity index (PI) of soil as given by Equation 5-4 provided by Garven and Vanapalli (2006):

$$\kappa = -0.0016 (PI)^2 + 0.0975 (PI) + 1 \tag{5-4}$$

Another estimation equation to explain the non-linear behavior of shear strength is given by Equation 2-10 as also shown in Equation 5-5 (Vanapalli et al. 1996).

$$\tan \phi^b = \left(\frac{\theta - \theta_r}{\theta_s - \theta_r} \right) \tan \phi' \tag{5-5}$$

where θ_r is the volumetric water content at residual suction.

Similarly, Equation 2-11, as also shown in Equation 5-6 (Khalili and Khabbaz 1998) , gives another estimation equation based on air entry value:

$$\tan \phi^b = \left[\frac{u_a - u_w}{(u_a - u_w)_b} \right]^{-0.55} \tan \phi' \tag{5-6}$$

where $(u_a\text{-}u_w)_b$ is the air entry value of the soil.

For the estimation of φ^b, the measured degree of saturation values shown in Table 4-1 were converted to volumetric water content values by using Equation 5-7 below.

$$\theta = S * n \tag{5-7}$$

where θ is the volumetric water content, S is the degree of saturation, and n is the porosity. Table 5-7 provides the results.

Table 5-7: Measured degree of saturation and respective volumetric water content

143.8 kPa compaction stress			229.2 kPa compaction stress			561.7 kPa compaction stress		
S (%)	n	θ	S (%)	n	θ	S (%)	n	θ
39.9	0.55	0.22	39.6	0.53	0.21	40.1	0.50	0.20
51.2	0.54	0.28	50.4	0.52	0.26	51.7	0.49	0.25
56.7	0.52	0.30	56.2	0.51	0.28	57.1	0.47	0.27
66.2	0.51	0.34	66.5	0.50	0.33	66.8	0.47	0.32
94.3	0.52	0.49	94.4	0.49	0.47	94.5	0.46	0.43

The volumetric water content at saturation (θ_s) and residual volumetric water content (θ_r) are provided by the "SWRC fit" web interface used to plot the full set of SWCCs as explained in Section 4.3. The fitting parameter κ was estimated to be 1.1 for the Fulton loess with a PI of 1 using Equation 5-4. Matric suction and air entry values are determined from the SWCCs shown in Figures 4-10 through 4-14 using the procedure described in Section 2.5. Table 5-8 provides the various parameters required to estimate ϕ^b using the various models described above. These parameters were determined using the "SWRC fit" web interface.

Table 5-8: Parameters required to estimate ϕ^b

Normal stress (kPa)	Air entry values (kPa)	Volumetric water content at saturation (θ_s)	Residual volumetric water content (θ_r)
110	40.7	0.494	0.023361
143.8	40.3	0.496	0.024194
229.2	36.7	0.491	1.91E-06
561.7	43.4	0.496	2.16E-06
600	39.7	0.499	2.95E-06

5.4.1 Estimation of angle φ^b using different models

Utilizing Equation 5-3 as provided by Fredlund et. al. (1996), calculated φ^b values are presented in Tables 5-9 through 5-11 for the different compaction stresses.

Table 5-9: φ^b values for 143.8 kPa compaction stress specimens

143.8 kPa Compaction Stress					
Volumetric water content	0.22	0.28	0.30	0.34	0.49
Normal Stress (kPa)	φ^b (°)				
110	11.2	14.4	15.5	17.6	25.6
143.8	11.1	14.3	15.4	17.6	25.5
229.2	11.2	14.5	15.6	17.7	25.7
561.7	11.1	14.3	15.4	17.6	25.5
600	11.1	14.2	15.3	17.5	25.3

Table 5-10: φ^b values for 229.2 kPa compaction stress specimens

229.2 kPa Compaction Stress					
Volumetric water content	0.21	0.26	0.28	0.33	0.47
Normal Stress (kPa)	φ^b (°)				
110	13.1	16.5	18.0	20.9	29.1
143.8	13.0	16.4	17.9	20.8	29.0
229.2	13.2	16.6	18.1	21.0	29.3
561.7	13.0	16.4	17.9	20.8	29.0
600	13.0	16.3	17.8	20.7	28.9

Table 5-11: φ^b values for 561.7 kPa compaction stress specimens

561.7 kPa Compaction Stress					
Volumetric water content	0.20	0.25	0.27	0.32	0.43
Normal Stress (kPa)	φ^b (°)				
110	14.6	18.6	19.9	23.4	31.1
143.8	14.6	18.5	19.8	23.3	31.0
229.2	14.7	18.7	20.0	23.6	31.3
561.7	14.6	18.5	19.8	23.3	31.0
600	14.5	18.4	19.7	23.2	30.9

Similarly, utilizing Equation 5-5 provided by Vanapalli et. al. (1996), calculated φ^b values are presented in Tables 5-12 through 5-14 for the different compaction stresses.

Table 5-12: φ^b values for 143.8 kPa compaction stress specimens

143.8 kPa Compaction Stress					
Volumetric water content	0.22	0.28	0.30	0.34	0.49
Normal Stress (kPa)	φ^b (°)				
110	11.3	14.6	15.7	17.9	25.6
143.8	11.3	14.5	15.6	17.8	25.5
229.2	12.1	15.2	16.3	18.4	25.7
561.7	12.0	15.1	16.2	18.2	25.5
600	11.9	15.0	16.1	18.1	25.4

Table 5-13: φ^b values for 229.2 kPa compaction stress specimens

229.2 kPa Compaction Stress					
Volumetric water content	0.21	0.26	0.28	0.33	0.47
Normal Stress (kPa)	φ^b (°)				
110	13.2	16.7	18.2	21.1	29.1
143.8	13.1	16.6	18.1	21.0	29.0
229.2	14.2	17.5	18.9	21.7	29.3
561.7	14.1	17.3	18.7	21.5	29.1
600	14.0	17.2	18.6	21.4	28.9

Table 5-14: φ^b values for 561.7 kPa compaction stress specimens

561.7 kPa Compaction Stress					
Volumetric water content	0.20	0.25	0.27	0.32	0.43
Normal Stress (kPa)	φ^b (°)				
110	14.7	18.8	20.1	23.6	31.1
143.8	14.6	18.7	20.0	23.5	31.0
229.2	15.8	19.6	20.9	24.2	31.3
561.7	15.6	19.5	20.7	24.0	31.0
600	15.6	19.3	20.6	23.8	30.9

Similarly, utilizing Equation 5-6 provided by Khalili & Khabbaz (1998), calculated φ^b values are presented in Tables 5-15 through 5-17 for the different compaction stresses.

Table 5-15: φ^b values for 143.8 kPa compaction stress specimens

143.8 kPa Compaction Stress					
Volumetric water content	0.22	0.28	0.30	0.34	0.49
Normal Stress (kPa)	φ^b (°)				
110	11.4	15.9	17.3	21.3	25.8
143.8	11.3	15.5	16.5	20.4	25.8
229.2	10.5	14.7	15.6	19.2	25.8
561.7	9.8	14.4	16.6	20.5	25.8
600	9.2	13.1	15.7	19.5	25.8

Table 5-16: φ^b values for 229.2 kPa compaction stress specimens

229.2 kPa Compaction Stress					
Volumetric water content	0.21	0.26	0.28	0.33	0.47
Normal Stress (kPa)	φ^b (°)				
110	13.2	18.4	19.7	24.8	29.3
143.8	12.9	17.7	18.9	23.7	29.3
229.2	12.1	16.5	17.7	22.3	29.3
561.7	11.3	15.8	19.0	23.7	29.3
600	10.5	14.6	18.0	22.7	29.3

Table 5-17: φ^b values for 561.7 kPa compaction stress specimens

561.7 kPa Compaction Stress					
Volumetric water content	0.20	0.25	0.27	0.32	0.43
Normal Stress (kPa)	φ^b (°)				
110	14.3	20.1	21.4	26.6	31.3
143.8	14.0	19.6	20.8	26.0	31.3
229.2	13.2	18.4	19.5	24.3	31.3
561.7	12.3	17.4	20.9	25.8	31.3
600	11.6	16.4	19.9	24.5	31.3

As observed in Tables 5-9 through 5-17, angle φ^b is influenced by the compaction stress. For example, in Tables 5-9 and 5-10, for a volumetric water content of 0.28 and normal stress of 110 kPa, the angle φ^b has a value of 14.4º for a compaction stress of 143.8 kPa and 18.0º for a

compaction stress of 229.2 kPa although the air-entry value, normal stress, volumetric water content at saturation, and residual volumetric water content are the same. This variance in angle φ^b is mainly due to the variance in drained friction angle (φ') values for different compaction stresses as seen in Table 5-1.

The next section presents a comparison of the Fulton loess results with the models used to estimate the angle indicating the rate of change of shear strength due to matric suction (φ^b).

5.4.2 Comparison of different models for estimating φ^b

The angles φ^b calculated using the various estimation equations in Section 5.4 are utilized to calculate a predicted apparent cohesion using Equation 5-2. The matric suction values for respective degrees of saturation are estimated from the SWCCs, and the values in Tables 5-9 through 5-17 are utilized for the angle φ^b. The predicted apparent cohesion values obtained from Equation 5-2 are then compared with the measured apparent cohesion (i.e., c') values from Table 4-2 to determine which models fit the best.

5.4.2.1 Comparison of apparent cohesion for 143.8 kPa compaction stress

Table 5-18 presents the measured and predicted apparent cohesion values for a compaction stress of 143.8 kPa. The table indicates the model predicted value(s) that is nearest to the measured value in bold font. For the reader to visually assess each model, a plot of predicted cohesion as a function of measured cohesion is provided in Figure 5-1. The plot also provides a line of measured cohesion equal to predicted cohesion to better assess the model fits.

Table 5-18: Comparison of apparent cohesion for 143.8 kPa compaction stress

Degree of saturation (%S)	Measured apparent cohesion (c, kPa)	Predicted apparent cohesion (Fredlund, 1996) (c, kPa)	Predicted apparent cohesion (Vanapalli, 1996) (c, kPa)	Predicted apparent cohesion (Khalili & Khabbaz, 1998) (c, kPa)
39.9	31.2	**39.7**	40.2	40.2
51.2	30.8	28.0	28.4	**30.6**
56.7	26.2	**27.1**	27.4	29.0
66.2	18.1	**20.6**	20.8	24.1
94.3	2.9	**0.4**	**0.4**	**0.4**

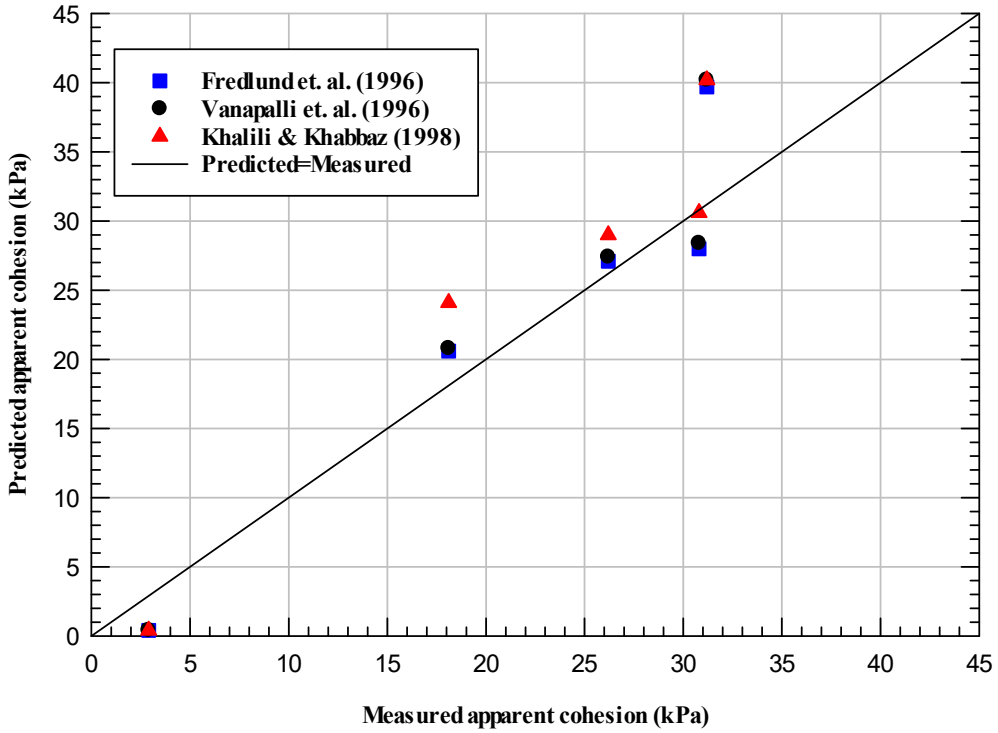

Figure 5-1: Predicted cohesion versus measured cohesion for compaction stress of 143.8 kPa

As observed in Table 5-18 and Figure 5-1, for a compaction stress of 143.8 kPa, overall, the predicted apparent cohesion values estimated using the equation provided by Fredlund et. al. (1996) are in better agreement with the measured apparent cohesion values. All three equations yield the same predicted cohesion value at 94.4% saturation.

5.4.2.2 Comparison of apparent cohesion for 229.2 kPa compaction stress

Table 5-19 presents the measured and predicted apparent cohesion values for a compaction stress of 229.2 kPa. The table indicates the model predicted value(s) that is nearest to the measured value in bold font. A plot of predicted cohesion as a function of measured cohesion is provided in Figure 5-2.

Table 5-19: Comparison of apparent cohesion for 229.2 kPa compaction stress

Degree of saturation (%S)	Measured apparent cohesion (c, kPa)	Predicted apparent cohesion (Fredlund, 1996) (c, kPa)	Predicted apparent cohesion (Vanapalli, 1996) (c, kPa)	Predicted apparent cohesion (Khalili & Khabbaz, 1998) (c, kPa)
39.6	39.5	49.7	53.6	**45.4**
50.4	31.3	35.1	37.1	**34.9**
56.2	27	33.4	35.0	**32.6**
66.5	26.6	25.0	25.8	**26.6**
94.4	2.2	**0.5**	**0.5**	**0.5**

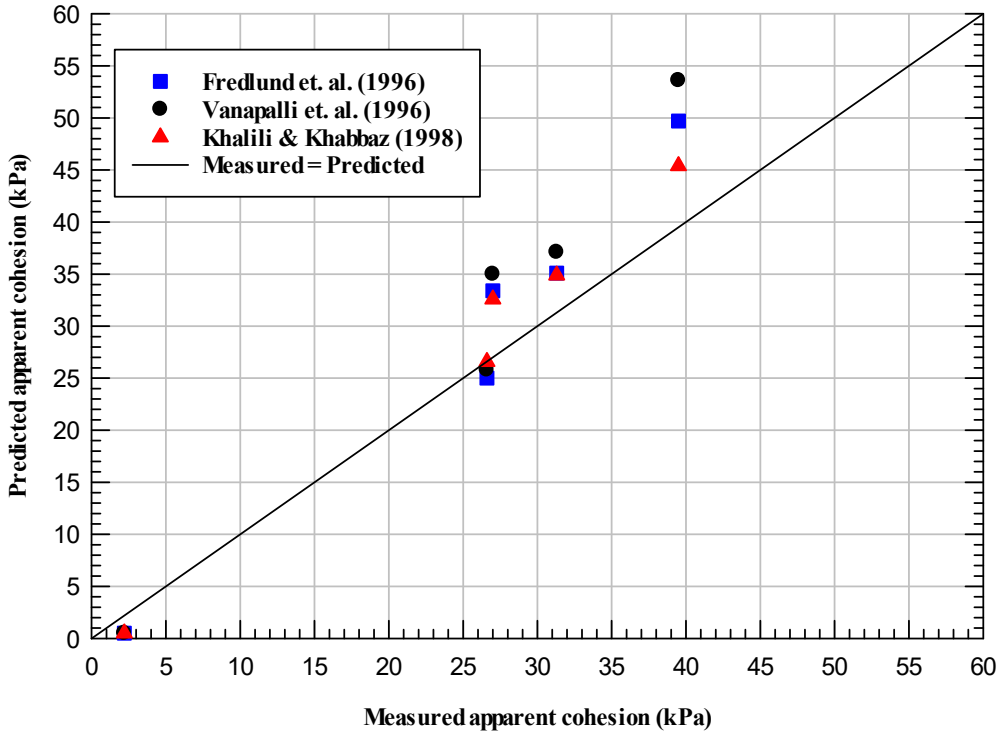

Figure 5-2: Predicted cohesion versus measured cohesion for compaction stress of 229.2 kPa

As observed in Table 5-19 and Figure 5-2, for a compaction stress of 229.2 kPa, overall, the predicted apparent cohesion values estimated using the equation provided by Khalili & Khabbaz (1998) are in better agreement with the measured apparent cohesion values than those predicted using the equations provided by Fredlund et. al. (1996) and Vanapalli et. al. (1996). All three equations yield the same predicted cohesion value at 94.4% saturation.

5.4.2.3 Comparison of apparent cohesion for 561.7 kPa compaction stress

Table 5-20 presents the measured and predicted apparent cohesion values for a compaction stress of 561.7 kPa. The table indicates the model predicted value(s) that is nearest to the measured value in bold font. A plot of predicted cohesion as a function of measured cohesion and degree of saturation is provided in Figure 5-3.

Table 5-20: Comparison of apparent cohesion for 561.7 kPa compaction stress

Degree of saturation (%S)	Measured apparent cohesion (c, kPa)	Predicted apparent cohesion (Fredlund, 1996) (c, kPa)	Predicted apparent cohesion (Vanapalli, 1996) (c, kPa)	Predicted apparent cohesion (Khalili & Khabbaz, 1998) (c, kPa)
40.1	63.2	72.3	77.9	**60.9**
51.7	43.2	48.6	51.2	**45.4**
57.1	41.4	36.4	38.1	**38.6**
66.8	30.8	28.5	29.3	**31.9**
94.5	7.3	**0.8**	**0.8**	**0.8**

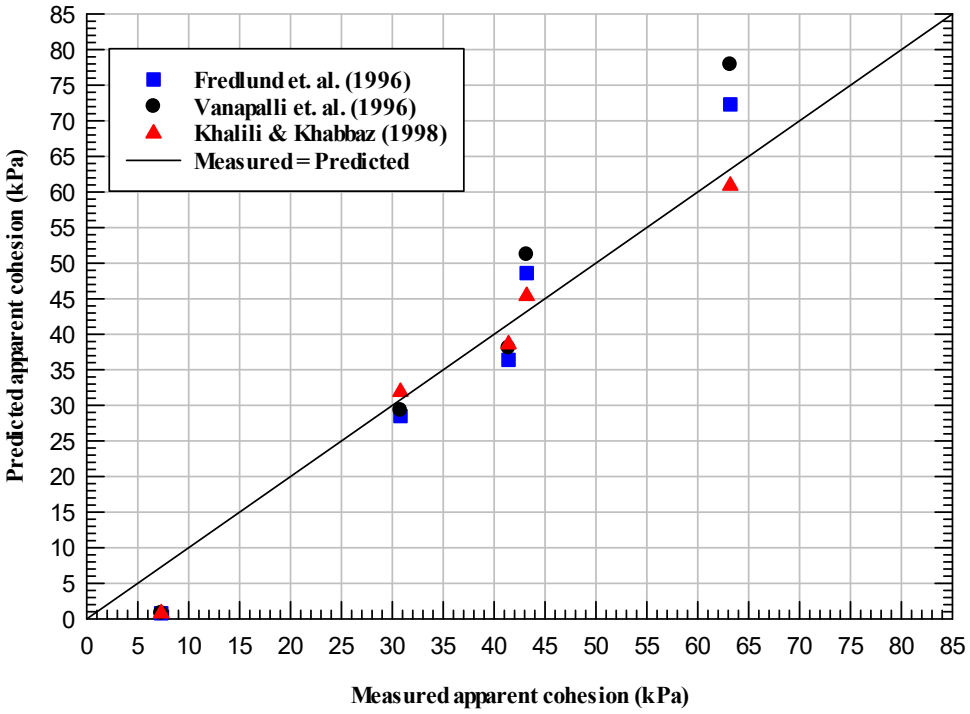

Figure 5-3: Predicted cohesion versus measured cohesion for compaction stress of 561.7 kPa

As observed in Table 5-20 and Figure 5-3, for a compaction stress of 561.7 kPa, overall, the predicted apparent cohesion values estimated using the equation provided by Khalili & Khabbaz (1998) provide better agreement with the measured apparent cohesion values as compared to Fredlund et. al. (1996) and Vanapalli et. al. (1996). All three equations yield the same predicted cohesion value at 94.4% saturation.

In summary, the Fredlund et. al. (1996) equation provides the best agreement with the measured cohesion values for the lower compaction stress of 143.8 kPa and the Khalili & Khabbaz (1998) equation provides better agreement for the higher compaction stresses of 229.2 kPa and 561.7 kPa. However, at the highest degree of saturation of 94.4%, all three equations provide the same predicted cohesions. The next section presents the resulting saturated and unsaturated shear strengths obtained on the Fulton loess tested in this study.

5.4.3 Saturated shear strength of Fulton loess

The drained shear strength of saturated Fulton loess is estimated using the first portion of Equation 5-1 and the drained shear strength parameters shown in Table 5-1 for net normal stress values of 110 kPa, 143.8 kPa, 229.2 kPa, 561.7 kPa, and 600 kPa. Table 5-11 presents the saturated shear strength values for Fulton loess for each compaction stress used to prepare the specimens. Also, a plot of saturated shear strength as a function of normal stress is provided in Figure 5-4.

Table 5-21: Saturated shear strength of Fulton loess

Normal stress (kPa)	Saturated shear strength at 143.8 kPa compaction stress	Saturated shear strength at 229.2 kPa compaction stress	Saturated shear strength at 561.7 kPa compaction stress
110	53.2	61.7	66.9
143.8	69.5	80.7	87.4
229.2	110.8	128.6	139.4
561.7	271.5	315.2	341.5
600	290.1	336.7	364.8

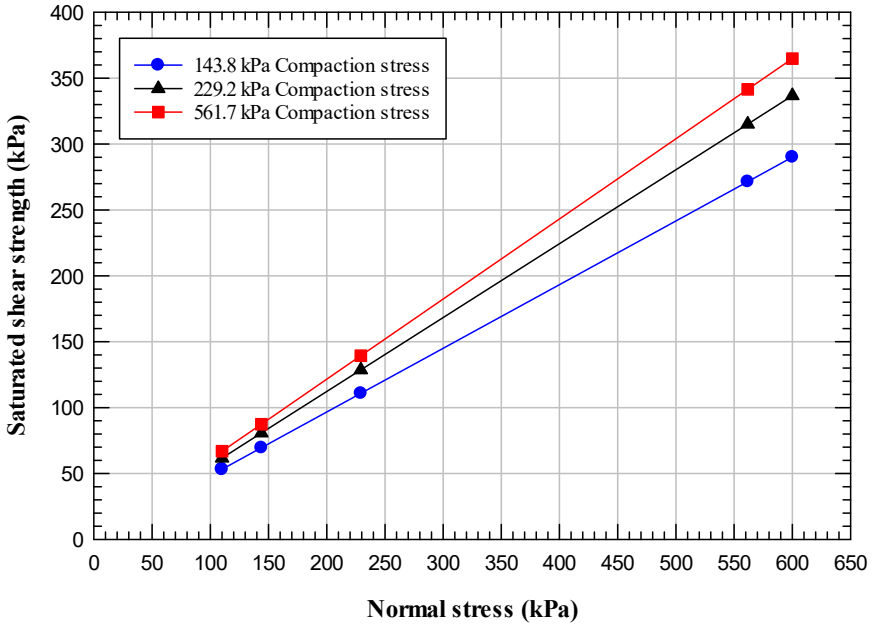

Figure 5-4: Saturated shear strength versus normal stress

From Table 5-21 and Figure 5-4, it is seen that for a given normal stress, the shear strength of the saturated specimens increases with the compaction stress. Similarly, for a given compaction stress, the shear strength also increases with an increase in normal stress.

5.4.4 Additional shear strength of the Fulton loess due to matric suction

As explained earlier, the additional shear strength of an unsaturated soil is provided by the matric suction. The second portion of Equation 5-1 was used to estimate the additional shear strength due to the matric suction in Section 5.4.2. In this section, the additional shear strength of Fulton loess due to matric suction at normal stresses of 110 kPa, 143.8 kPa, 229.2 kPa, 561.7 kPa, and 600 kPa is determined using each φ^b model and the effects of degree of saturation and normal stress are evaluated. The matric suction values listed in Tables 5-2 through 5-6 for each normal stress used to obtain the SWCCs are used. Moreover, the angles φ^b presented in Tables 5-9 through 5-11 are used. This section is further divided into subsections to make it easier to look into each model separately.

5.4.4.1 Additional shear strength due to matric suction based on angle φ^b estimated using Fredlund et. al. (1996)

Data for the additional shear strength due to matric suction and the corresponding compaction stress, saturation levels, and normal stress are provided in Tables 5-22 through 5-24. Also, Figures 5-5 through 5-7 provide a summary of the additional shear strength due to matric suction as a function of the degree of saturation. The figure caption provides the compaction stress used to prepare the specimens.

Table 5-22: Additional **s**hear strength due to matric suction for compaction stress of 143.8 kPa

Compaction stress of 143.8 kPa					
Degree of saturation (%S)	Normal stress (kPa)				
	110	143.8	229.2	561.7	600
	Shear strength due to matric suction (kPa)				
39.9	39.11	39.73	41.77	55.08	57.06
51.2	27.14	28.05	28.88	35.19	38.25
56.7	24.96	27.06	27.92	28.72	29.08
66.2	19.07	20.57	21.44	21.84	22.01
94.3	0.38	0.38	0.43	0.62	0.80

Table 5-23: Additional shear strength due to matric suction for compaction stress of 229.2 kPa

Compaction stress of 229.2 kPa					
Degree of saturation (%S)	Normal stress (kPa)				
	110	143.8	229.2	561.7	600
	Shear strength due to matric suction (kPa)				
39.6	46.53	47.26	49.66	66.03	68.59
50.4	31.06	32.99	35.14	44.19	46.82
56.2	29.87	32.01	33.35	33.96	34.37
66.5	22.16	23.97	25.01	25.87	25.70
94.4	0.45	0.44	0.51	0.72	0.94

Table 5-24: Additional **s**hear strength due to matric suction for compaction stress of 561.7 kPa

Compaction stress of 561.7 kPa					
Degree of saturation (%S)	Normal stress (kPa)				
	110	143.8	229.2	561.7	600
	Shear strength due to matric suction (kPa)				
40.1	51.68	52.77	54.67	72.27	73.60
51.7	34.34	35.87	37.29	48.62	49.30
57.1	32.57	34.24	35.71	36.40	36.52
66.8	25.13	25.89	27.49	28.48	28.72
94.5	0.48	0.48	0.55	0.78	1.02

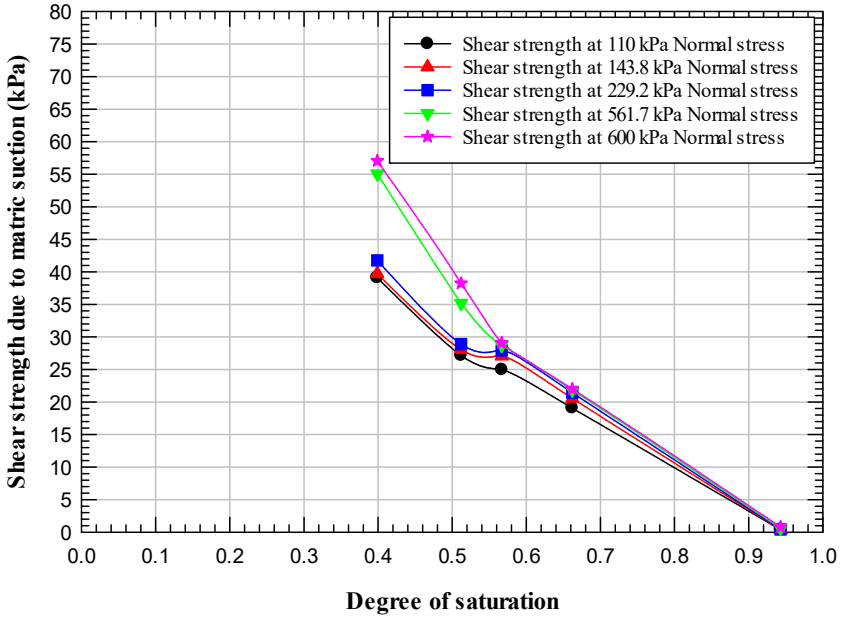

Figure 5-5: Additional shear strength due to matric suction for specimens prepared using 143.8 kPa compaction stress

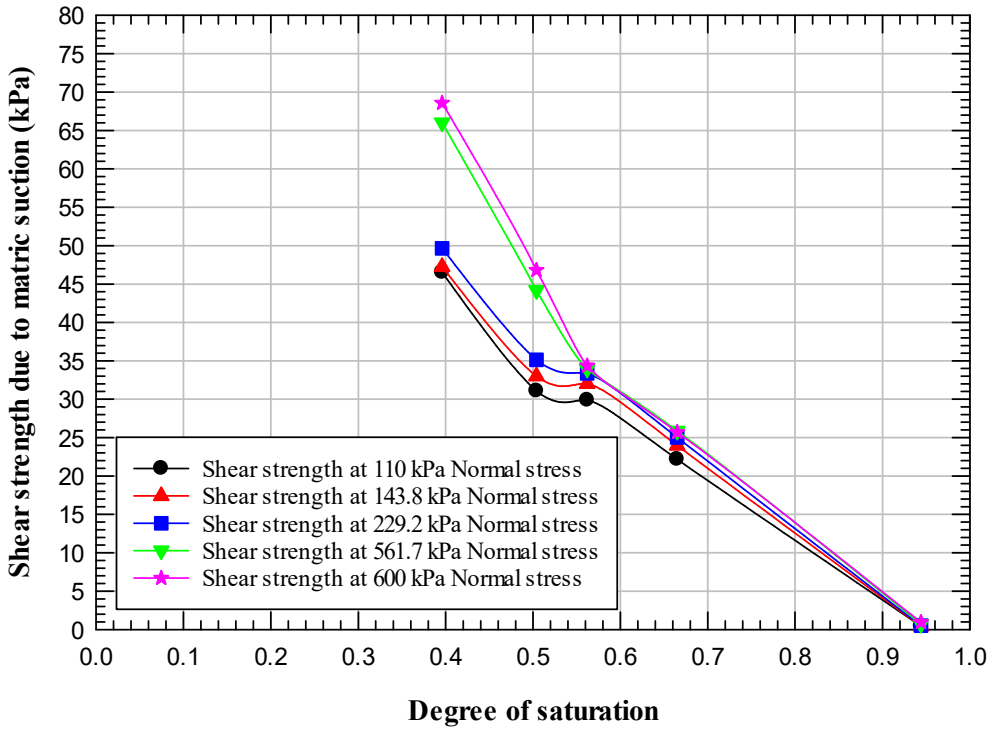

Figure 5-6: Additional shear strength due to matric suction for specimens prepared using 229.2 kPa compaction stress

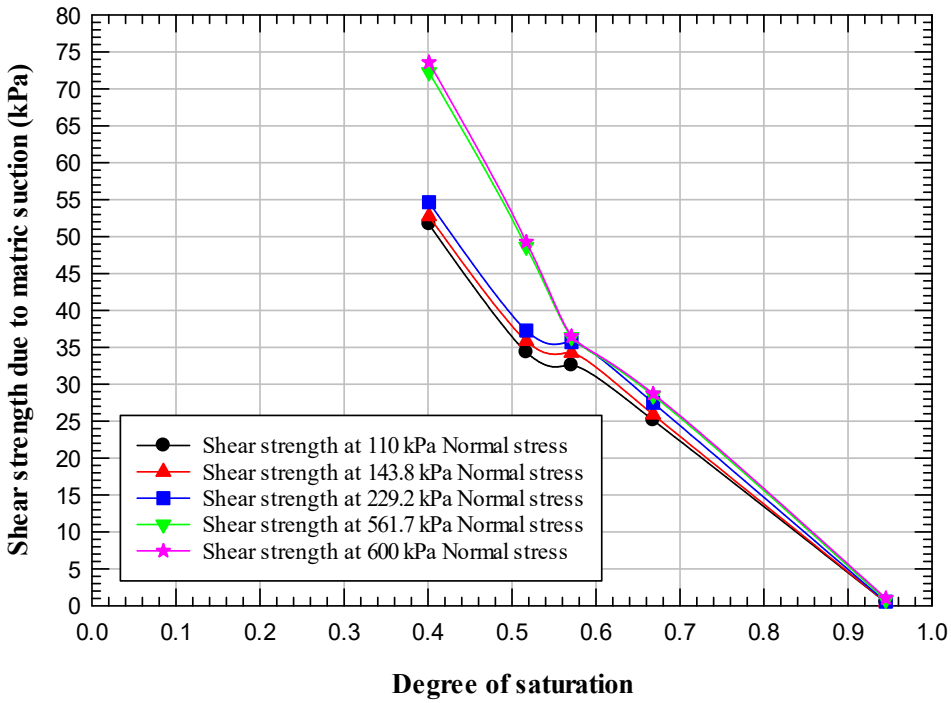

Figure 5-7: Additional shear strength due to matric suction for specimens prepared using 561.7 kPa compaction stress

5.4.4.2 Additional shear strength due to matric suction based on angle φ^b estimated using Vanapalli et.al. (1996)

Data for the additional shear strength due to matric suction and the corresponding compaction stress, saturation level, and normal stress are provided in Tables 5-25 through 5-27. Also, Figures 5-8 through 5-10 provide a summary of the additional shear strength due to matric suction as a function of the degree of saturation. The figure caption provides the compaction stress used to prepare the specimens.

Table 5-25: Additional shear strength due to matric suction for compaction stress of 143.8 kPa

Compaction stress of 143.8 kPa					
Degree of saturation (%S)	Normal stress (kPa)				
	110	143.8	229.2	561.7	600
	Shear strength due to matric suction (kPa)				
0.399	39.64	40.18	45.14	59.59	61.77
0.512	27.58	28.46	30.51	37.22	40.48
0.567	25.34	27.45	29.30	30.17	30.56
0.662	19.32	20.83	22.23	22.66	22.85
0.943	0.38	0.38	0.43	0.62	0.81

Table 5-26: Additional shear strength due to matric suction for compaction stress of 229.2 kPa

Compaction stress of 229.2 kPa					
Degree of saturation (%S)	Normal stress (kPa)				
	110	143.8	229.2	561.7	600
	Shear strength due to matric suction (kPa)				
0.399	47.01	47.63	53.61	71.35	74.15
0.512	31.48	33.39	37.15	46.75	49.57
0.567	30.27	32.41	34.96	35.63	36.09
0.662	22.41	24.23	25.85	26.77	26.61
0.943	0.45	0.44	0.51	0.72	0.94

Table 5-27: Additional shear strength due to matric suction for compaction stress of 561.7 kPa

Compaction stress of 561.7 kPa					
Degree of saturation (%S)	Normal stress (kPa)				
	110	143.8	229.2	561.7	600
	Shear strength due to matric suction (kPa)				
0.399	51.96	52.92	58.83	77.85	79.33
0.512	34.69	36.19	39.25	51.22	51.96
0.567	32.91	34.55	37.35	38.11	38.25
0.662	25.35	26.10	28.30	29.35	29.61
0.943	0.48	0.48	0.55	0.78	1.02

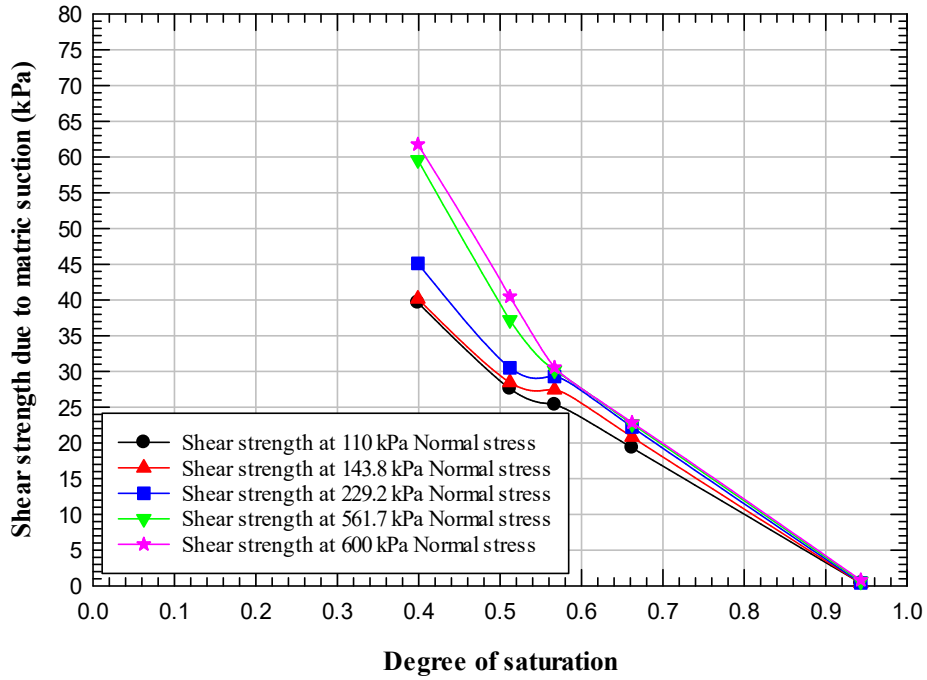

Figure 5-8: Additional shear strength due to matric suction for specimens prepared using 143.8 kPa compaction stress

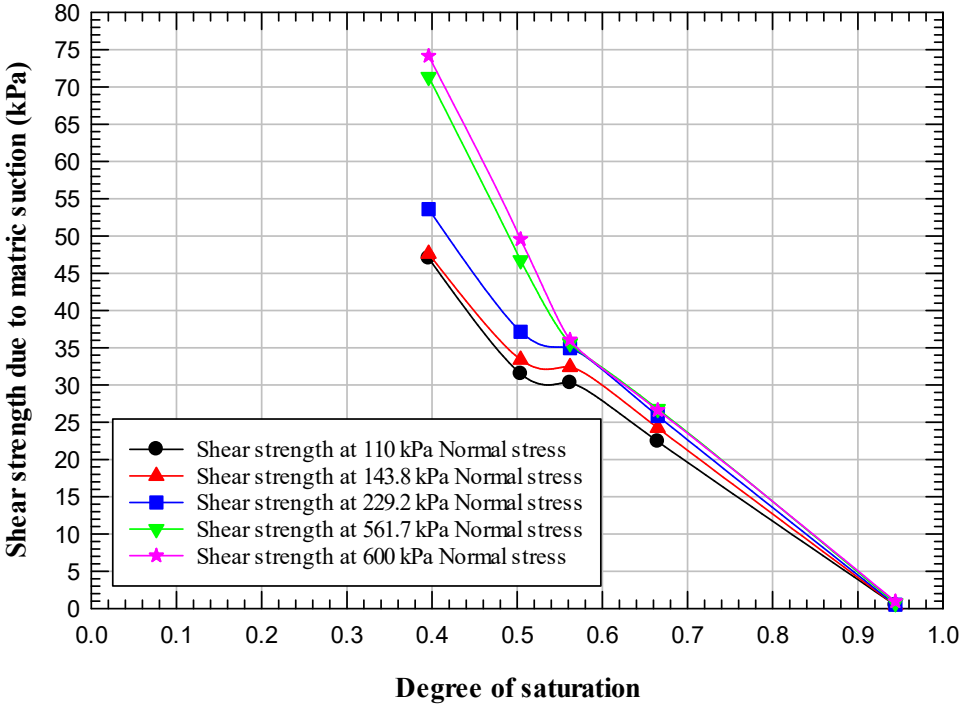

Figure 5-9: Additional shear strength due to matric suction for specimens prepared using 229.2 kPa compaction stress

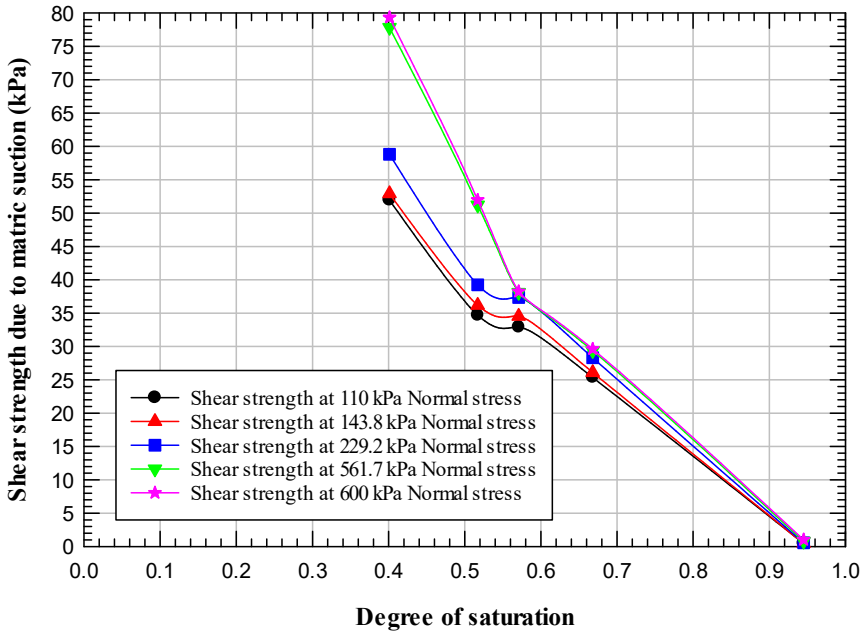

Figure 5-10: Additional shear strength due to matric suction for specimens prepared using 561.7 kPa compaction stress

5.4.4.3 Additional shear strength due to matric suction based on angle φ^b estimated using Khalili & Khabbaz (1998)

Data for the additional shear strength due to matric suction and the corresponding compaction stress, saturation level, and normal stress are provided in Tables 5-28 through 5-30. Figures 5-11 through 5-13 provide a summary of the additional shear strength due to matric suction as a function of the degree of saturation. The figure caption provides the compaction stress used to prepare the specimens.

Table 5-28: Additional shear strength due to matric suction for compaction stress of 143.8 kPa

Compaction stress of 143.8 kPa					
Degree of saturation (%S)	Normal stress (kPa)				
	110	143.8	229.2	561.7	600
	Shear strength due to matric suction (kPa)				
0.399	40.08	40.23	38.91	48.55	47.10
0.512	30.26	30.60	29.33	35.31	35.00
0.567	28.11	29.05	27.87	31.09	29.85
0.662	23.42	24.15	23.27	25.85	24.77
0.943	0.39	0.39	0.44	0.63	0.82

Table 5-29: Additional shear strength due to matric suction for compaction stress of 229.2 kPa

Compaction stress of 229.2 kPa					
Degree of saturation (%S)	Normal stress (kPa)				
	110	143.8	229.2	561.7	600
	Shear strength due to matric suction (kPa)				
0.399	46.74	46.91	45.37	56.81	55.18
0.512	34.98	35.81	34.85	42.56	41.71
0.567	32.96	33.88	32.64	36.25	34.80
0.662	26.78	27.64	26.65	29.81	28.38
0.943	0.45	0.45	0.51	0.73	0.95

Table 5-30: Additional shear strength due to matric suction for compaction stress of 561.7 kPa

Compaction stress of 561.7 kPa					
Degree of saturation (%S)	Normal stress (kPa)				
	110	143.8	229.2	561.7	600
	Shear strength due to matric suction (kPa)				
0.399	50.41	50.71	48.73	60.86	58.59
0.512	37.40	38.01	36.59	45.41	43.63
0.567	35.36	36.03	34.73	38.59	36.90
0.662	29.01	29.30	28.47	31.87	30.54
0.943	0.49	0.49	0.55	0.79	1.03

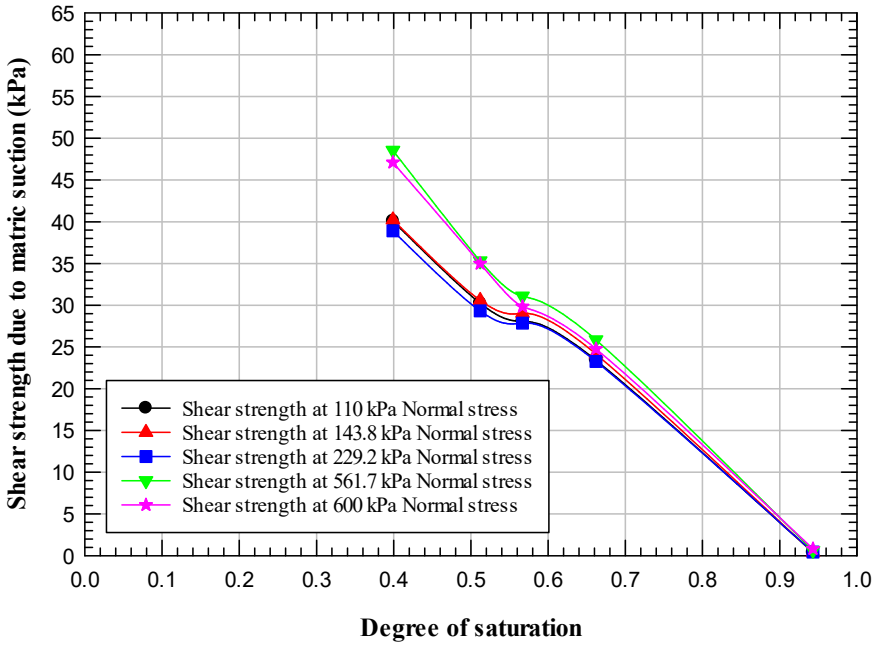

Figure 5-11: Additional shear strength due to matric suction for specimens prepared using143.8 kPa compaction stress

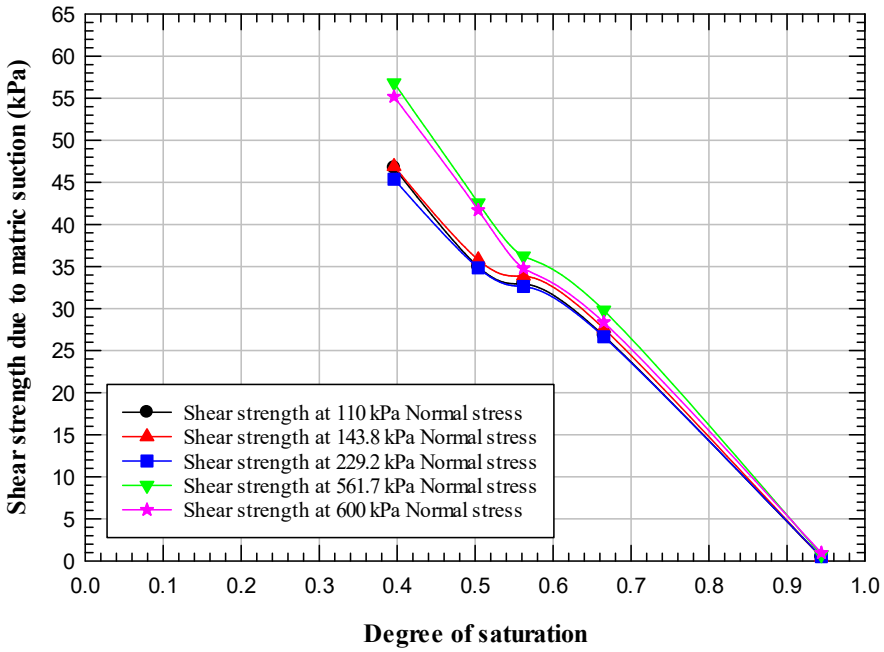

Figure 5-12: Additional shear strength due to matric suction for specimens prepared using 229.2 kPa compaction stress

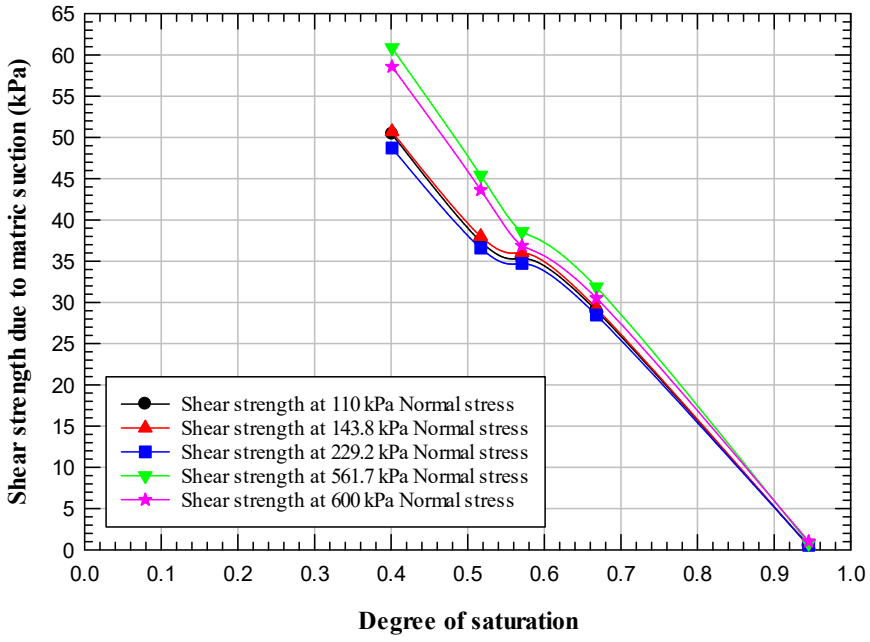

Figure 5-13: Additional shear strength due to matric suction for specimens prepared using 561.7 kPa compaction stress

Observations on Figures 5-5 through 5-13 show that the additional shear strength due to matric suction rapidly decreases with an increase in the degree of saturation and ultimately

reaches zero at 100% saturation for all three models utilized. Zhong et. al. (2015) made a similar conclusion in his study on Shanxi, China loess. It can also be noted that the additional shear strength due to matric suction for the specimens tested at a higher normal stress have higher values because the matric suction increases with increasing applied normal stress as shown in Tables 5-2 through 5-6. In Figures 5-5 through 5-13, the specimens tested with normal stresses of 561.7 kPa and 600 kPa have higher shear strength values at low degrees of saturation, since the matric suction values increase exponentially at low degree of saturation and higher applied normal stress. This fact can be seen in Tables 5-2 through 5-6. It is also seen that at higher degrees of saturation, greater than 57%, the difference in shear strength is almost negligible with changes in normal stress. This suggests that the matric suction of the Fulton loess is almost independent of the normal stress at higher degrees of saturation. Figure 4-14 also supports this conclusion.

5.4.5 Influence of degree of saturation on the shear strength of unsaturated Fulton loess

The shear strength of unsaturated Fulton loess was estimated using Equation 5-1 per the procedure explained in Section 5.4. The saturated shear strength and the additional shear strength due to matric suction were combined to estimate the shear strength of unsaturated loess. The additional shear strength due to matric suction is calculated for different models to estimate angle φ^b as described in Section 5.4.4. Tables 5-31 through 5-48 present the unsaturated shear strength for the Fulton loess utilizing different models to determine angle φ^b as described in Section 5.4.4. The table captions for unsaturated shear strength provide the compaction stress used to prepare the specimens and the model used to determine angle φ^b. Similarly, Figures 5-14 through 5-22 show plots of the unsaturated shear strength as a function of degree of saturation for the Fulton loess utilizing different models for estimating angle φ^b as described in Section 5.4.4 to study the

influence of the degree of saturation on the shear strength. The figure caption provides the compaction stress used to prepare the specimens and the model used to determine angle φ^b.

Table 5-31: Unsaturated shear strength of Fulton loess specimens using compaction stress of 143.8 kPa and utilizing Fredlund et. al. (1996) relationship

Compaction stress of 143.8 kPa					
Degree of saturation (%S)	Normal stress (kPa)				
	110	143.8	229.2	561.7	600
	Unsaturated shear strength of Fulton loess (kPa)				
0.399	92.28	109.25	152.56	326.62	347.11
0.512	80.32	97.57	139.68	306.73	328.31
0.567	78.13	96.58	138.72	300.26	319.13
0.662	72.24	90.09	132.24	293.38	312.06
0.943	53.56	69.90	111.23	272.16	290.86

Table 5-32: Unsaturated shear strength of Fulton loess specimens using compaction stress of 229.2 kPa and utilizing Fredlund et. al. (1996) relationship

Compaction stress of 229.2 kPa					
Degree of saturation (%S)	Normal stress (kPa)				
	110	143.8	229.2	561.7	600
	Unsaturated shear strength of Fulton loess (kPa)				
0.396	108.26	127.96	178.28	381.25	405.29
0.504	92.79	113.69	163.77	359.40	383.53
0.562	91.60	112.71	161.97	349.17	371.08
0.665	83.89	104.67	153.63	341.09	362.41
0.944	62.17	81.14	129.13	315.93	337.64

Table 5-33: Unsaturated shear strength of Fulton loess specimens using compaction stress of 561.7 kPa and utilizing Fredlund et. al. (1996) relationship

Compaction stress of 561.7 kPa					
Degree of saturation (%S)	Normal stress (kPa)				
	110	143.8	229.2	561.7	600
	Unsaturated shear strength of Fulton loess (kPa)				
0.401	118.56	140.20	194.03	413.79	438.41
0.517	101.22	123.31	176.65	390.14	414.10
0.571	99.45	121.67	175.07	377.92	401.33
0.668	92.01	113.32	166.84	370.00	393.53
0.945	67.36	87.91	139.90	342.30	365.82

Table 5-34: Unsaturated shear strength of Fulton loess specimens using compaction stress of 143.8 kPa and utilizing Vanapalli et. al. (1996) relationship

Compaction stress of 143.8 kPa					
Degree of saturation (%S)	Normal stress (kPa)				
	110	143.8	229.2	561.7	600
	Unsaturated shear strength of Fulton loess (kPa)				
0.399	92.82	109.70	155.94	331.12	351.82
0.512	80.75	97.97	141.31	308.76	330.53
0.567	78.52	96.97	140.10	301.70	320.61
0.662	72.50	90.35	133.03	294.20	312.91
0.943	53.56	69.90	111.23	272.16	290.86

Table 5-35: Unsaturated shear strength of Fulton loess specimens using compaction stress of 229.2 kPa and utilizing Vanapalli et. al. (1996) relationship

Compaction stress of 229.2 kPa					
Degree of saturation (%S)	Normal stress (kPa)				
	110	143.8	229.2	561.7	600
	Unsaturated shear strength of Fulton loess (kPa)				
0.396	108.74	128.33	182.23	386.56	410.86
0.504	93.21	114.09	165.77	361.96	386.27
0.562	92.00	113.10	163.59	350.85	372.80
0.665	84.14	104.92	154.47	341.98	363.31
0.944	62.18	81.14	129.13	315.93	337.64

Table 5-36: Unsaturated shear strength of Fulton loess specimens using compaction stress of 561.7 kPa and utilizing Vanapalli et. al. (1996) relationship

Compaction stress of 561.7 kPa					
Degree of saturation (%S)	Normal stress (kPa)				
	110	143.8	229.2	561.7	600
	Unsaturated shear strength of Fulton loess (kPa)				
0.401	118.84	140.35	198.19	419.37	444.13
0.517	101.57	123.62	178.60	392.74	416.77
0.571	99.79	121.98	176.70	379.63	403.06
0.668	92.23	113.53	167.65	370.87	394.42
0.945	67.36	87.91	139.90	342.30	365.82

Table 5-37: Unsaturated shear strength of Fulton loess specimens using compaction stress of 143.8 kPa and utilizing Khalili & Khabbaz (1998) relationship

Compaction stress of 143.8 kPa					
Degree of saturation (%S)	Normal stress (kPa)				
	110	143.8	229.2	561.7	600
	Unsaturated shear strength of Fulton loess (kPa)				
0.399	93.26	109.74	149.71	320.08	337.15
0.512	83.43	100.12	140.13	306.85	325.05
0.567	81.29	98.57	138.67	302.63	319.90
0.662	76.60	93.67	134.07	297.38	314.82
0.943	53.56	69.90	111.23	272.16	290.87

Table 5-38: Unsaturated shear strength of Fulton loess specimens using compaction stress of 229.2 kPa and utilizing Khalili & Khabbaz (1998) relationship

Compaction stress of 229.2 kPa					
Degree of saturation (%S)	Normal stress (kPa)				
	110	143.8	229.2	561.7	600
	Unsaturated shear strength of Fulton loess (kPa)				
0.396	108.47	127.60	173.99	372.02	391.88
0.504	96.70	116.51	163.47	357.77	378.41
0.562	94.69	114.58	161.26	351.46	371.50
0.665	88.51	108.34	155.27	345.02	365.08
0.944	62.18	81.15	129.13	315.94	337.66

Table 5-39: Unsaturated shear strength of Fulton loess specimens using compaction stress of 561.7 kPa and utilizing Khalili & Khabbaz (1998) relationship

Compaction stress of 561.7 kPa					
Degree of saturation (%S)	Normal stress (kPa)				
	110	143.8	229.2	561.7	600
	Unsaturated shear strength of Fulton loess (kPa)				
0.401	117.29	138.14	188.09	402.38	423.40
0.517	104.28	125.45	175.94	386.93	408.43
0.571	102.24	123.46	174.09	380.11	401.71
0.668	95.89	116.73	167.83	373.38	395.35
0.945	67.37	87.92	139.90	342.31	365.84

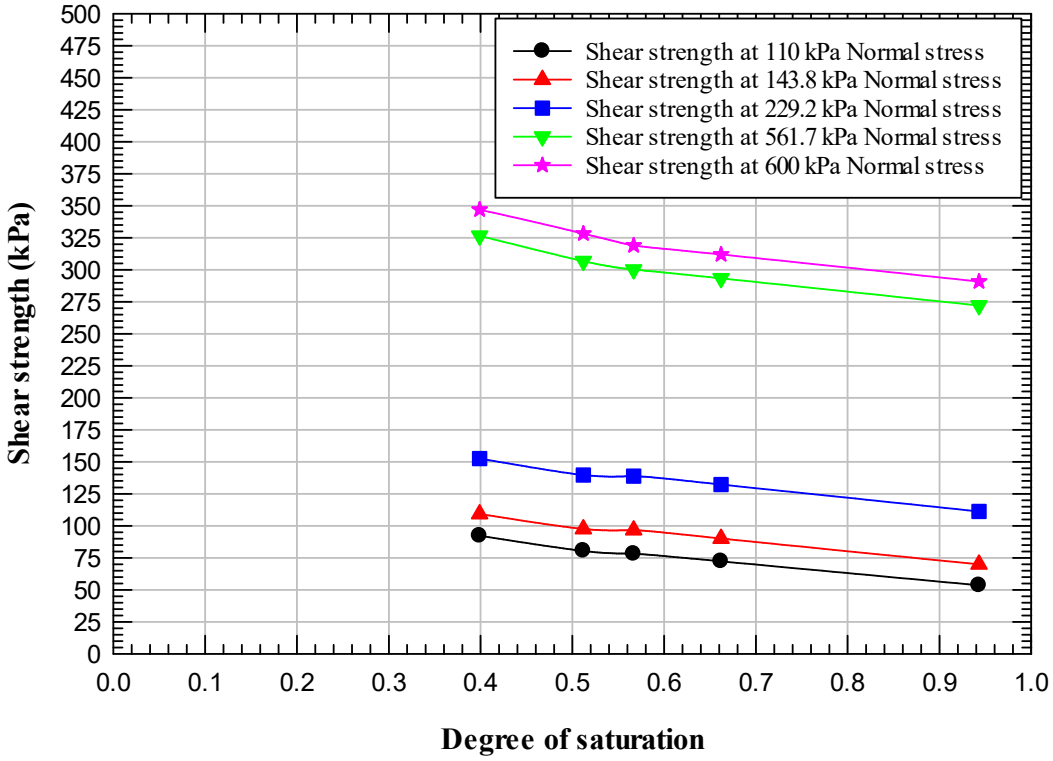

Figure 5-14: Shear strength versus degree of saturation for specimens prepared with compaction stress of 143.8 kPa and utilizing Fredlund et. al. (1996) relationship

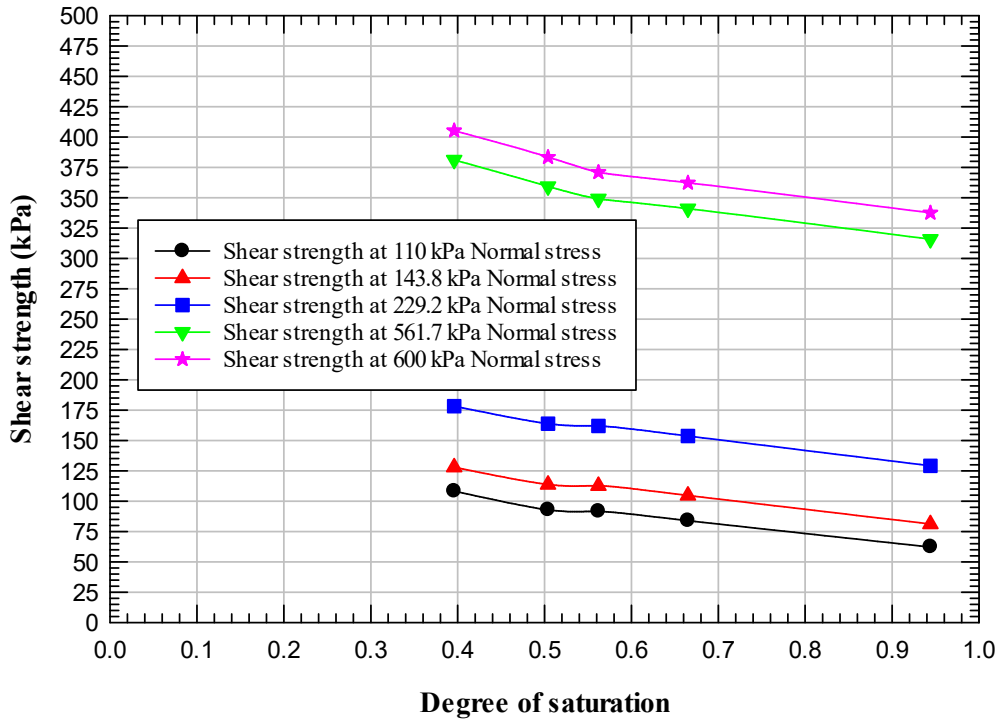

Figure 5-15: Shear strength versus degree of saturation for specimens prepared with compaction stress of 229.2 kPa and utilizing Fredlund et. al. (1996) relationship

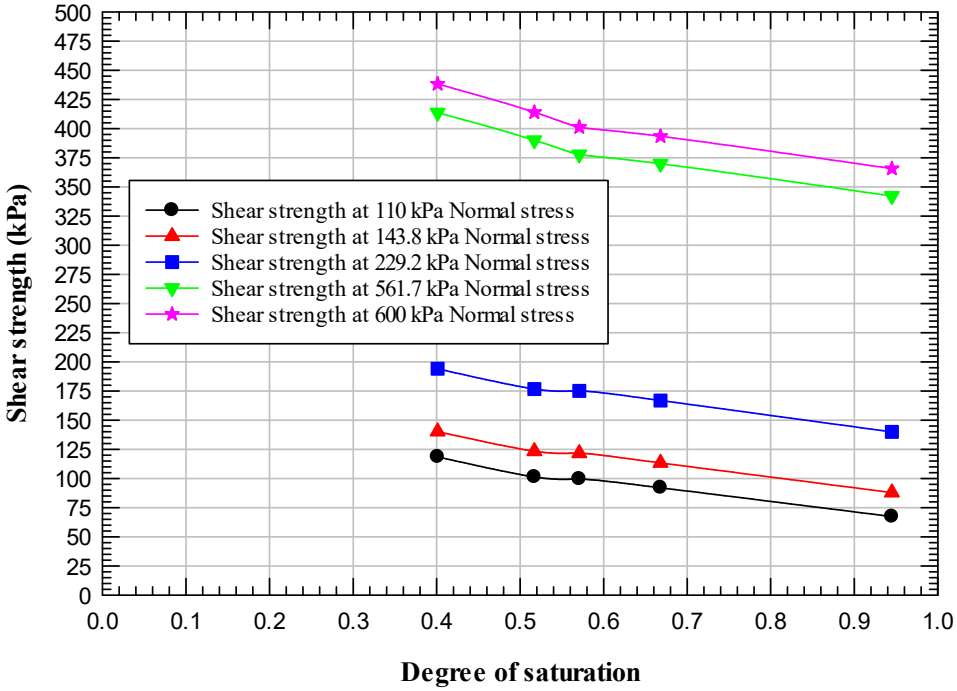

Figure 5-16: Shear strength versus degree of saturation for specimens prepared with compaction stress of 561.7 kPa and utilizing Fredlund et. al. (1996) relationship

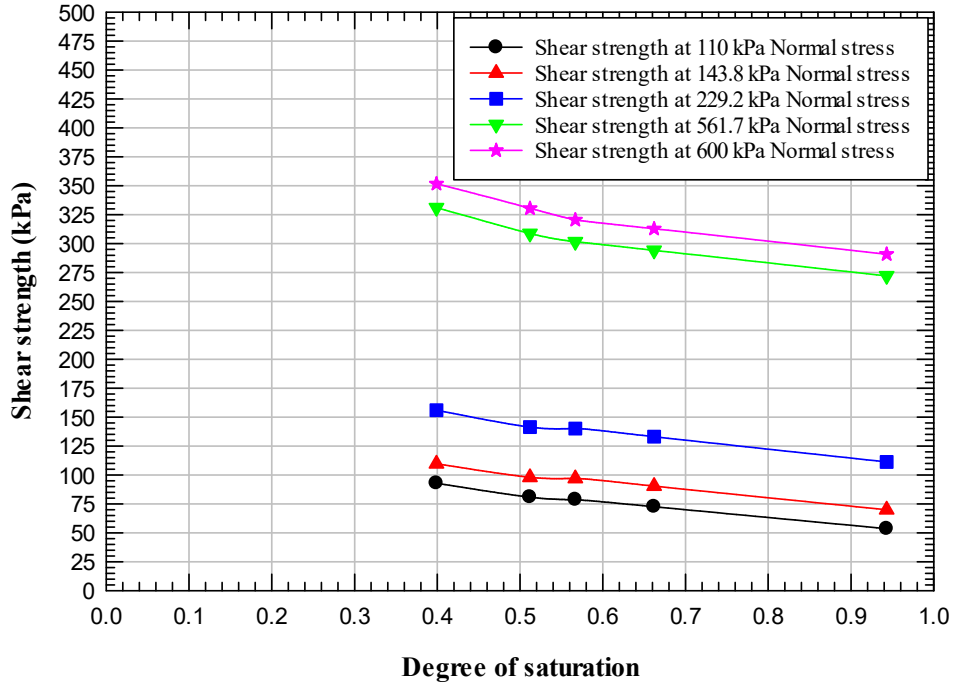

Figure 5-17: Shear strength versus degree of saturation for specimens prepared with compaction stress of 143.8 kPa and utilizing Vanapalli et. al. (1996) relationship

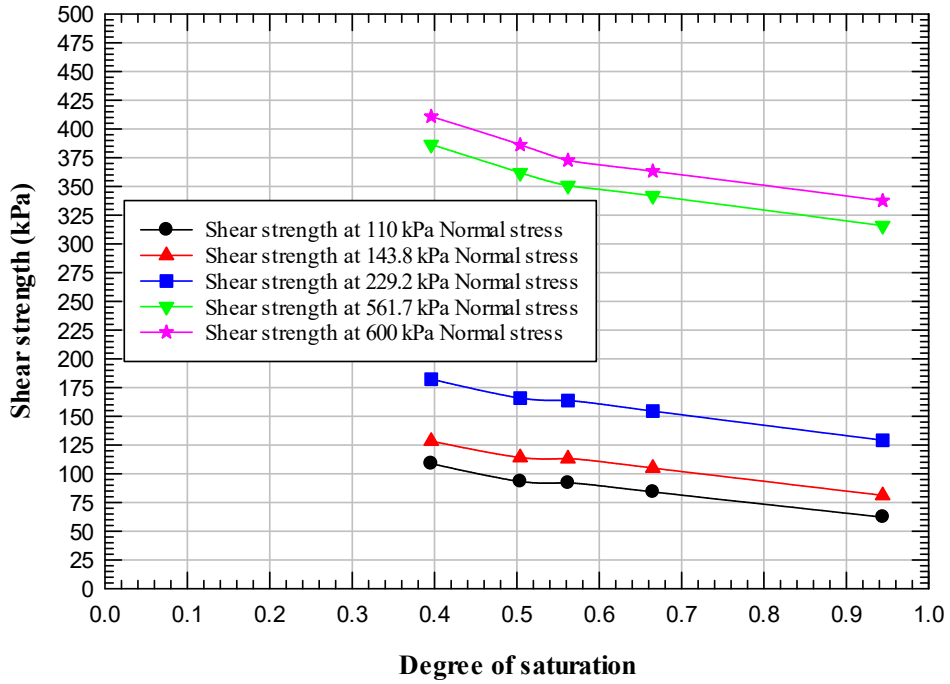

Figure 5-18: Shear strength versus degree of saturation for specimens prepared with compaction stress of 229.2 kPa and utilizing Vanapalli et. al. (1996) relationship

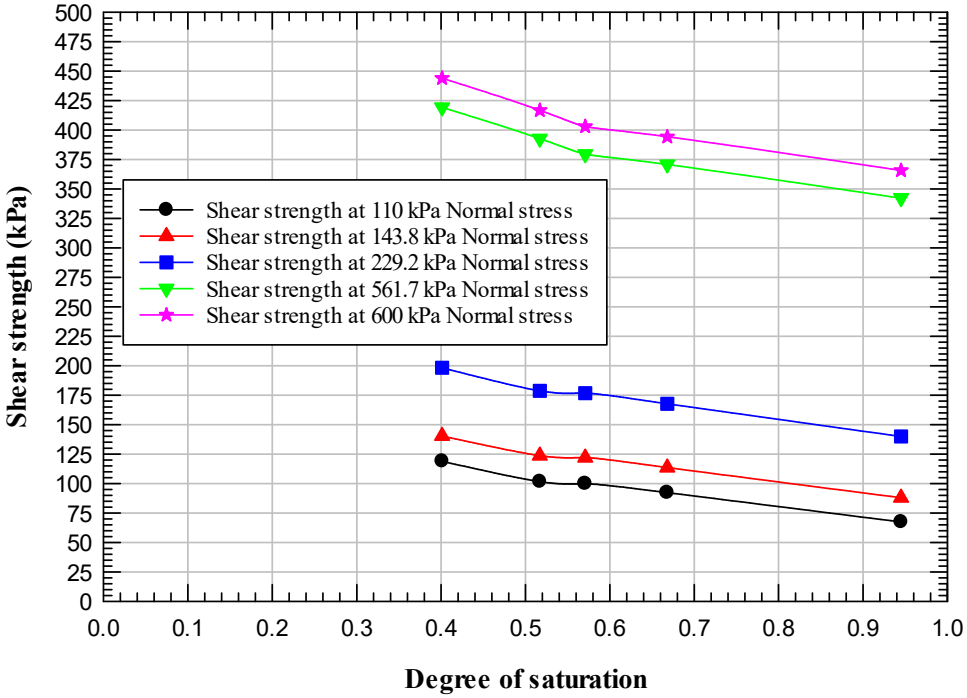

Figure 5-19: Shear strength versus degree of saturation for specimens prepared with compaction stress of 561.7 kPa and utilizing Vanapalli et. al. (1996) relationship

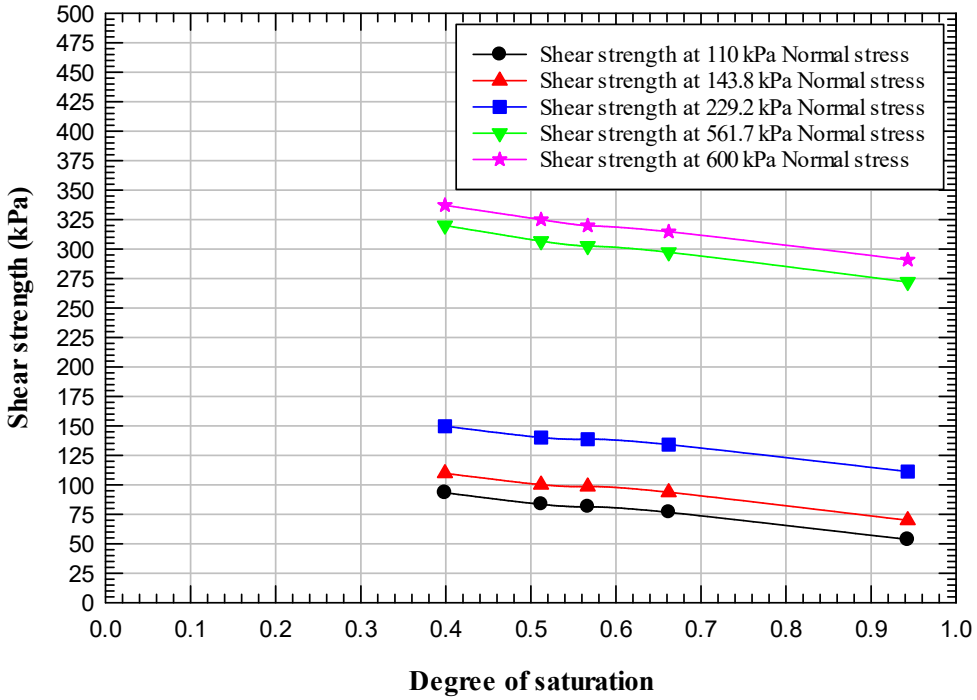

Figure 5-20: Shear strength versus degree of saturation for specimens prepared with compaction stress of 143.8 kPa and utilizing Khalili & Khabbaz (1998) relationship

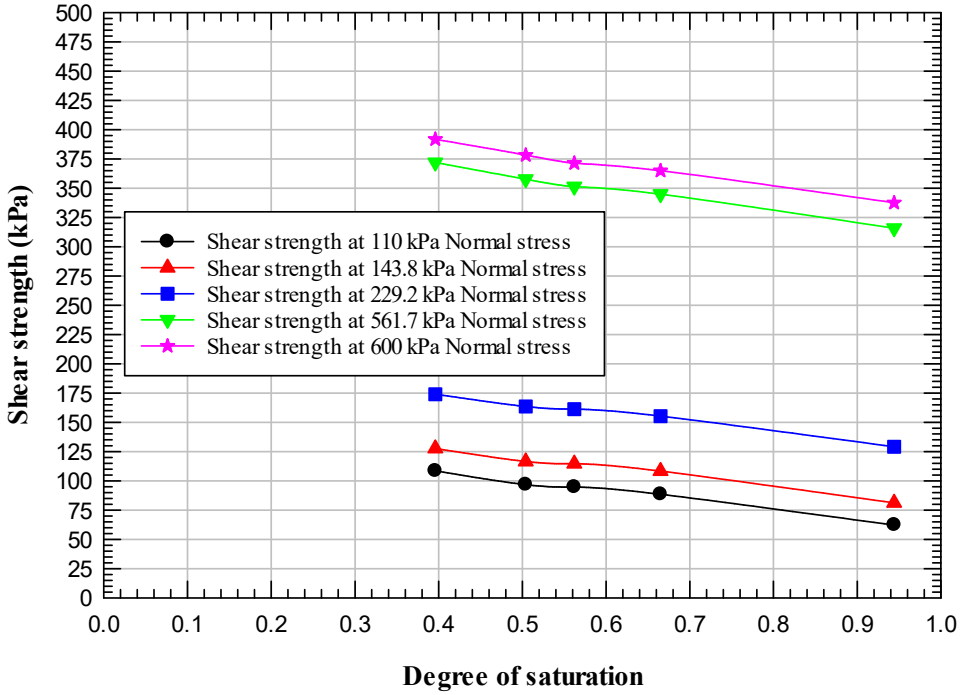

Figure 5-21: Shear strength versus degree of saturation for specimens prepared with compaction stress of 229.2 kPa and utilizing Khalili & Khabbaz (1998) relationship

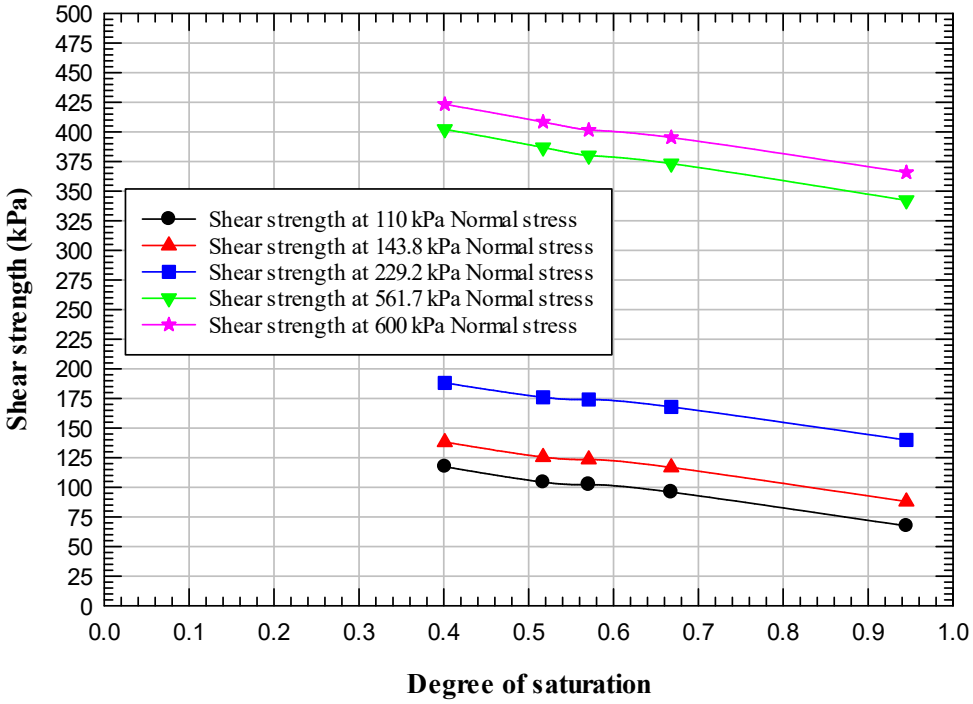

Figure 5-22: Shear strength versus degree of saturation for specimens prepared with compaction stress of 561.7 kPa and utilizing Khalili & Khabbaz (1998) relationship

Observations made on Figures 5-14 through 5-22 suggest that the shear strength of the Fulton loess decreases with increasing degree of saturation. This agrees with the results obtained for Lanzhou, China loess, as studied by Wen and Yan (2014). The decrease in shear strength can be explained by the decrease in apparent cohesion values with the increase in degree of saturation. This change in apparent cohesion is primarily due to the decrease in matric suction values with the increase in degree of saturation as explained in Section 4.3 and illustrated in Tables 5-2 through 5-6. Wen and Yan (2014) indicated that the primary mechanism for the reduction in the shear strength of unsaturated loess is the breaking up of inter-particle bonds between particles provided by clay and calcium carbonate binding and secondly by dissolution of soluble salts and reduction in matric suction. However, Fredlund and Rahardjo (1993) and

Muñoz-Castelblanco et al. (2012) suggest that the primary mechanism responsible for the reduction of shear strength with an increase in the degree of saturation is the reduction in matric suction.

For this research, the reduction in apparent cohesion was the primary contribution to the reduction in shear strength of Fulton loess with increasing saturation. Since the cementation due to calcium carbonate, ferric oxide, sodium chloride, etc., is lost during the specimen remolding process, the primary contribution to cohesion for the Fulton loess specimens in this research is clay binding and matric suction. As the degree of saturation increases, the saturation of clay particles increases, and the bonding provided between silt particles by the clay particles decreases. Once the soil gets fully saturated, the clay binding and matric suction can be completely lost and the cohesion intercept is nearly zero as shown by Figure 4-5 and discussed in Section 4.2.1.1.

The reduction in matric suction with an increase in saturation contributes to the reduction in apparent cohesion and the decrease in the shear strength of the loess. The matric suction in soil is a combined effect of capillarity and short-range adsorption as explained in Section 2.4.2. As the moisture content increases, the meniscus connecting two soil particles becomes larger and the inter-particle forces between the soil particles decreases. Additionally, the inter-particle forces between soil particles decreases with an increase in saturation because short-range adsorption of particles decreases as water molecules replace air molecules in the voids of the soil. The combined effect of capillarity and short-range adsorption reduction causes a decrease in matric suction and a decrease in the shear strength.

In summary, the decrease in apparent cohesion due to the reduction in matric suction with increasing degree of saturation contributed to the decrease in shear strength of loess. A similar

conclusion was made about Shanxi loess in China by Zhong et. al. (2015). As per their study, the decrease in cohesion that included matric suction was the primary reason for the decrease of shear strength of unsaturated loess with the increase in the degree of saturation.

As also depicted in Figures 5-14 through 5-22, the shear strength of loess increases with normal stress and agrees with the general behavior of soils as defined by Equation 5-1. Figures 5-14 through 5-22 also show that the shear strength of loess increases with compaction stress applied during specimen preparation. Higher compaction stresses applied during specimen preparation results in a denser soil specimen and an increase in both the cohesion and internal friction angle components of shear strength.

5.4.6 Influence of dry unit weight on the shear strength of unsaturated Fulton loess

Figures 5-23 through 5-37 show unsaturated shear strength as a function of dry unit weight for the Fulton loess for each normal stress used to calculate the unsaturated shear strength and different models used to determine angle φ^b. The normal stress values used, and the models utilized to calculate angle φ^b are provided in the figure caption. In each of the plots shown in Figures 5-23 through 5-37, the first point in each curve represents the specimens prepared at 143.8 kPa compaction stress, the second point represents the specimens prepared at 229.2 kPa compaction stress, and the third point represents the specimens prepared at 561.7 kPa compaction stress.

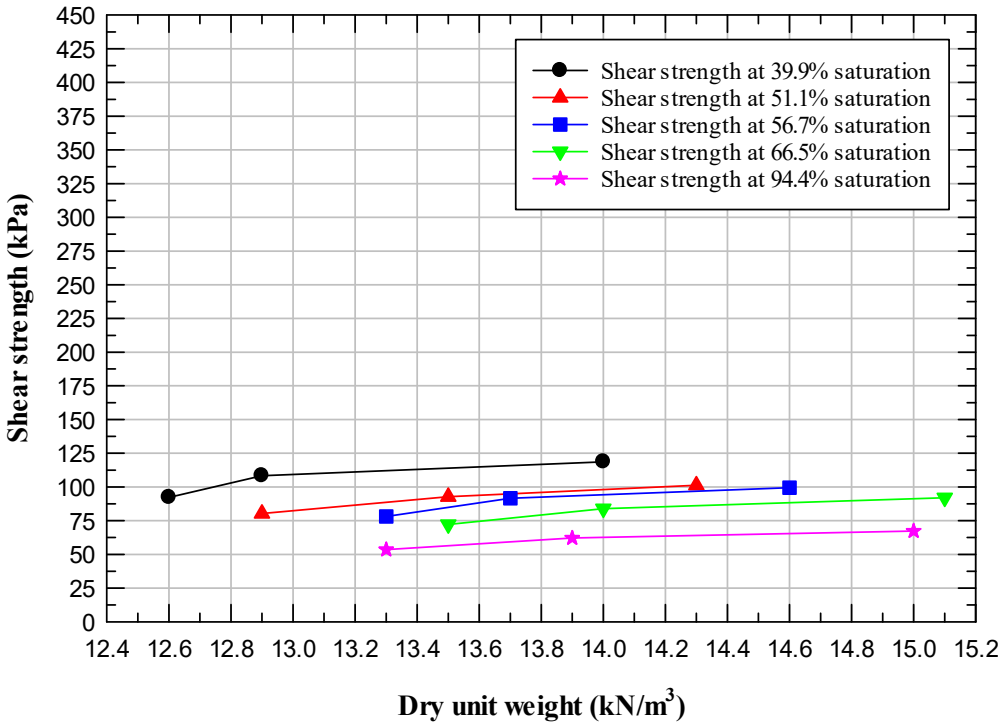

Figure 5-23: Shear strength versus dry unit weight at 110 kPa normal stress and utilizing Fredlund et. al. (1996) relationship

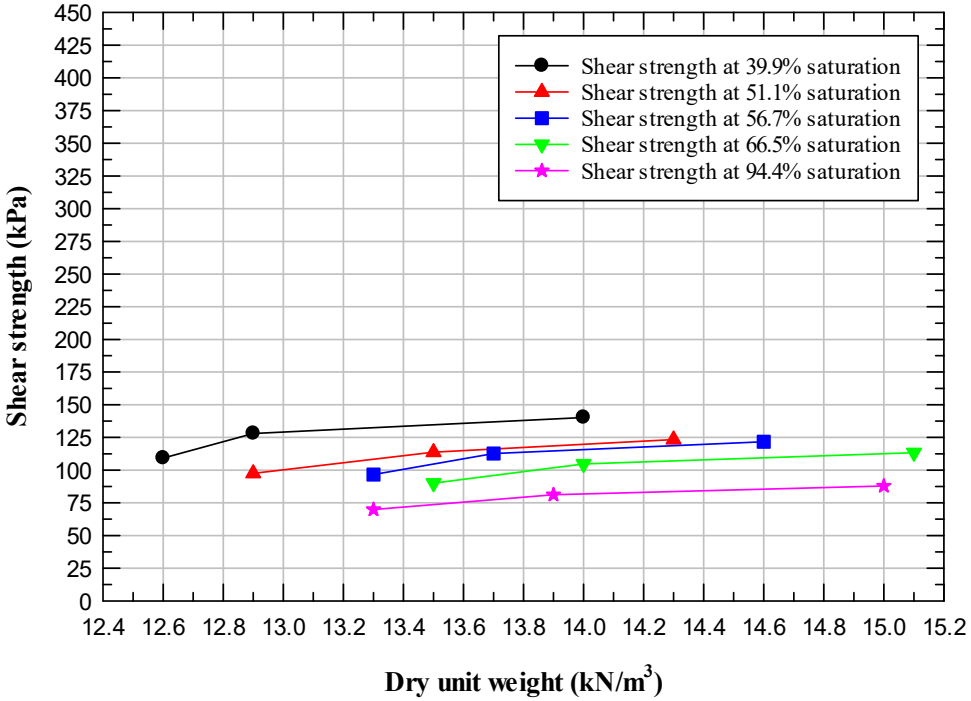

Figure 5-24: Shear strength versus dry unit weight at 143.8 kPa normal stress and utilizing Fredlund et. al. (1996) relationship

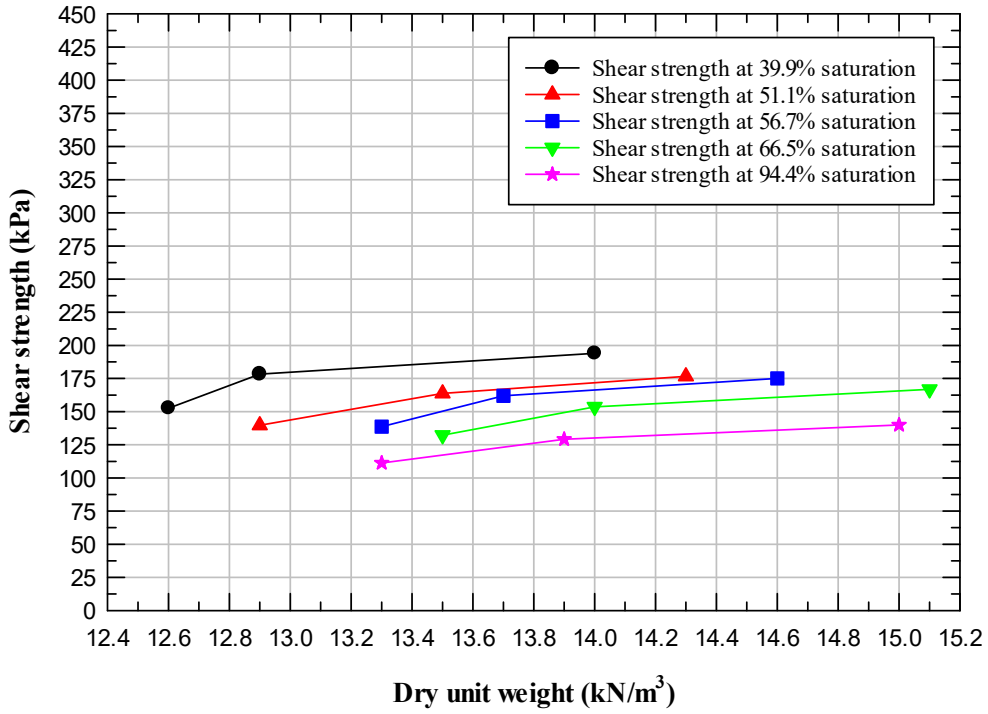

Figure 5-25: Shear strength versus dry unit weight at 229.2 kPa normal stress and utilizing Fredlund et. al. (1996) relationship

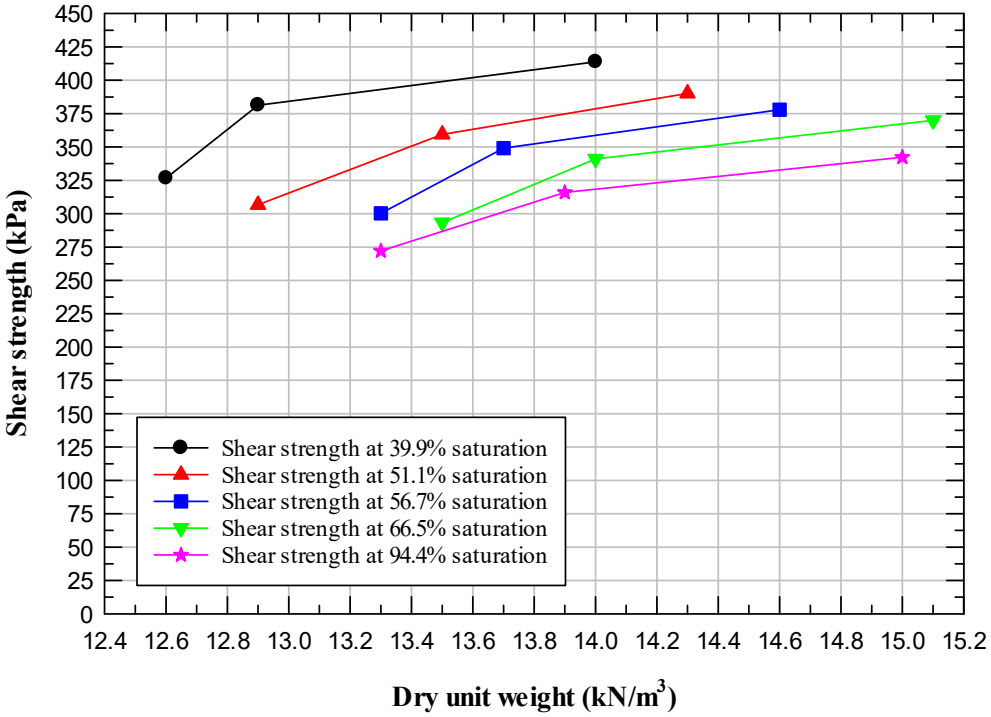

Figure 5-26: Shear strength versus dry unit weight at 561.7 kPa normal stress and utilizing Fredlund et. al. (1996) relationship

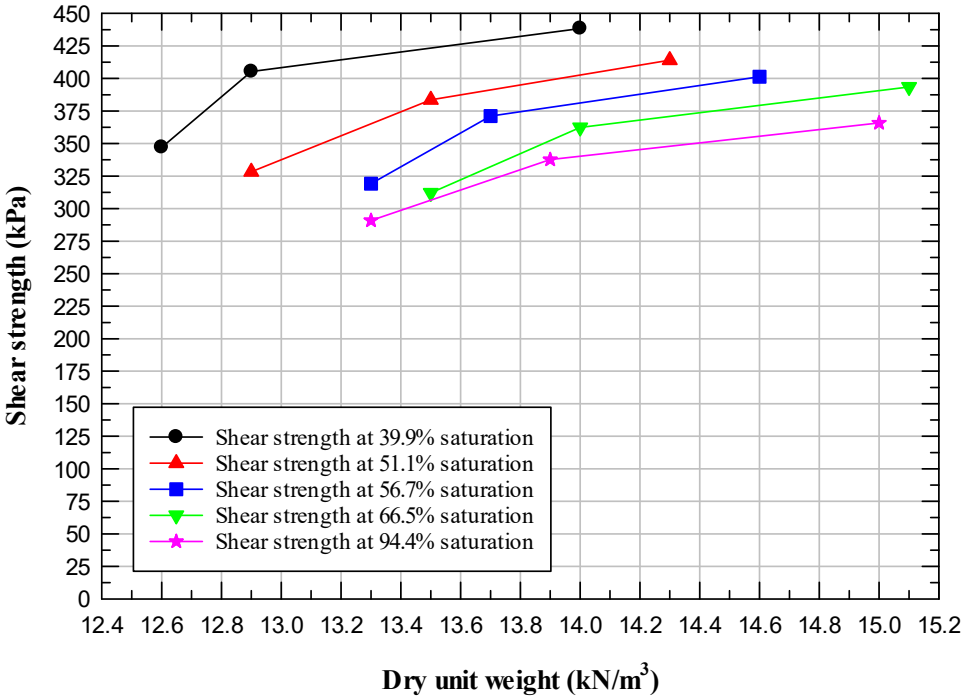

Figure 5-27: Shear strength versus dry unit weight at 600 kPa normal stress and utilizing Fredlund et. al. (1996) relationship

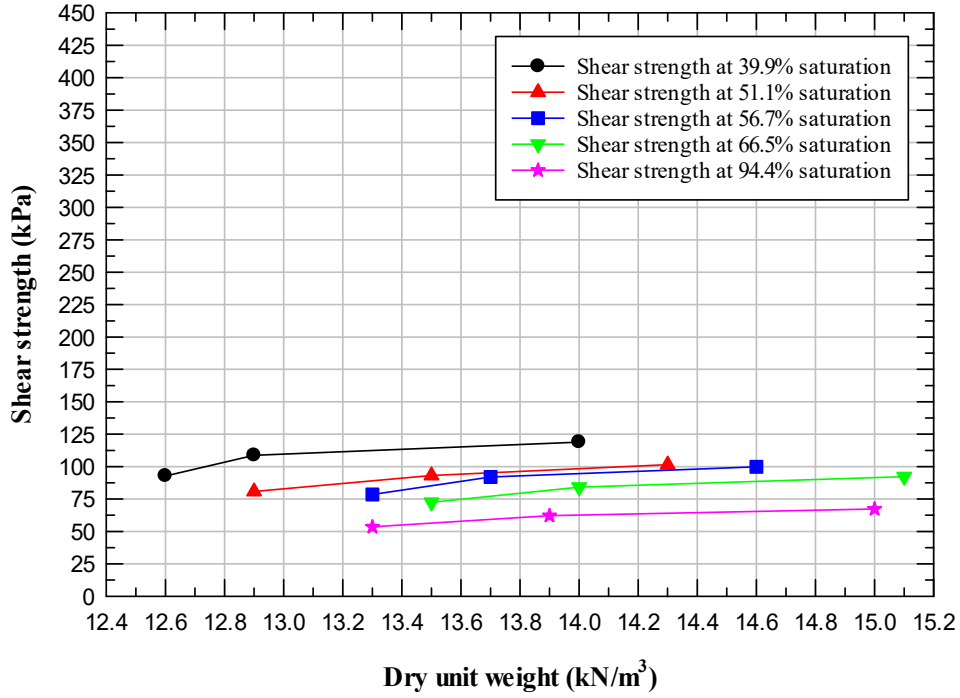

Figure 5-28: Shear strength versus dry unit weight at 110 kPa normal stress and utilizing Vanapalli et. al. (1996) relationship

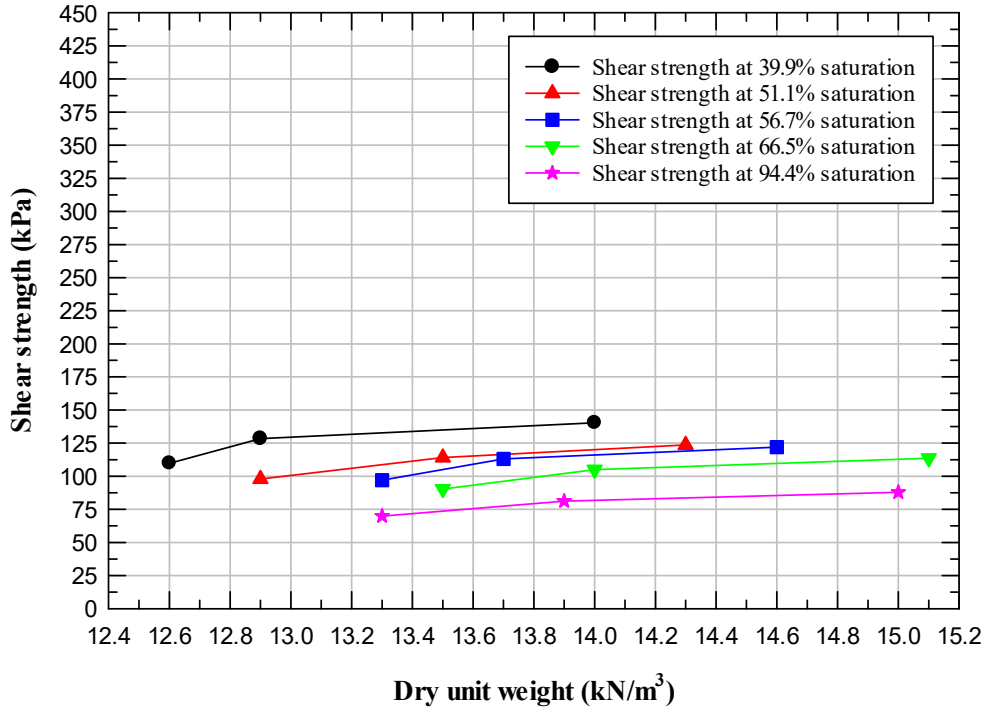

Figure 5-29: Shear strength versus dry unit weight at 143.8 kPa normal stress and utilizing Vanapalli et. al. (1996) relationship

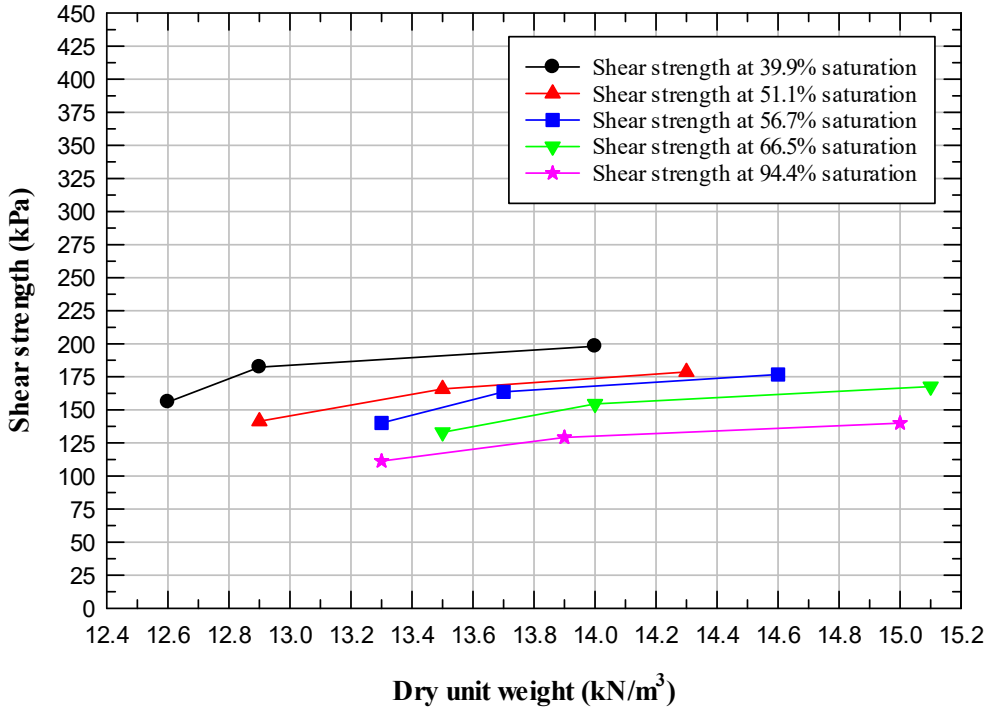

Figure 5-30: Shear strength versus dry unit weight at 229.2 kPa normal stress and utilizing Vanapalli et. al. (1996) relationship

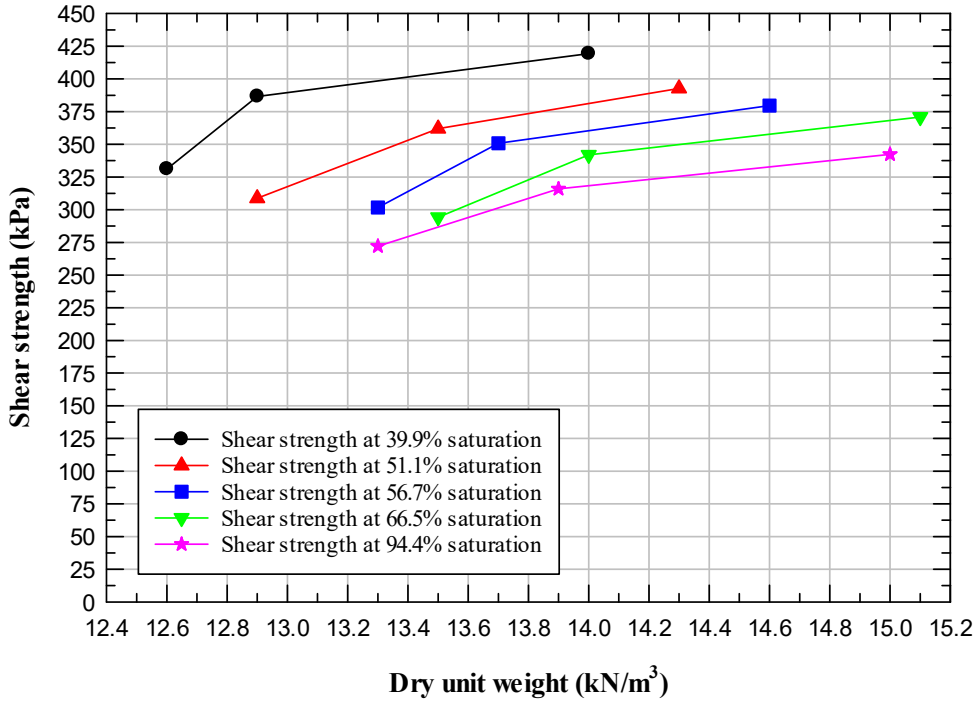

Figure 5-31: Shear strength versus dry unit weight at 561.7 kPa normal stress and utilizing Vanapalli et. al. (1996) relationship

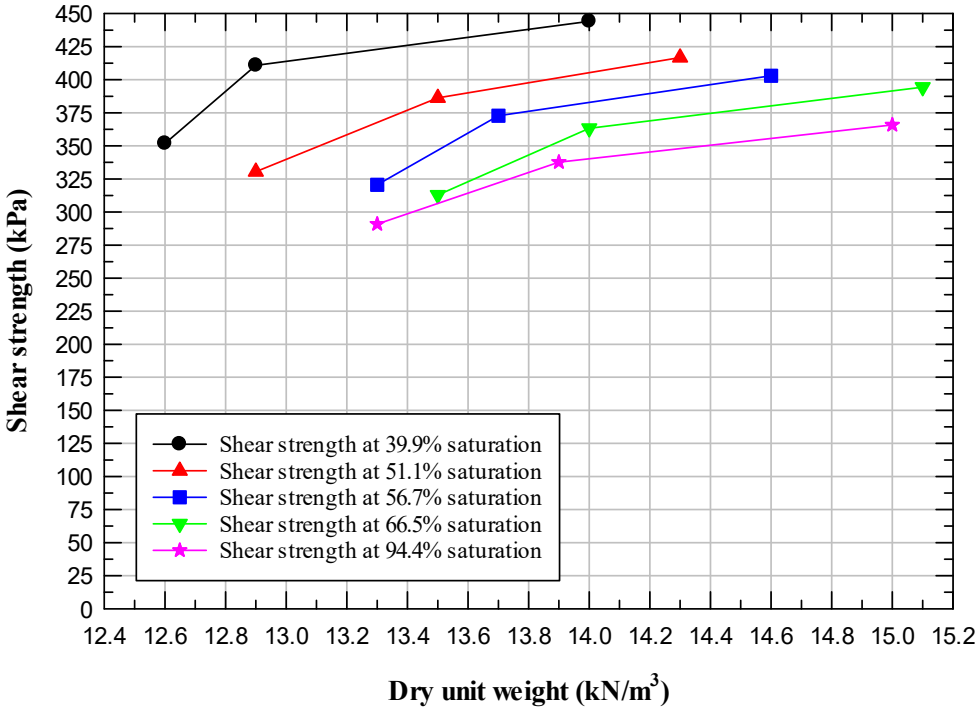

Figure 5-32: Shear strength versus dry unit weight at 600 kPa normal stress and utilizing Vanapalli et. al. (1996) relationship

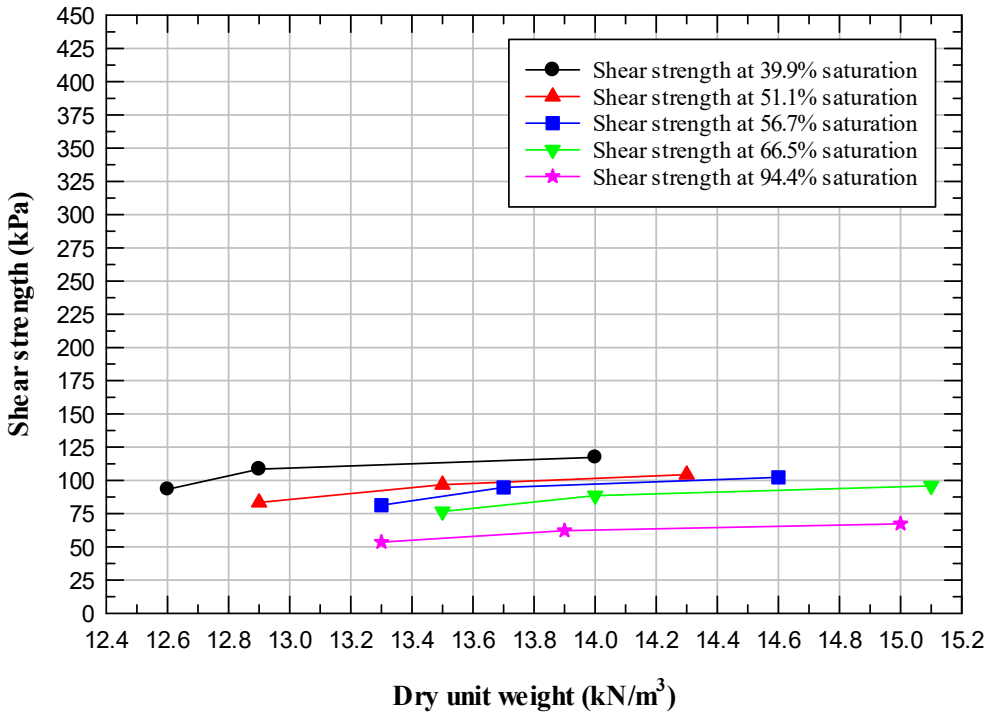

Figure 5-33: Shear strength versus dry unit weight at 110 kPa normal stress and utilizing Khalili & Khabbaz (1998) relationship

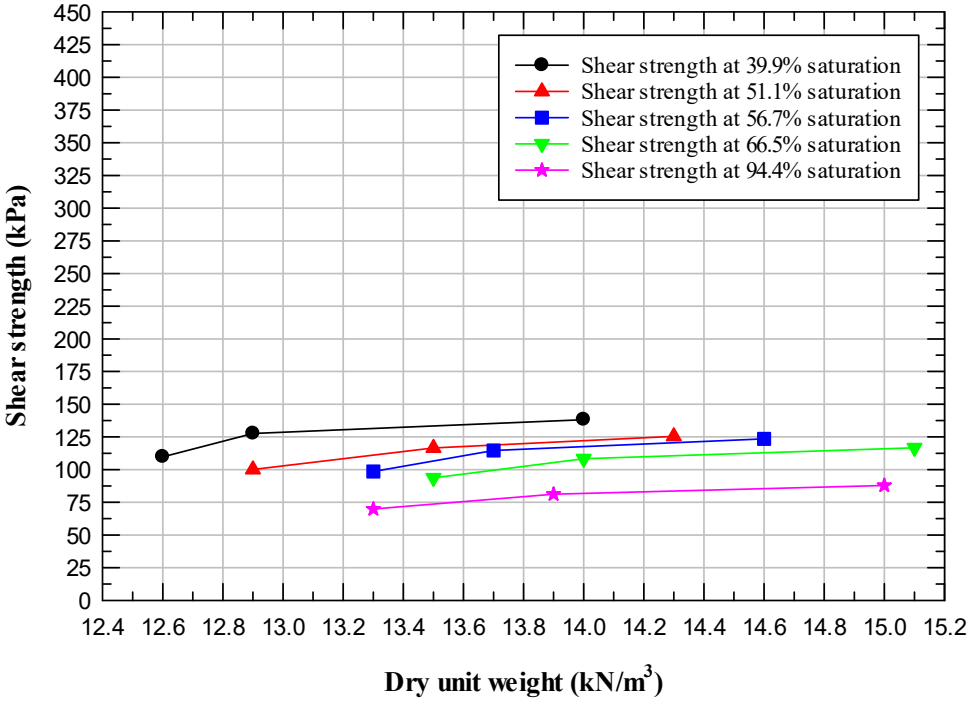

Figure 5-34: Shear strength versus dry unit weight at 143.8 kPa normal stress and utilizing Khalili & Khabbaz (1998) relationship

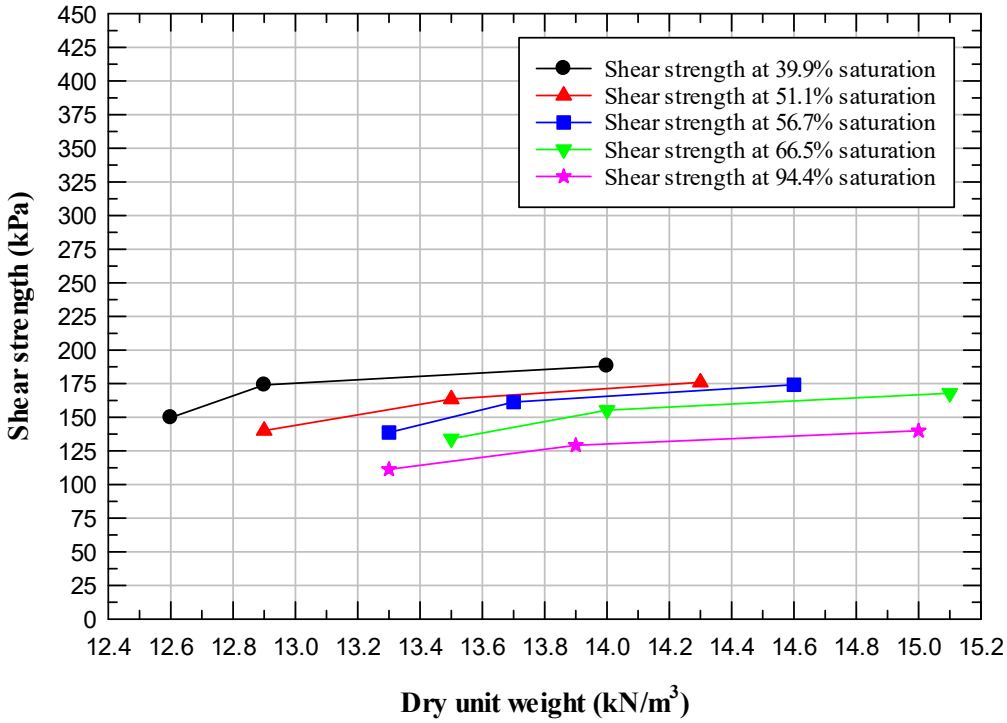

Figure 5-35: Shear strength versus dry unit weight at 229.2 kPa normal stress and utilizing Khalili & Khabbaz (1998) relationship

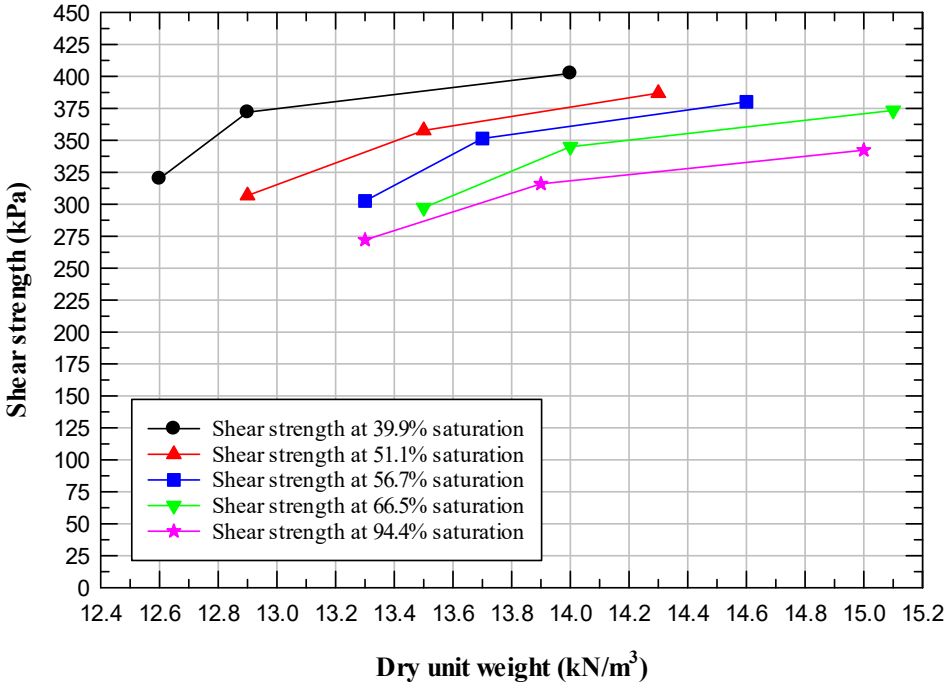

Figure 5-36: Shear strength versus dry unit weight at 561.7 kPa normal stress and utilizing Khalili & Khabbaz (1998) relationship

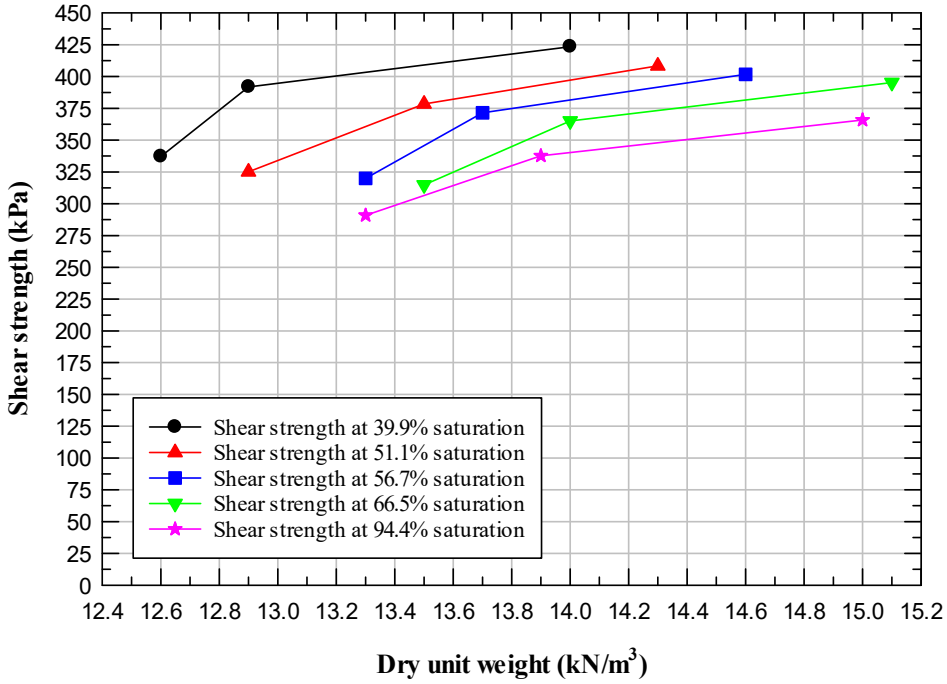

Figure 5-37: Shear strength versus dry unit weight at 600 kPa normal stress and utilizing Khalili & Khabbaz (1998) relationship

Observations on Figures 5-23 through 5-37 show that the shear strength increases with increasing dry unit weight for all the models utilized to calculate angle φ^b. For a given degree of saturation, the specimens with higher dry unit weight have higher shear strength as also discussed in Sections 4.2.1.2 and 4.2.1.4 and shown by Figures 4-6 and 4-8. Observations also show that the shear strength is dependent on the degree of saturation and the normal stress in addition to the dry unit weight. As clearly observed, the specimens having higher dry unit weight and lower degree of saturation have the highest shear strength. Similarly, the specimens with higher normal stress give a higher value of shear strength as depicted. Also, the change in shear strength for all the specimens continues to increase as the normal stress increases. For instance, for specimens at 94.4% saturation, the change in shear strength is lower, as shown in Figure 5-23, compared to the change in shear strength shown in Figure 5-27. Similar conclusions that the

shear strength of the unsaturated soil and its strength parameters are related to overburden pressure and dry density were made by Wen and Yan (2014).

5.5 Summary

This chapter presents the results of saturated shear strength along with the results of the additional shear strength due to matric suction. In addition, a discussion on the influence of degree of saturation and dry unit weight on the shear strength of unsaturated loess is presented.

The saturated shear strength increases with compaction stress for a given normal stress. Also, for a given compaction stress, the saturated shear strength increases with an increase in normal stress.

A comparison made of the three relationships for estimating φ^b revealed that the Fredlund et al. (1996) equation provides the best agreement with the measured cohesion values for the lower compaction stress of 143.8 kPa and the Khalili & Khabbaz et al. (1998) equation provides the better agreement for the higher compaction stresses of 229.2 kPa and 561.7 kPa. However, at the highest degree of saturation of 94.4%, all three equations provide the same predicted cohesions. Each relationship revealed a variance in φ^b , which indicates the rate of change of shear strength due to matric suction, that is due to the primarily to the variance in drained friction angle values for different compaction stress.

The additional shear strength due to matric suction rapidly decreases with an increase in the degree of saturation and ultimately reaches zero at 100% saturation for all three relationships. The additional shear strength due to matric suction for the specimens tested at higher normal stresses have higher values because the matric suction increases with increasing normal stress. At higher degrees of saturation, greater than 57%, the difference in shear strength due to matric

suction is almost negligible with changes in normal stress. This suggests that the matric suction of Fulton loess is almost independent of the normal stress at higher degrees of saturation.

The overall shear strength of Fulton loess decreases with increasing degree of saturation. This decrease in shear strength is due to the decrease in apparent cohesion values with increasing degree of saturation resulting from the decrease in matric suction values with increase in saturation level. Additionally, the shear strength of loess increases with the increase in normal stress and agrees with the general behavior of soils. Higher compaction stresses applied during specimen preparation results in a denser soil specimen with higher cohesion and friction angle. Thus, shear strength increases with the increase in compaction stress. Finally, the shear strength increases with increasing dry unit weight and is dependent on the degree of saturation and normal stress too.

6 Conclusions and Recommendations

6.1 Introduction

This chapter provides the overall summary and conclusions of this research to find the influence of the degree of saturation and dry unit weight on the shear strength of unsaturated Peoria loess at Fulton, TN. To achieve this overall research goal, direct shear tests were performed on loess specimens obtained near Fulton in West Tennessee. The influence of degree of saturation and dry unit weight on the drained shear strength parameters of loess (i.e., drained cohesion and drained internal friction angle) were studied. Since matric suction plays an important role in the shear strength of unsaturated soil, the influence of normal stress on the matric suction values was also studied. To find the matric suction values, soil-water characteristic curves for loess were prepared. Finally, the overall shear strength of the unsaturated loess was estimated and the influence of degree of saturation and dry unit weight on the shear strength of the unsaturated loess was evaluated. Recommendations for future research are also provided in this chapter.

6.2 Overall summary and conclusions

- Changes in the degree of saturation have significant influence on the drained cohesion. As the degree of saturation increases, the drained cohesion of the loess specimens decreases for all the compaction stress levels used to prepare the specimens. In addition, the dry unit weight also influences the drained cohesion values. Denser specimens have higher drained cohesion values.
- The influence of degree of saturation on the drained internal friction angle is especially seen at higher degrees of saturation.

- For a given degree of saturation, the drained friction angle increases with an increase in dry unit weight. However, the drained friction angle values at saturation levels of 66% did not have the same trend as other specimens. This might be due to inherent property differences in soil specimens that arise during specimen preparation.
- For a given degree of saturation, the matric suction values increase with an increase in the vertical stress applied to obtain the soil-water characteristic curve.
- For a given normal stress, the saturated shear strength increases with the compaction stress used to prepare the specimens. Also, for a given compaction stress, the saturated shear strength increases with an increase in normal stress.
- A comparison made of the three relationships for estimating φ^b revealed that the Fredlund et al. (1996) equation provides the best agreement with the measured cohesion values for the lower compaction stress of 143.8 kPa and the Khalili & Khabbaz et al. (1998) equation provides the better agreement for the higher compaction stresses of 229.2 kPa and 561.7 kPa.
- At the highest degree of saturation of 94.4%, all three φ^b equations provide the same predicted cohesions. Each relationship revealed a variance in φ^b, which indicates the rate of change of shear strength due to matric suction, that is due to the primarily to the variance in drained friction angle values for different compaction stress.
- The additional shear strength due to matric suction decreases rapidly with an increase in degree of saturation and ultimately reaches zero at 100% saturation. The additional shear strength due to matric suction for the specimens tested at higher normal stresses have higher values because the matric suction increases with increasing normal stress.

But for degrees of saturation greater than 57%, the influence of normal stress is almost negligible.

- The overall shear strength of Fulton loess decreases with an increase in degree of saturation. This decrease in shear strength is due to the decrease in apparent cohesion resulting from the reduction in the matric suction values with an increase in degree of saturation.
- The overall shear strength of Fulton loess increases with an increase in dry unit weight and is dependent on the degree of saturation and normal stress too. The specimens tested at a higher normal stress give higher shear strength and agrees with the general behavior of soils. The shear strength also increases with the increase in compaction stress because higher compaction stresses applied during specimen preparation results in a denser soil specimen with higher cohesion and friction angle.

6.3 Recommendations for future research

- In order to have a better understanding on the shear behavior of loess, triaxial tests need to be performed. In addition, the stress-strain relationship must be understood which can be provided by the triaxial tests.
- Ring shear tests must be conducted to find the ultimate shear stress of the loess as the direct shear test limits the horizontal displacement.
- To study the influence of degree of saturation and dry unit weight on the shear strength of loess, wider ranges of saturation levels and dry unit weights should be utilized. Additionally, to better understand the shear strength of unsaturated soil, a modified direct shear test apparatus may be utilized that can control suction levels and pore water pressures.

- This research has a limitation on the degree of saturation of the specimens between 66% and 94% due to the expulsion of water from the specimens during specimen preparation. A better estimate of drained cohesion and drained friction angle may be achieved if specimens could be prepared within those ranges using a different specimen preparation method.
- Loess samples from different locations should be tested and compared in order to better understand the shear strength of loess and its behavior upon saturation.
- The SWCCs were prepared within the suction range of 0 to 800 kPa due to the laboratory constraints. The full set of SWCCs were generated using the "SWRC fit" web interface and the Fredlund and Xing (1994) model to estimate the behavior at higher levels of matric suction. The SWCCs can be prepared at greater suction range to get more precise data.

REFERENCES

Adrian, D. B. (2012). "The collapse behavior of compacted West Tennessee loess". Thesis, Master's in Science. The University of Memphis, Memphis, TN.

Akiyama, F. M. (1964). "Shear strength properties of western Iowa loess".

Bowders, J. J., Loehr, J. E., and Owen, J. W. (2000). "Shear behavior of compacted silty loess." *Advances in Unsaturated Geotechnics,* 235-246.

Corbet, J. H. "Department of Geography, Memphis State University." *Department of Geography, Memphis State University*.

Delage, P., Cui, Y., and Antoine, P. (2005). "Geotechnical problems related with loess deposits in Northern France." *Proceedings of International Conference on Problematic Soils,* 1-24.

Doris Asmani, M., Hafez, M., and Shakri, M. (2013). "Comparison between static and dynamic compaction for California Bearing Ratio (CBR)." *The Electronic Journal of Geotechnical Engineering,* 18 5857-5869.

Ekawita, R., and Nawir, H. (2015). "A simple unconsolidated undrained triaxial compression test emulator." *Applied Mechanics and Materials,* Trans Tech Publications, 104-107.

Elkady, T. Y., and Al-Mahbashi, A. M. (2012). "Effect of vertical stress on the soil water characteristic curve of highly expansive soils." *Unsaturated Soils: Research and Applications,* Springer, 165-172.

Fredlund, D. G., Rahardjo, H., and Gan, J. (1987). "Non-linearity of strength envelope for unsaturated soils." 49-54.

Fredlund, D. G., and Rahardjo, H. (1993). *Soil mechanics for unsaturated soils.* John Wiley & Sons, .

Fredlund, D. G., Rahardjo, H., and Fredlund, M. D. (2012). *Unsaturated soil mechanics in engineering practice.* John Wiley & Sons.

Fredlund, D. G., and Xing, A. (1994). "Equations for the soil-water characteristic curve." *Canadian Geotechnical Journal,* 31(4), 521-532.

Fredlund, D. G., Xing, A., Fredlund, M. D., and Barbour, S. (1996). "The relationship of the unsaturated soil shear to the soil-water characteristic curve." *Canadian Geotechnical Journal,* 33(3), 440-448.

Garven, E., and Vanapalli, S. (2006). "Evaluation of empirical procedures for predicting the shear strength of unsaturated soils." *Unsaturated Soils 2006,* 2570-2592.

GCTS, T. S. (2007). "SWC-150 Fredlund Soil Water Characteristic Device: User's Guide & Reference Manual." 27p.

Gibbs, H. J., and Holland, W. (1960). "Petrographic and engineering properties of loess." *Engineering Monographs. Bureau of Reclamation. United States Department of the Interior (no. 28),* (28), 37p.

Higgins, J. D., and Modeer Jr, V. A. (1996). "Landslides: Investigation and Mitigation. Chapter 23- Loess." *Transportation Research Board Special Report,* (247), 585-606.

Holtz, W., and Gibbs, H. (1951). "Consolidation and related properties of loessial soils. Special technical publication No. 126." *American Society for testing materials,* 9-33.

Kane, H. (1968). "A mechanistic explanation of the physical properties of undisturbed loess." *University of Iowa Research Project HR-126. Iowa State Highway Commission, Iowa City.,* 113p.

Khalili, N., and Khabbaz, M. (1998). "A unique relationship of chi for the determination of the shear strength of unsaturated soils." *Geotechnique,* 48(5), 681-687.

Krinitzsky, E. L., and Turnbull, W. J. (1967). "Loess deposits of Mississippi." *Geological Society of America Special Papers,* 94 1-62.

Li, J., Sun, D., Sheng, D., Sloan, S., and Fredlund, D. (2007). "Preliminary study on soil water characteristics of Maryland clay." *Proceedings of the 3rd Asian Conference on Unsaturated Soils, Nanjing, China,* 569-574.

Liu, S. (2006). "Simulating a direct shear box test by DEM." *Canadian Geotechnical Journal,* 43(2), 155-168.

Muhs, D. R., Aleinikoff, J. N., Stafford, T. W., Kihl, R., Been, J., Mahan, S. A., and Cowherd, S. (1999). "Late Quaternary loess in Northeastern Colorado: Part I—Age and Paleoclimatic significance." *Geological Society of America Bulletin,* 111(12), 1861-1875.

Muñoz-Castelblanco, J., Pereira, J., Delage, P., and Cui, Y. (2012). "The water retention properties of a natural unsaturated loess from northern France." *Géotechnique,* 62(2), 95.

Ng, C. W., and Pang, Y. (2000). "Influence of stress state on soil-water characteristics and slope stability." *Journal of Geotechnical and Geoenvironmental Engineering,* 126(2), 157-166.

Oh, S., and Lu, N. (2014). "Uniqueness of the suction stress characteristic curve under different confining stress conditions." *Vadose Zone Journal,* 13(5), 10p.

Olson, R. E. (2004). "Direct Shear Testing." 1-14.

Olson, R. E., and Langfelder, L. J. (1965). "Pore water pressures in unsaturated soils." *Journal of Soil Mechanics & Foundations Division,* 97(SM4), 127-150.

Parsons, R. L., Johnson, R. M., Brown, D. A., Dapp, S., and Brennan, J. J. (2009). "Characterization of loess for deep foundations." *DFI Journal-the Journal of the Deep Foundations Institute,* 3(2), 14-24.

Perez-Garcia, N., Houston, S. L., Houston, W. N., and Padilla, J. M. (2007). "An oedometer-type pressure plate SWCC apparatus".

Seki, K. (2007). "SWRC fit? a nonlinear fitting program with a water retention curve for soils having unimodal and bimodal pore structure." *Hydrology and Earth System Sciences Discussions,* 4(1), 407-437.

Stinson, G. T. (2014). "Maximum collapse potential of remolded West Tennessee loess". Thesis, Master of Science. The University of Memphis, Memphis, TN.

Vanapalli, S. K., Fredlund, D. G., and Pufahl, D. E. (1996). "The relationship between the soil-water characteristic curve and the unsaturated shear strength of a compacted glacial till." *Geotechnical Testing Journal, GTJODJ,* 19(3), 259-268.

Wen, B., and Yan, Y. (2014). "Influence of structure on shear characteristics of the unsaturated loess in Lanzhou, China." *Engineering Geology,* 168, 46-58.

Zhong, Z., Liu, Y., Liu, X., Li, X., and Wang, S. (2015). "Influence of moisture content on shearing strength of unsaturated undisturbed quaternary system middle Pleistocene." *Journal of Central South University,* 22(7), 2776-2782.

APPENDIX A: Consolidation test data

Table A-1: Square root of time vs axial strain

Square root of time ($min^{1/2}$)	**Axial strain, ε (%)**
2.45	0.108
3.87	0.107
5.48	0.107
7.75	0.106
10.95	0.105
15.49	0.105
21.91	0.104
30.00	0.103
42.43	0.103
60.00	0.102
84.85	0.102
120.00	0.101
169.71	0.101
293.94	0.100

Table A-2: Consolidation test data

Load (kPa)	Void-ratio (e)
13.4	1.02
26.4	1.00
51.4	0.98
101.4	0.94
201.4	0.89
401.4	0.85
801.4	0.81

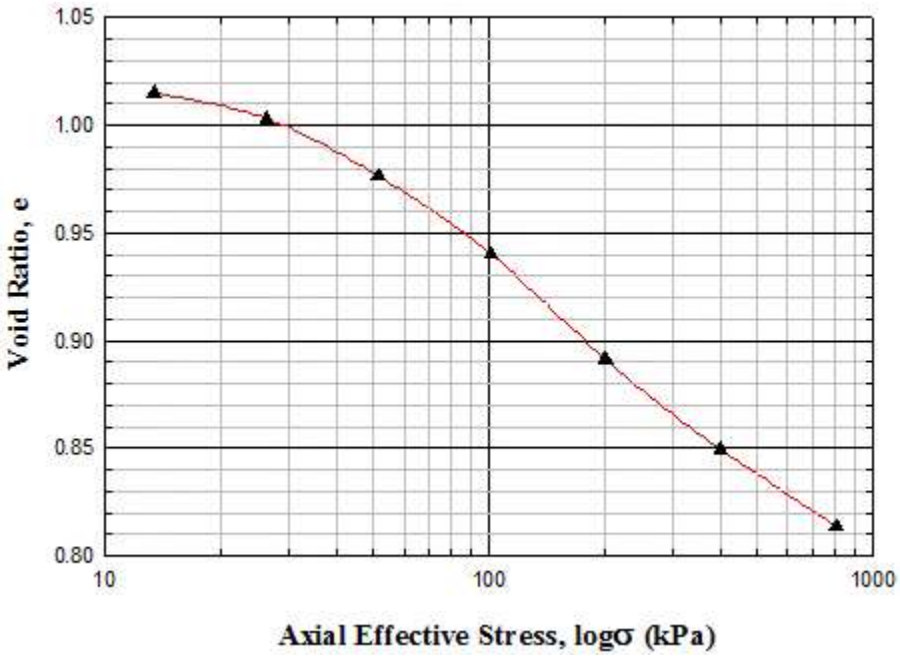

Figure A-1: e versus logσ consolidation curve

APPENDIX B: Direct shear test results

The following figures include the plots of corrected shear stress versus horizontal displacement and vertical displacement versus horizontal displacement for loess with different compaction stress and different saturation levels. The solid lines represent the plots of shear stress versus horizontal displacement whereas the dashed lines represent the plots of vertical displacement versus horizontal displacement.

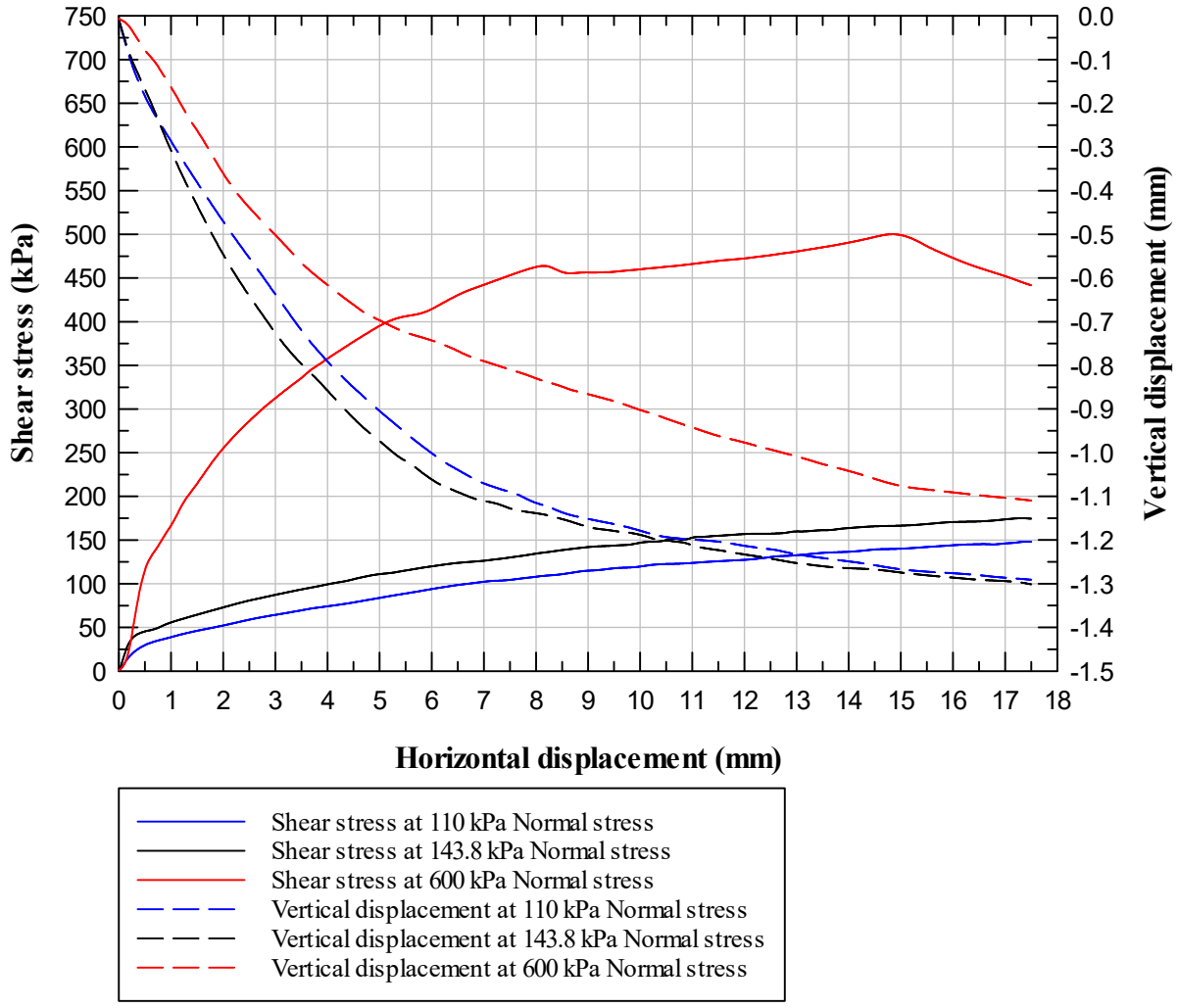

Figure B-1: Corrected shear stress and vertical displacement versus horizontal displacement for specimens with 39.9% saturation level and 143.8 kPa compaction stress

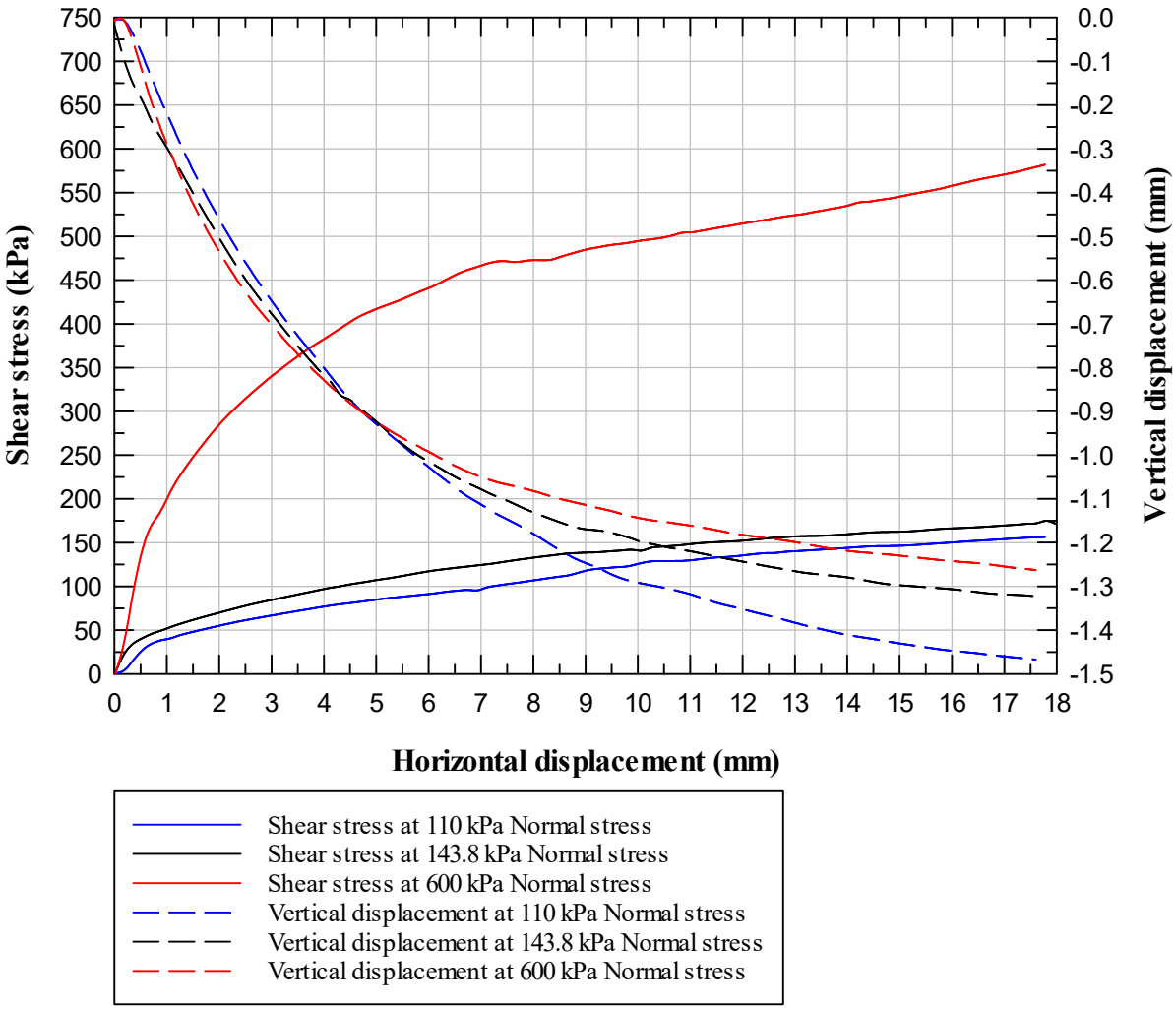

Figure B-2: Corrected shear stress and vertical displacement versus horizontal displacement for specimens with 51.2% saturation level and 143.8 kPa compaction stress

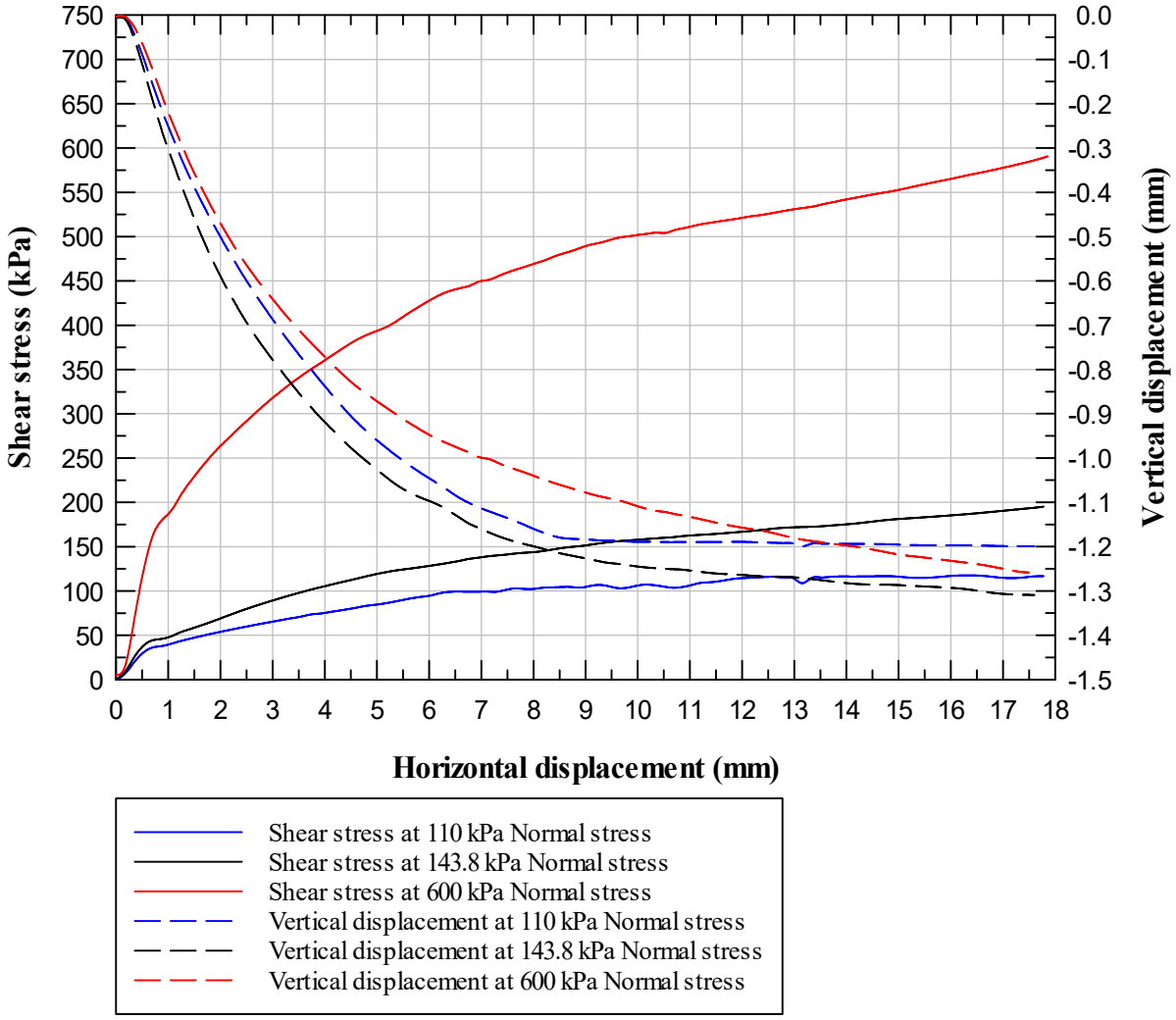

Figure B-3: Corrected shear stress and vertical displacement versus horizontal displacement for specimens with 56.7% saturation level and 143.8 kPa compaction stress

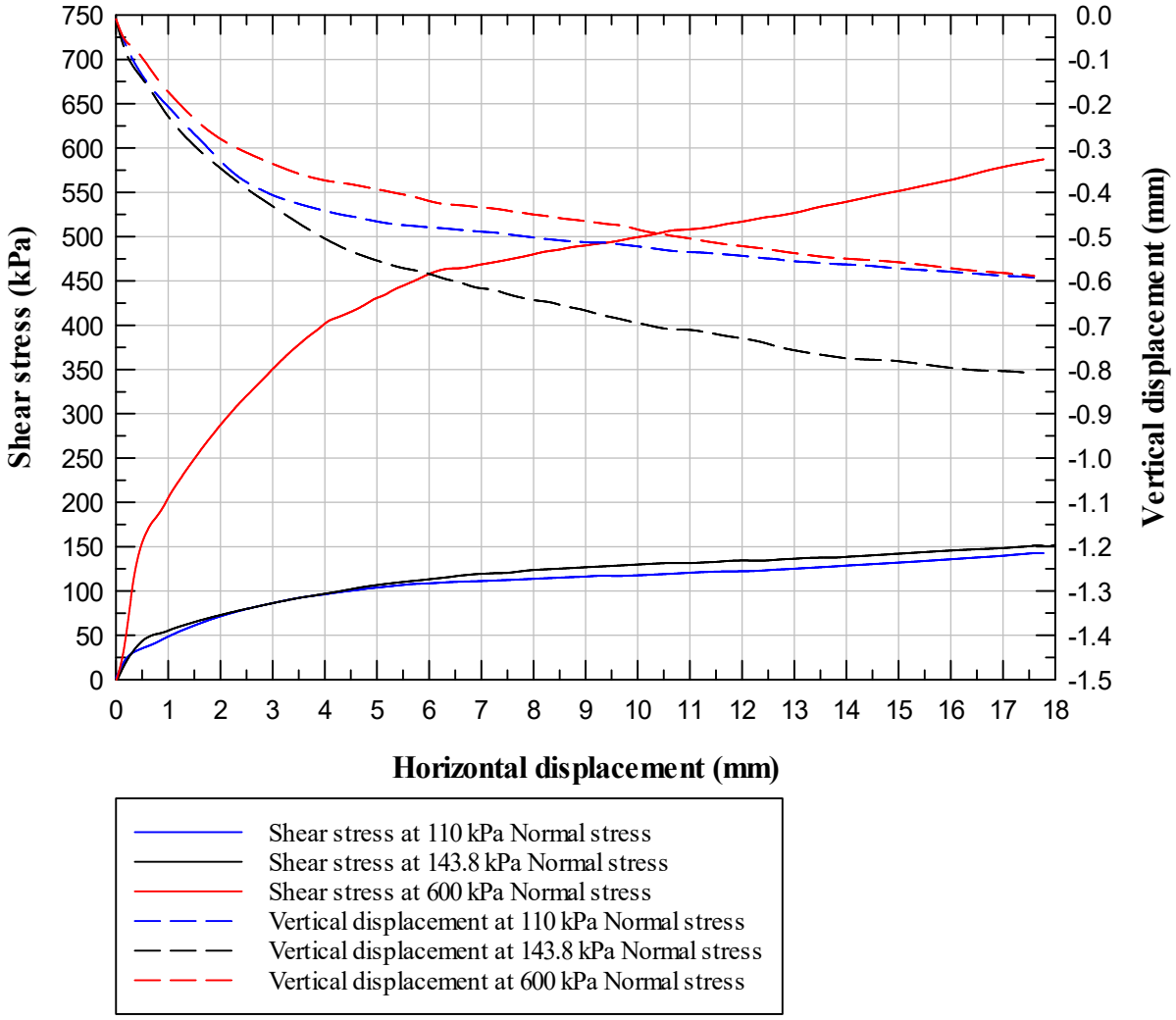

Figure B-4: Corrected shear stress and vertical displacement versus horizontal displacement for specimens with 66.2% saturation level and 143.8 kPa compaction stress

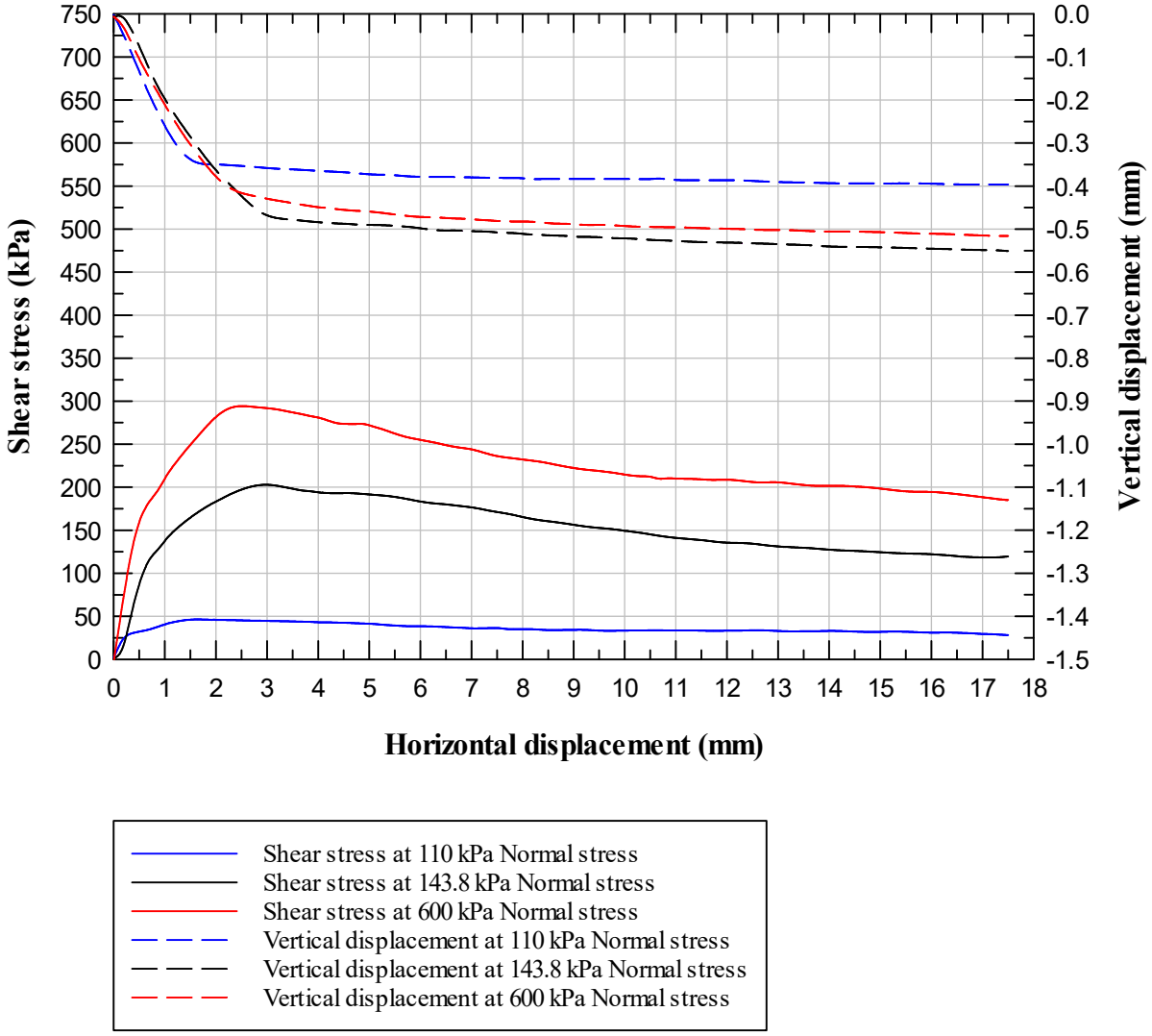

Figure B-5: Corrected shear stress and vertical displacement versus horizontal displacement for specimens with 94.3% saturation level and 143.8 kPa compaction stress

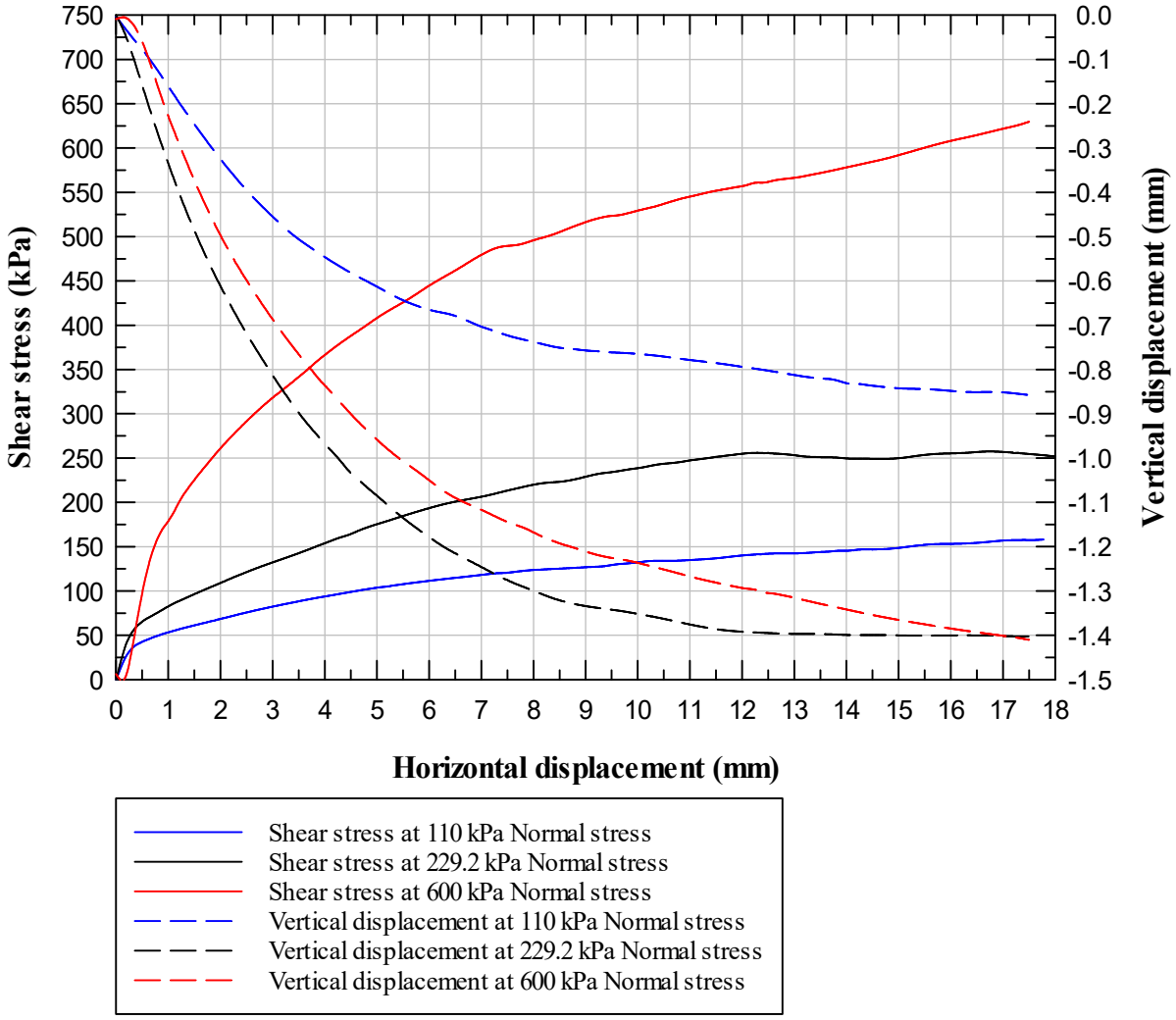

Figure B-6: Corrected shear stress and vertical displacement versus horizontal displacement for specimens with 39.6% saturation level and 229.2 kPa compaction stress

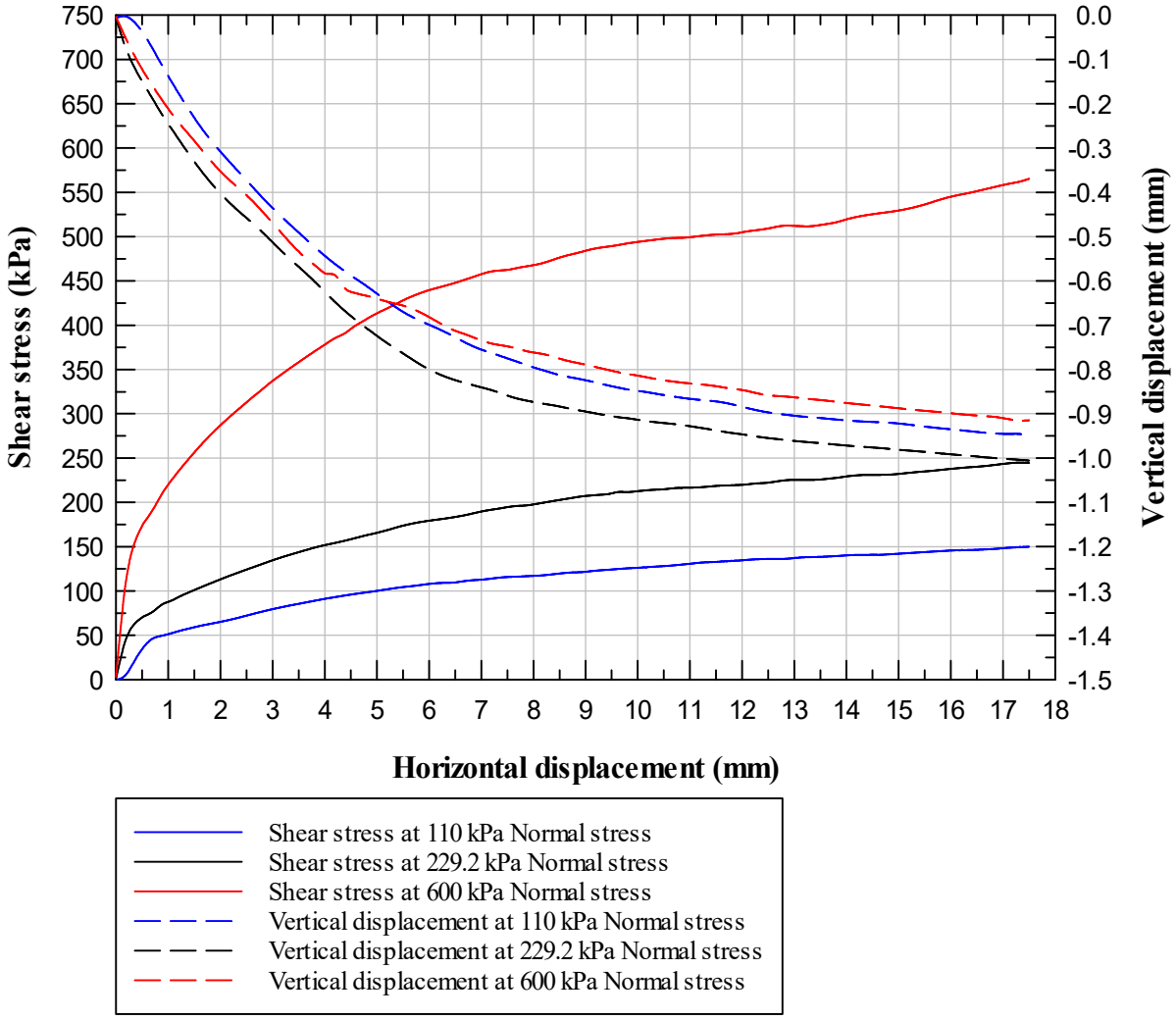

Figure B-7: Corrected shear stress and vertical displacement versus horizontal displacement for specimens with 50.4% saturation level and 229.2 kPa compaction stress

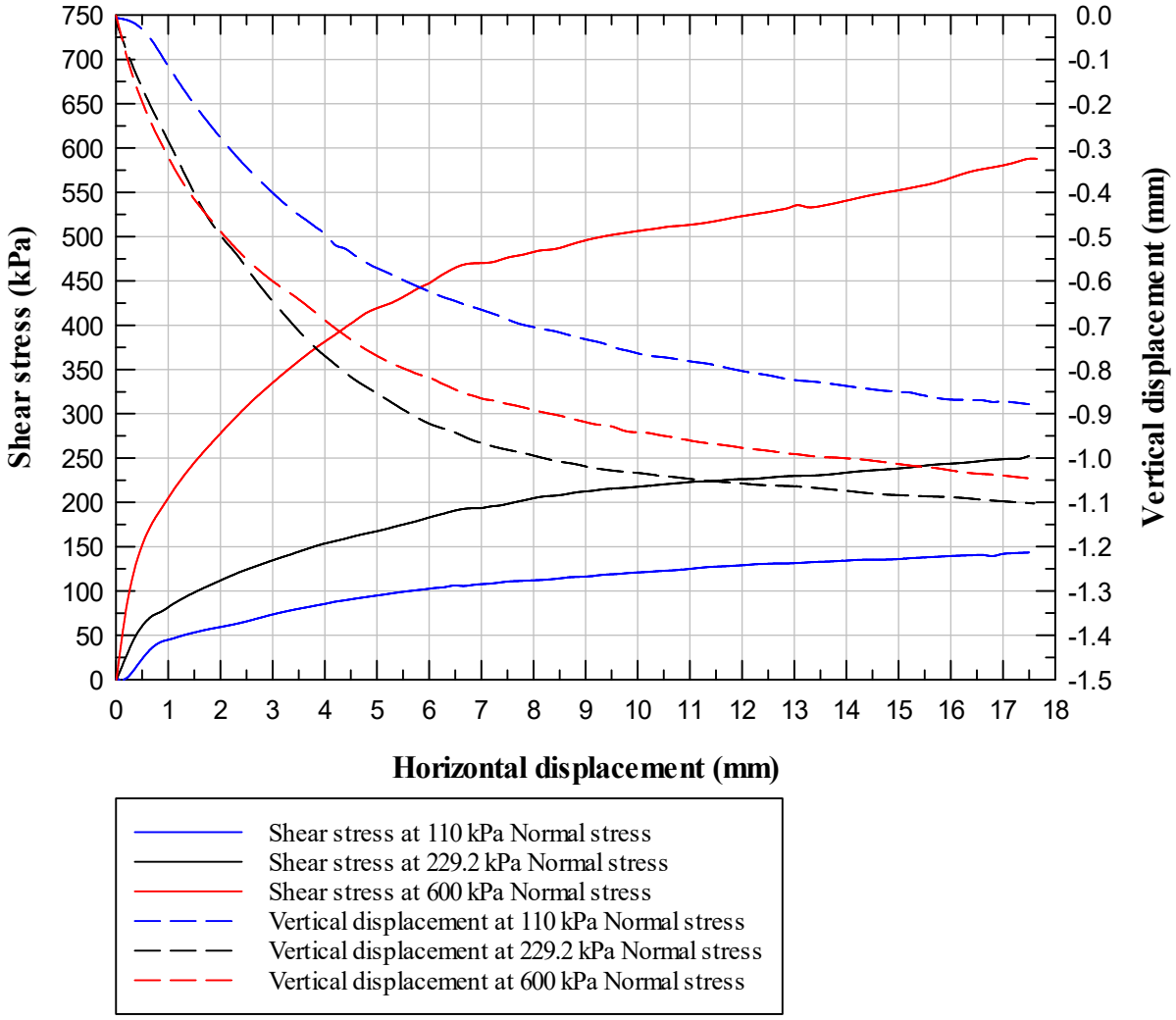

Figure B-8: Corrected shear stress and vertical displacement versus horizontal displacement for specimens with 56.2% saturation level and 229.2 kPa compaction stress

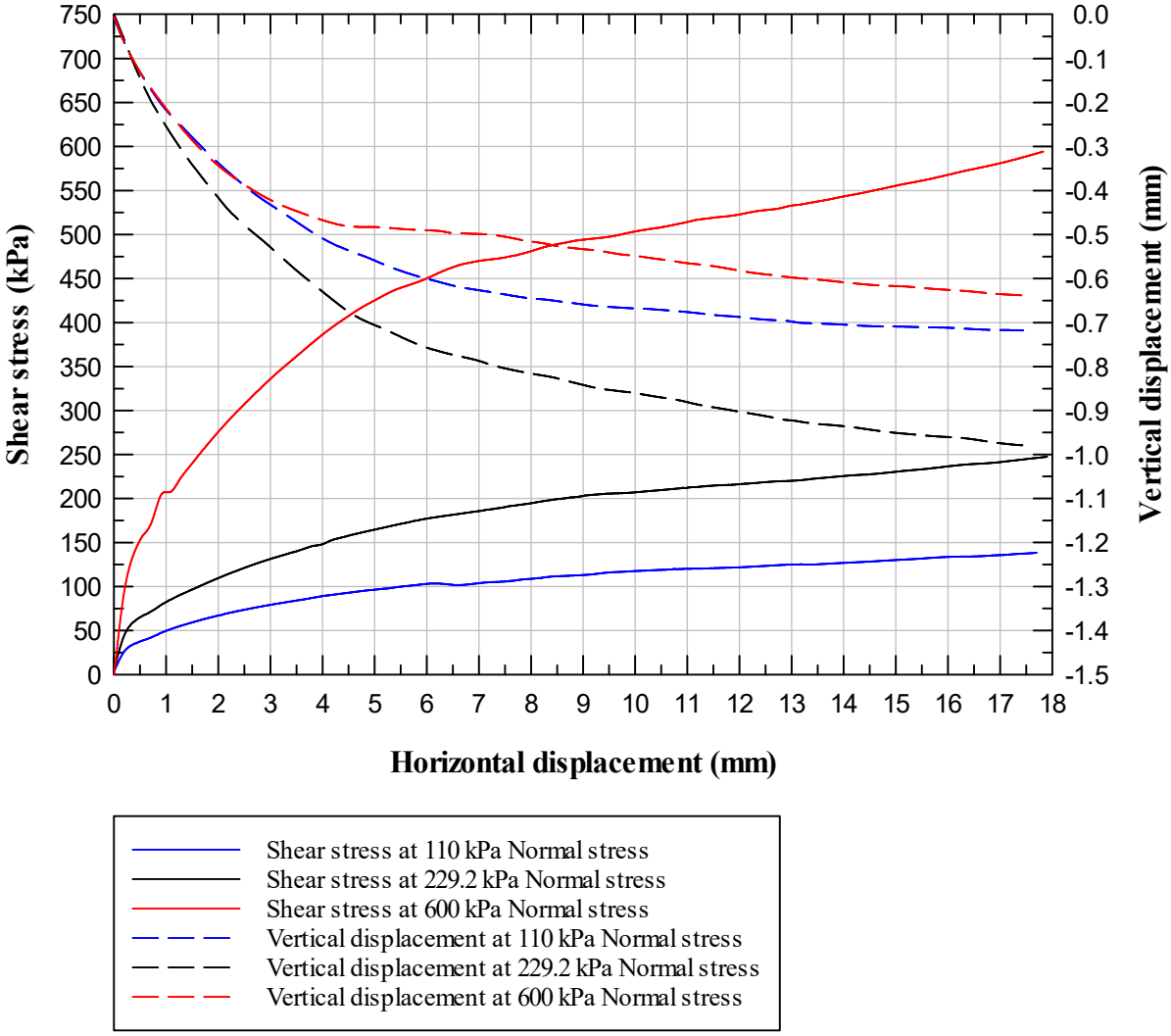

Figure B-9: Corrected shear stress and vertical displacement versus horizontal displacement for specimens with 66.5% saturation level and 229.2 kPa compaction stress

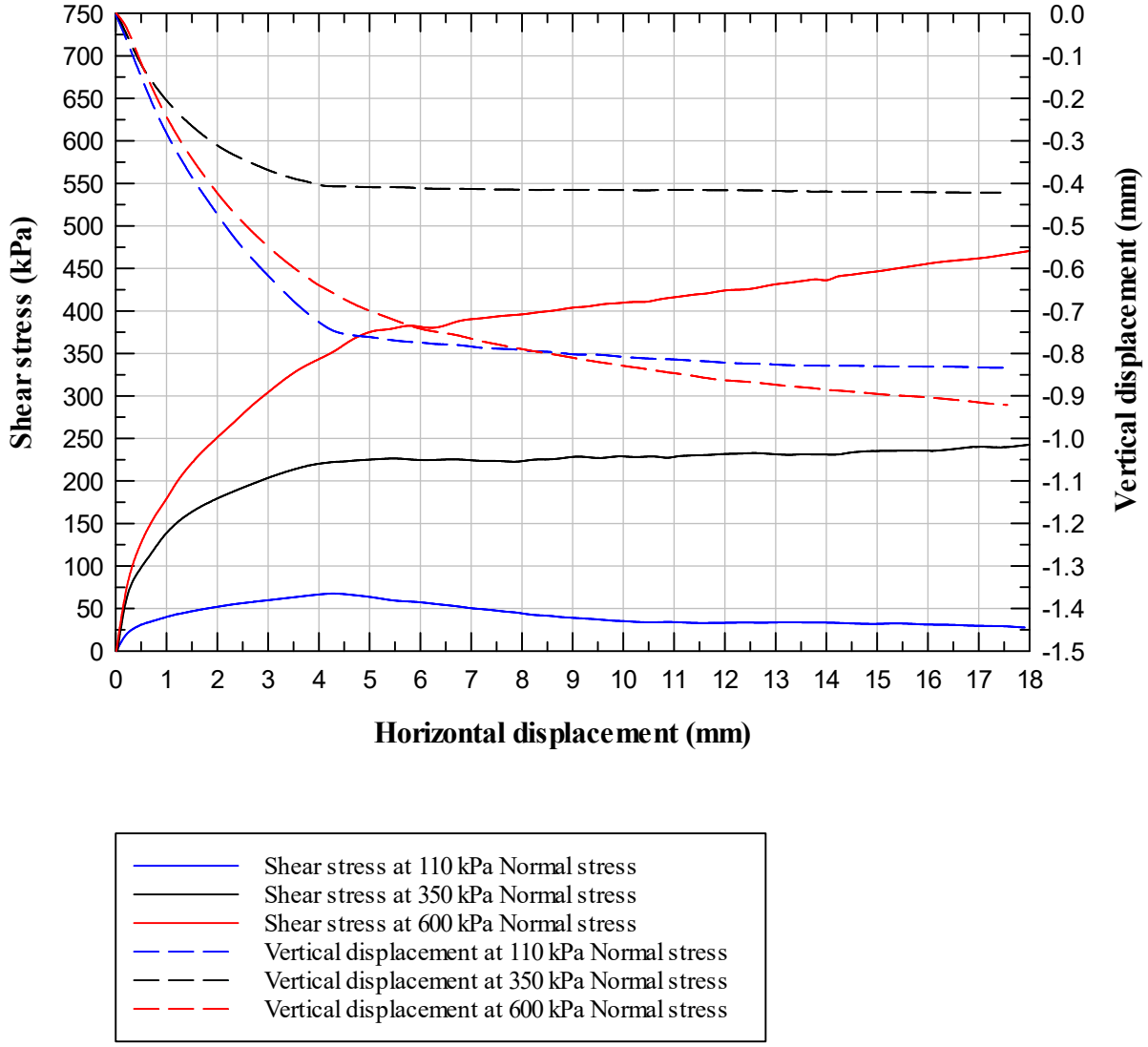

Figure B-10: Corrected shear stress and vertical displacement versus horizontal displacement for specimens with 94.4% saturation level and 229.2 kPa compaction stress

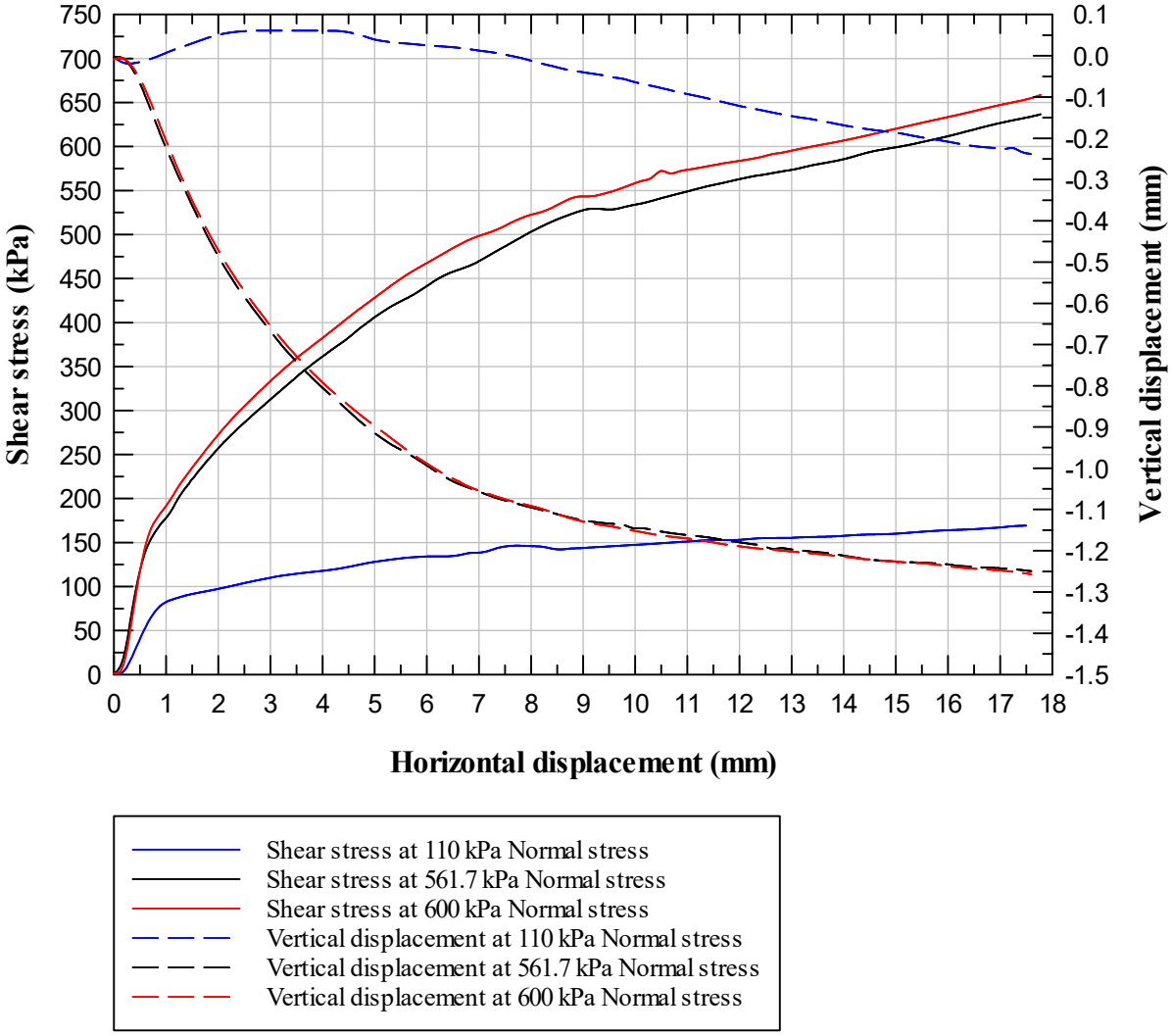

Figure B-11: Corrected shear stress and vertical displacement versus horizontal displacement for specimens with 40.1% saturation level and 561.7 kPa compaction stress

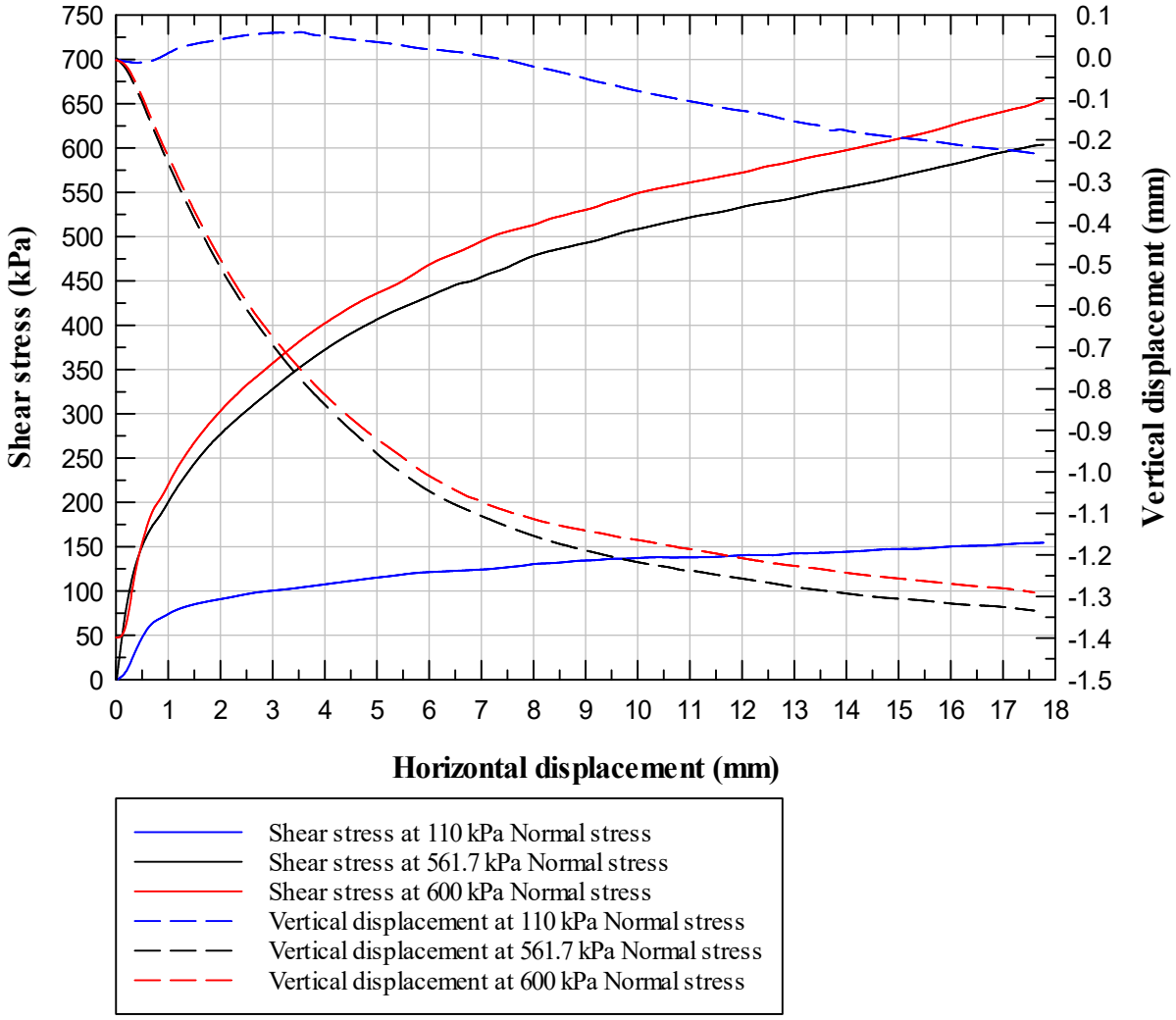

Figure B-12: Corrected shear stress and vertical displacement versus horizontal displacement for specimens with 51.7% saturation level and 561.7 kPa compaction stress

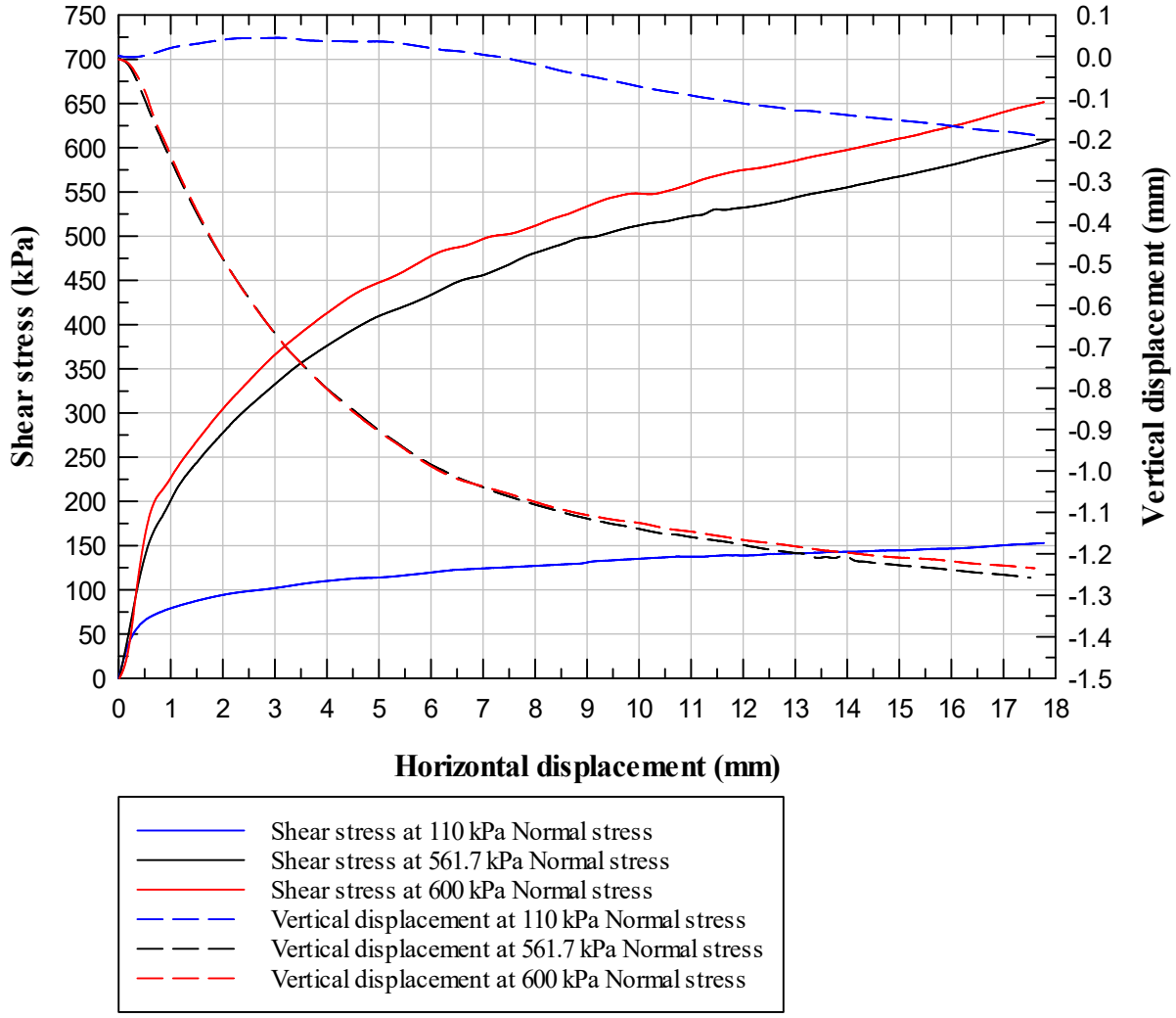

Figure B-13: Corrected shear stress and vertical displacement versus horizontal displacement for specimens with 57.1% saturation level and 561.7 kPa compaction stress

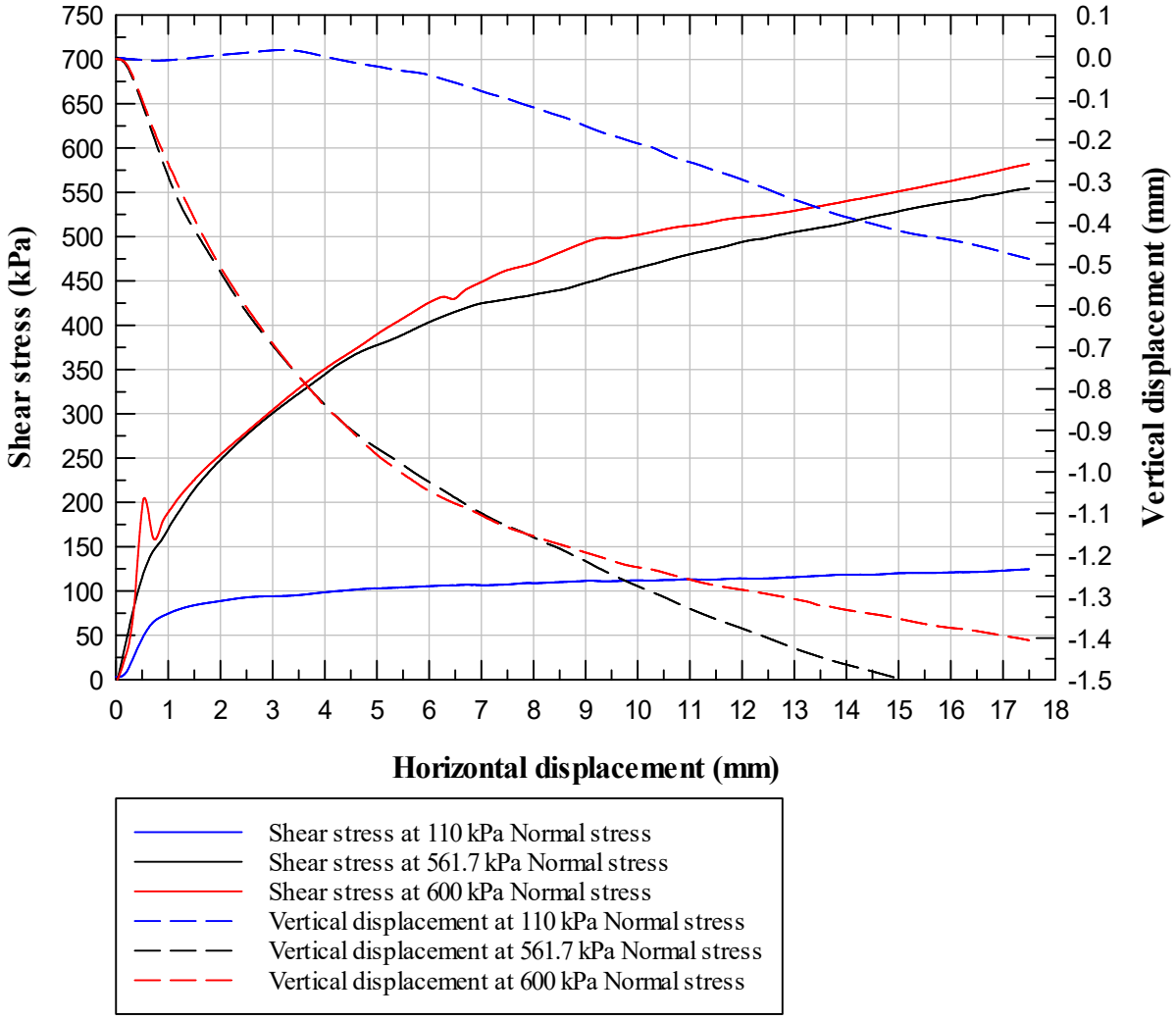

Figure B-14: Corrected shear stress and vertical displacement versus horizontal displacement for specimens with 66.8% saturation level and 561.7 kPa compaction stress

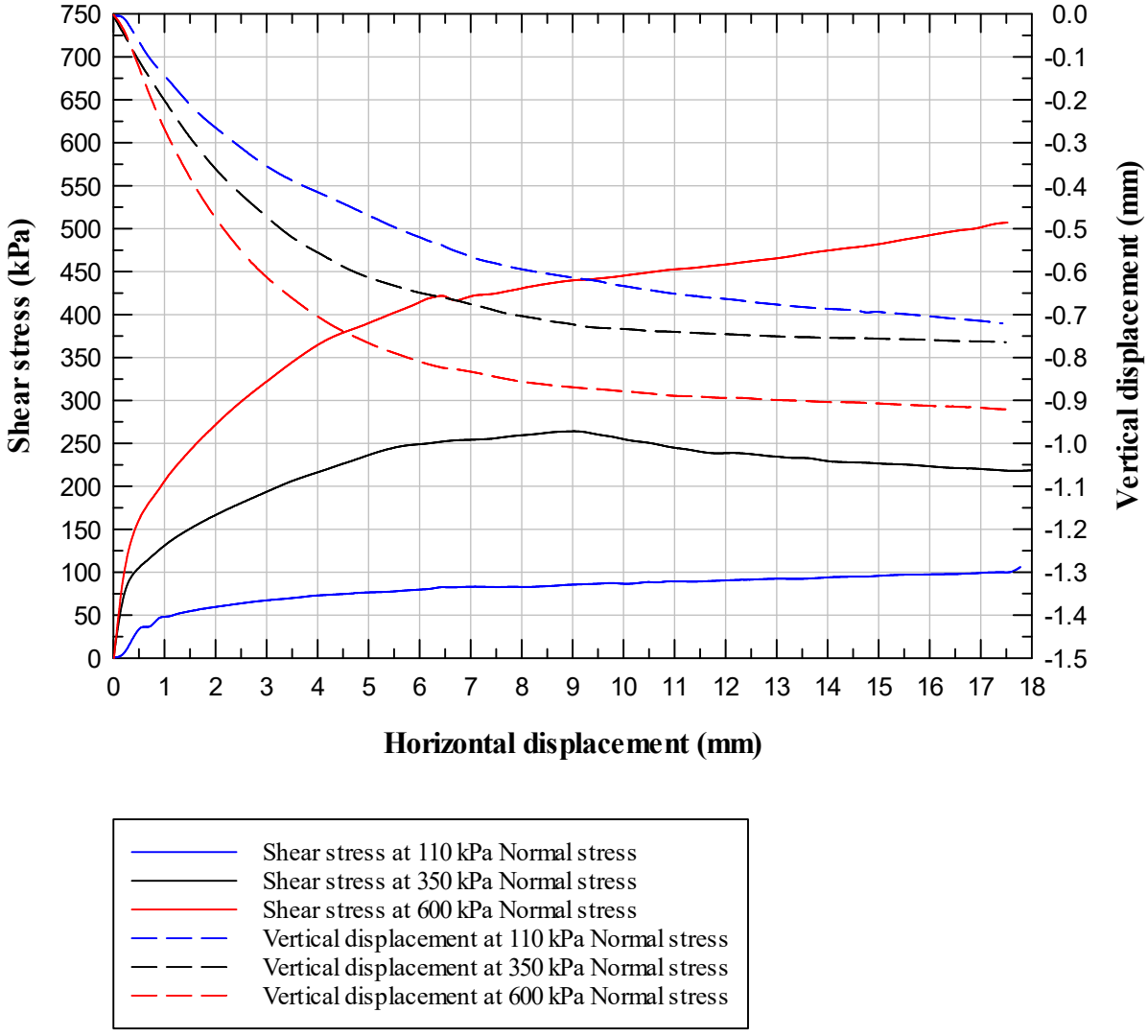

Figure B-15: Corrected shear stress and vertical displacement versus horizontal displacement for specimens with 94.5% saturation level and 561.7 kPa compaction stress